Materials Today: Proceedings xxx (xxxx) xxx

Contents lists available at ScienceDirect

Materials Today: Proceedings

journal homepage: www.elsevier.com/locate/matpr

X-ray analysis and size-strain plot of zinc oxide nanoparticles by Williamson-Hall

M. Antony Lilly Grace [a], Kodumuri Veerabhadra Rao [b], K. Anuradha [b], A. Judith Jayarani [c], A. Arun kumar [b,*], A. Rathika [d]

[a] Department of Physics, CMR Institute of Technology, Bangalore 560037, India
[b] Department of Physics, Methodist College of Engineering and Technology, Abids, Hyderabad, Telangana 500001, India
[c] Department of Physics, Bishop Heber College (Autonomous), Trichy 620017, India
[d] Department of Physics, Stanley College of Engineering and Technology for Women, Hyderabad 500001, India

ARTICLE INFO

Article history:
Available online xxxx

Keywords:
Combustion
X-ray analysis
ZnO
Nanoparticles
Williamson- Hall uniform stress deformation model
Scherer's Formula

ABSTRACT

Zinc oxide (ZnO) nanoparticles were made by burning zinc nitrate, Glycine, and Citric acid at a 1:4 Stochiometric ratio. ZnO-NPs were produced at 350 °C and 500 °C for 4 h. XRD validates the crystalline nature of ZnO nanoparticles with a hexagon structure, whereas SEM shows single-crystal ZnO-NPs with approximately cubical morphologies. Involvement of tiny crystallite sizes and lattice strain in peak broadening at 350 °C and 500 °C. (W-H) analysis and size-strain plot approach were used to examine ZnO nanoparticles' peak broadening. Physical parameters like strain, stress,lattice stain and energy density value were calculated for all XRD reflection peaks of peak broadening at 350 °C and 500 °C. By using W- H Plot deformation, Stress deformation, energy density is calculated. Relation between xrd analysis and sem analysis also discussed.

Selection and peer-review under responsibility of the scientific committee of the 2nd International Conference on Multifunctional Materials.

1. Introduction

The length of a flawless crystal would be infinite in all directions. Crystals can't be perfect since they can only grow so much. The diffraction peaks are more dispersed because to this deviation from perfect crystallinity. The two most important findings from an analysis of form factor and lattice tension at a peak width. The size of the crystallites is not always the same as the size of the particle because of polycrystalline aggregates [1]. Due to its significance in both life and technology, zinc oxide (ZnO), a well-known material, has received extensive study in recent years. A broad energygap (3.37 eV), a high exciton energy, and strong substance constancy are just a few of its advantageous characteristics. These characteristics imply that it could be utilized in a variety of applications, such as sensing applications, earthenware, physical hardware, and materials that light in the dark. [2–4] Table 1.

Particle size, not crystallite size, is typically measured using the BET experiment, light (laser) scattering experiment and scanning electron microscopy (SEM). Strain of the lattice quantifies how dislocations affect lattice constants. Strain is brought on by the triple junction at the grain border, contacting or thermal decomposition pressures, layering flaws, internal consistency stresses, and other factors. [5]. X-ray line broadening analyzes spreading dislodgment. These traits broaden, strengthen, and align the peaks. Crystallite size (1/cosθ) and strain determine peak width (tanθ). Size or strain causes peak broadening as a function of 2θ. Crystallite size opposes Bragg width [6]. W-H analysis separates widening caused by pressure and shape [7]. For years, researchers have created nanocrystalline ZnO because particle size and crystal structure matter for numerous applications. Due to this, many methods have been devised to make ZnO nanopowders, including solgel, solo-chemical, precipitation, ignition blend, pyrolysis and others [8–9]. X-ray profile analysis measures grain size most often. ZnO-NP mean particle size is compared by powder XRD and SEM. he W-H-UDM calculated structural distortion strain in ZnO-NPs calcined at 350oC and 500oC. USDM, UEDM, and SSP provided stress-strain data and dynamism compactness (u) measurements. UDM adopts crystal's surroundings, while USDM and UEDM don't. Layer space strain is compared to the hexagonal crystal's non-uniform surroundings.

* Corresponding author at: Department of Physics, Methodist College of Engineering & Technology (Autonomous), Abids, Hyderabad, India
E-mail address: arunkumr@gmail.com (A. Arun kumar).

https://doi.org/10.1016/j.matpr.2023.05.492
2214-7853/
Selection and peer-review under responsibility of the scientific committee of the 2nd International Conference on Multifunctional Materials.

Please cite this article as: M. Antony Lilly Grace, K. Veerabhadra Rao, K. Anuradha et al., X-ray analysis and size-strain plot of zinc oxide nanoparticles by Williamson-Hall, Materials Today: Proceedings, https://doi.org/10.1016/j.matpr.2023.05.492

RESEARCH ARTICLE

CRYSTAL RESEARCH & TECHNOLOGY

www.crt-journal.org

Studies on the Nucleation, Photoluminescence, and Photoconductivity of Semi-Organic Lithium Fumarate Crystals

G. Padmasree, Kodumuri Veerabhadra Rao, K. Anuradha, A. Arun kumar, and S. Rama*

Semi-organic materials consisting of organic and inorganic semiconductors, exhibit the characteristic properties like strong optical nonlinearity and thermal stability. Lithium Fumarate (LF) is grown as a semi-organic single crystal using lithium hydroxide and fumaric acid employing a slow evaporation method with de-ionized water as the solvent. Classical Nucleation Theory (CNT) is used to calculate the speed of LF nucleation. By altering the temperature, the thermogravimetric (TG) models, namely Coats–Redfern and Piloyan–Novikova equations are used to calculate the kinetic parameters such as enthalpy, Gibbs free energy, real heat power, and entropy of activation values. The width of the metastable zone in the LF crystal is determined by evaluating the relationship between supersaturation and temperature and it is found to exhibit a linear dependence on temperature and possess positive solubility. Lithium Fumarate's (LF) photoconductivity test shows that the grown crystal has positive photoconductivity. Photoluminescence studies conclude that Correlated Colour Temperature (CCT) values and color purity of LF crystal are suited to the green light emitting devices and flat panel displays.

1. Introduction

A new class of optical crystals like semi-organic crystals are developed to overcome the disadvantages seen in organic materials. The organic materials have disadvantages like low transparency, narrow optical band gap, low laser damage threshold, and unfavorable thermal and mechanical properties.[1,2] Because of these restrictions in organic materials, it is difficult to grow large size optical-quality crystals for device applications.[3] Some semi-organic materials have both the qualities of organic materials such as high thermal stability, strong optical non-linearity, and transmittance property of inorganic materials. Solution growth technique is a simple method used for synthesizing semi-organic crystals.[4] The quality of crystal is determined by its form, size, purity, and state of the solid. The crystallization process is profoundly affected by the nucleation behavior. The kinetics of primary nucleation may be inferred from a variety of parameters like the size of the metastable zone, the length of the induction period, and the yield of nuclei.[5,6]

Classical Nucleation Theory (CNT) describes the principles of nucleation mechanisms for bulk developing crystals and Density Functional Theory (DFT) is utilized to determine atomic level values. CNT is based on experimental evidence, whereas DFT is based on structure knowledge. When compared to CNT, the density profile is shown to permit quick approximation of several crystal thermodynamic parameters.[7]

In this investigation, nucleation parameters of LF crystals such as interfacial energy (σ), volume of free energy (ΔG_v), critical energy barrier for nucleation (ΔG^*), radius of the critical nucleus (r^*), and nucleation rate (J) are calculated. In order to back up the research, graphical representations of the thermo dynamical parameters at various temperatures are presented. The width of the metastable zone is calculated using CNT and DFT. During various steps of decomposition, the fractional weight loss (α) is determined using the TG graph at various temperatures. Non-isothermal techniques are used to evaluate the kinetics of decomposition processes.[8] Using suitable equations from non-isothermal kinetic investigations of decomposition processes, thermogravimetric data is analyzed. Kinetic parameters are determined and a reaction model is created and the model with the best linear fit to the equations is chosen.

2. Experimental Section

Synthesis of Lithium Fumarate and its crystal growth characterization is reported in the literature.[9] The Lithium Fumarate single crystal was synthesized by using analar grade lithium hydroxide and fumaric acid as starting materials. Lithium hydroxide was

G. Padmasree
Department of Physics
Stanley College of Engineering and Technology for Women
Abids, Hyderabad, Telangana 500001, India
K. V. Rao, K. Anuradha, A. A. kumar
Department of Physics
Methodist College of Engineering and Technology
Abids, Hyderabad, Telangana 500001, India
E-mail: anunkajini@gmail.com
S. Rama
Department of Physics
St. Joseph's College of Engineering
OMR, Chennai 600119, India

DOI: 10.1002/crat.202300112

Journal of Biomolecular Structure and Dynamics

ISSN: (Print) (Online) Journal homepage: https://www.tandfonline.com/loi/tbsd20

Hypothetical confirmation for the anti-bacterial compound potassium succinate-succinic acid in comparison with certain succinate derivatives

X. D. Divya Dexlin, J. D. Deephlin Tarika, A. Arun Kumar & T. Joselin Beaula

To cite this article: X. D. Divya Dexlin, J. D. Deephlin Tarika, A. Arun Kumar & T. Joselin Beaula (2023): Hypothetical confirmation for the anti-bacterial compound potassium succinate-succinic acid in comparison with certain succinate derivatives, Journal of Biomolecular Structure and Dynamics, DOI: 10.1080/07391102.2023.2199078

To link to this article: https://doi.org/10.1080/07391102.2023.2199078

J Mater Sci: Mater Electron (2023)34:939

Investigation on the growth, structure and physical properties of pyridin-1-ium-2-carboxylate benzimidazole (1:1) hydrate single crystal

S. Sivapriya[1,2], R. Subramaniyan Raja[3], A. Arun Kumar[4], K. Balasubramanian[1,*], T. Joselin Beaula[5], and G. Padmasree[6]

[1] PG & Research, Department of Physics (Reg. No: 12122), The M.D.T. Hindu College, Pettai, Tirunelveli, TN 627010, India
[2] Affiliated to Manonmaniam Sundaranar University, Abishekapatti, Tirunelveli, TN 627 012, India
[3] Department of Physics, KPR Institute of Engineering and Technology, Coimbatore, TN 641407, India
[4] Department of Physics, Methodist College of Engineering and Technology (Autonomous), Abids, Hyderabad 500001, India
[5] Department of Physics and Research Centre, Malankara Catholic College, Mariagiri, TN 629153, India
[6] Department of Physics, Stanley College of Engineering for Women, Hyderabad, India

Received: 2 November 2022
Accepted: 2 March 2023

ABSTRACT

Pyridin-1-ium-2-carboxylate Benzimidazole hydrate (PCBH) crystals was synthesized from Benzimidazole and Pyridine 1-ium-2-carboxylic acid in 1:1 ratio and were grown as single crystals using methanol solvent by conventional evaporation growth method. The unit cell parameters were obtained using single crystal X-Ray Diffraction. The presence of the functional groups in the PCBH compound have been identified using the FTIR spectra. The linear optical properties of solution grown PCBH crystals were analyzed using UV–Vis spectrometer. The DFT was used to figure out the best molecular structures, frontier molecular orbitals, and quantum chemical properties of the grown compound. The calculations were done at the B3LYP/6-311G (d,p) level. Vickers Microhardness Tester was employed for the analysis of mechanical properties of the crystal. The dielectric characteristics were investigated. The laser damaged threshold of PCBH crystal was identified. The molecular docking study suggests that it possesses antibacterial action and displays minimal binding energy. The ADMET factors and drug-likeness are used to predict the pharmacokinetic features of PCBH molecule. PCBH compound is clearly well-optimized and recommended for the prevention of any bacterial illness according to the results.

Address correspondence to E-mail: kbcrystalmdt@gmail.com

https://doi.org/10.1007/s10854-023-10216-0
Published online: 12 April 2023

J Mater Sci: Mater Electron (2023)34:939

Investigation on the growth, structure and physical properties of pyridin-1-ium-2-carboxylate benzimidazole (1:1) hydrate single crystal

S. Sivapriya[1,2], R. Subramaniyan Raja[3], A. Arun Kumar[4], K. Balasubramanian[1,*], T. Joselin Beaula[5], and G. Padmasree[6]

[1] PG & Research, Department of Physics (Reg. No: 12122), The M.D.T. Hindu College, Pettai, Tirunelveli, TN 627010, India
[2] Affiliated to Manonmaniam Sundaranar University, Abishekapatti, Tirunelveli, TN 627 012, India
[3] Department of Physics, KPR Institute of Engineering and Technology, Coimbatore, TN 641407, India
[4] Department of Physics, Methodist College of Engineering and Technology (Autonomous), Abids, Hyderabad 500001, India
[5] Department of Physics and Research Centre, Malankara Catholic College, Mariagiri, TN 629153, India
[6] Department of Physics, Stanley College of Engineering for Women, Hyderabad, India

Received: 2 November 2022
Accepted: 2 March 2023

ABSTRACT

Pyridin-1-ium-2-carboxylate Benzimidazole hydrate (PCBH) crystals was synthesized from Benzimidazole and Pyridine 1-ium-2-carboxylic acid in 1:1 ratio and were grown as single crystals using methanol solvent by conventional evaporation growth method. The unit cell parameters were obtained using single crystal X-Ray Diffraction. The presence of the functional groups in the PCBH compound have been identified using the FTIR spectra. The linear optical properties of solution grown PCBH crystals were analyzed using UV–Vis spectrometer. The DFT was used to figure out the best molecular structures, frontier molecular orbitals, and quantum chemical properties of the grown compound. The calculations were done at the B3LYP/6-311G (d,p) level. Vickers Microhardness Tester was employed for the analysis of mechanical properties of the crystal. The dielectric characteristics were investigated. The laser damaged threshold of PCBH crystal was identified. The molecular docking study suggests that it possesses antibacterial action and displays minimal binding energy. The ADMET factors and drug-likeness are used to predict the pharmacokinetic features of PCBH molecule. PCBH compound is clearly well-optimized and recommended for the prevention of any bacterial illness according to the results.

Address correspondence to E-mail: kbcrystalmdt@gmail.com

https://doi.org/10.1007/s10854-023-10216-0
Published online: 12 April 2023

Journal of Physics and Chemistry of Solids xxx (xxxx) 110938

Contents lists available at ScienceDirect

Journal of Physics and Chemistry of Solids

journal homepage: www.elsevier.com/locate/jpcs

Irradiative thermoluminescence, and defect center analysis in Ni^{2+} ionic $CaAl_2SiO_6$ glass lattice

K. Veerabhadra Rao [a], Ch Ramesh [b], S. Shesha Devi [c], Padala Ashok [a], Ravi Kumar Guntu [d, *], G. Bhikshamaiah [e], B. Appa Rao [a]

[a] Department of Physics, University College of Science, Osmania University, Hyderabad, 500 007, Telangana, India
[b] Department of Physics, University College of Science, Mahathma Gandhi University, Hyderabad, 508 254, Telangana, India
[c] Department of Physics, Vardaman College of Engineering, and Technology, JNT University, Hyderabad, 501 218, Telangana, India
[d] Department of Physics, Sreenidhi Institute of Science and Technology, JNT University, Hyderabad, 501 301, Telangana, India
[e] Department of Physics, CVR College of Engineering, JNT University, Hyderabad, 501 510, India

ARTICLE INFO

Keywords:
Alumina silicate glasses
Elastic glass lattice
DC conductivity
Irradiative thermoluminescence
Photoluminescence

ABSTRACT

In this study, we obtained nickel oxide-doped $CaAl_2SiO_6$ glasses and analyzed their structural, optical, thermoluminescent, and photoluminescent properties. In general, NiO-doped glasses are useful as optical materials. However, optical materials such as glasses containing Ni^{2+} ions require refinement of their properties in terms of their structure, thermal stability, microhardness, electrical conductivity, and luminescence to facilitate the development of advanced thermoluminescent materials. Thus, Ni^{2+} ionic $CaAl_2SiO_6$ glasses were synthesized and tested in this study. We observed the amorphous behavior of samples by X-ray diffraction, scanning electron microscopy, differential thermal analysis, and Fourier transform-infrared (FT-IR) spectroscopy. The order of density, oxygen packing density, polaronic radius, molar volume, and refractive index were evaluated for the glasses. The glass transition temperatures were identified using DTA to assess the order of the thermal stabilities, where the highest was found for the $Ni_{0.4}Ca_{9.4}Al_{30}Si_{60}$ glass. The modes of molecular vibrations for Ni–O–Ni, Ca–O–Ca, Al–O–Al, and Si–O–Si molecules were identified using FT-IR. The highest transmittance intensities were determined for the $Ni_{0.6}Ca_{9.4}Al_{30}Si_{60}$ glass. The order of the electrical conductivity and activation energy were obtained for glasses using DC conductivity measurements, where the highest was found for the $Ni_{0.2}Ca_{9.4}Al_{30}Si_{60}$ glass. Optical absorption spectra were recorded for the glasses to determine the order of the band gap (~0.78 eV) and nephelauxetic ratio (0.799). The photoluminescence was recorded for the glasses at an excitation wavelength of 400 nm to determine the order of the transition probability (~1.85 S^{-1}) and luminescence emission cross section (~0.819 × 10^{-14} cm^2). The highest transmittance intensities were obtained for the $Ni_{0.4}Ca_{9.4}Al_{30}Si_{60}$ glass. Thermoluminescence was recorded for the glasses under gamma irradiation at a dose of 30 kGy, which yielded the shape symmetry factor (~0.536%), frequency factor (1.31 S^{-1}), and activation energy (~0.551 eV). Irradiative thermoluminescent analysis suggested a higher order octahedral tendency, and the divalent oxidation states for nickel ions in the glass with an NiO concentration of 0.6 mol% obtained the best thermoluminescent intensities. The orders of the elastic modulus, nephelauxetic ratio, and microhardness for the glasses suggested covalently connected elastic lattices.

1. Introduction

SiO_2 glass materials are highly transparent, rigid, non-corrosive, and thermally stable. Their structural and optical characteristics, such as a high refractive index and optical bandgap, make them useful for various spectroscopic applications [1,2]. In the last three decades, many studies have investigated silicate glass materials doped with various transition and rare earth metal ions due to their mechanical, dielectric, and spectroscopic properties [3,4]. The dielectric and spectroscopic properties of glasses containing SiO_2 and Ni^{2+} transition metal ions make them suitable for various applications, such as in semiconducting lasers and light-emitting diodes (LEDs) [5,6]. The metal oxide Al_2O_3 is not a conventional glass former but adding Al_2O_3 to SiO_2 glasses improves the elastic strength and non-corrosion behavior, as

* Corresponding author.
E-mail address: drgrk1985@gmail.com (R.K. Guntu).

https://doi.org/10.1016/j.jpcs.2022.110938
Received 11 March 2022; Received in revised form 27 July 2022; Accepted 28 July 2022
0022-3697/

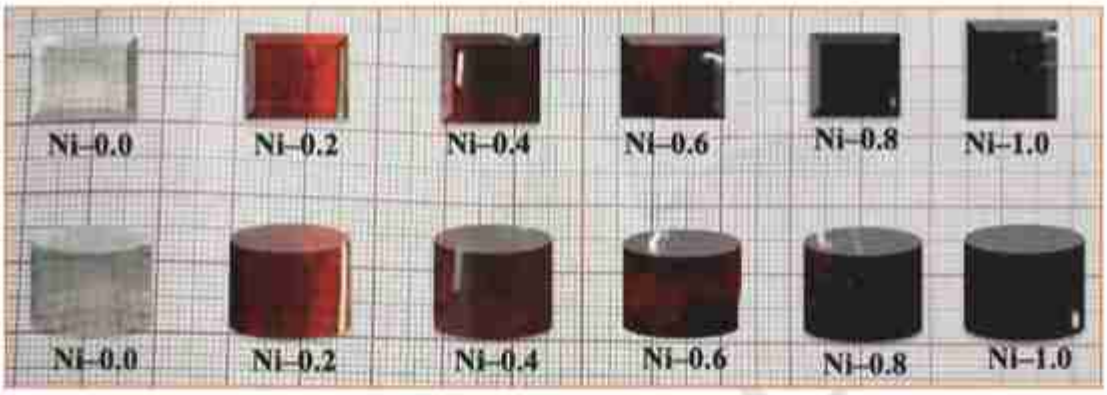

Fig. 1. Represents the photograph of $Ca_{(10-x)}Al_{30}Si_{60}Ni_x$ glasses, where, $0.0 = x \leq 1.0$, step size = 0.2 mol %.

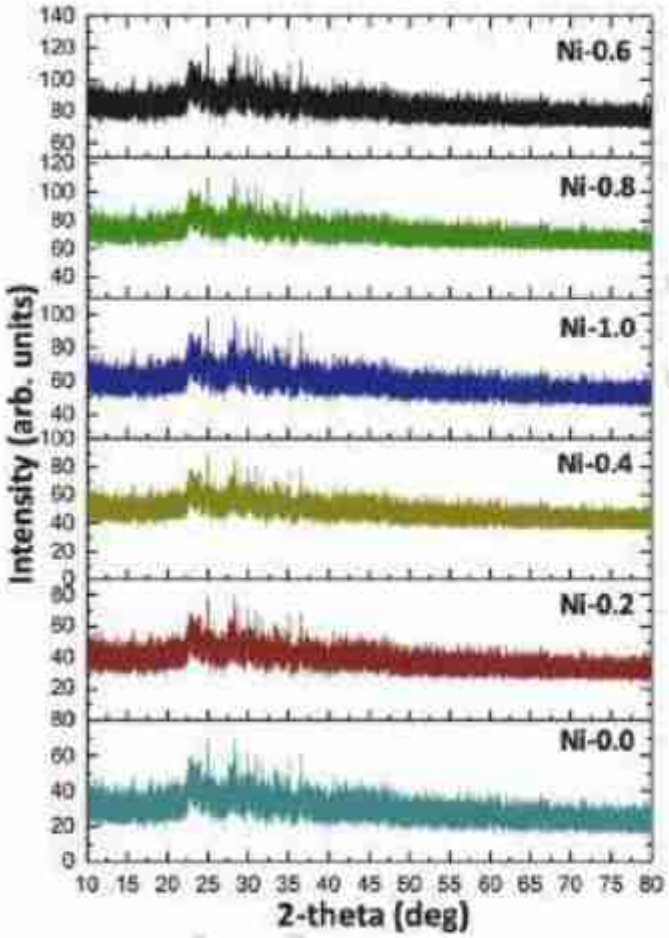

Fig. 2. X-Ray diffraction pattern of $Ca_{(10-x)}Al_{30}Si_{60}Ni_x$ glasses, where, 'x' varies 0–1 mol% with a step size of 0.2 mol%. The diffraction angles are taken up to an accuracy of $\pm 0.1^{\circ}$. Lines drawn back ground of image only for better view of eye guiding.

well as increasing the microhardness and thermal stability of silicate glasses [7–9]. The added Al^{3+} ions change Si–O–Si linkages into Al–O–Si linkages, thereby greatly enhancing the strength, chemical endurance, and mechanical properties of silicate glasses [10–12]. In addition, Al_2O_3-containing SiO_2 glasses have high order trap centers and thus more orders of thermally stimulated luminescence, which are useful for various applications in radiation dosimetry. Under gamma irradiation, Al_2O_3-containing SiO_2 glasses generate high order trap centers with excellent thermoluminescence outputs [13–15].

The addition of CaO to a pure silicate host enhances the refractive index, reduces the glass transition temperature, and improves the optical inertness. The added Ca^{2+} ions change Si–O–Si linkages into Ca–O–Si linkages, thereby greatly changing the strength, chemical endurance, and mechanical properties of the silicate glasses [16,17]. In addition, CaO-containing SiO_2 glasses have high order trap centers, and thus more orders of trap centers are obtained by replacing Si^{4+} ions with Ca^{2+} ions, which is useful for advanced radiation dosimetry applications. In general, CaO silicate materials doped with 3d block elements such as NiO, MnO, CoO, CuO, Sc_2O_3, and V_2O_3 are the most favorable candidates for use in semiconductors, laser diodes, and LEDs. Replacing Ni^{2+} ions with Ca^{2+} ions in Ca–O–Ca linkages in the SiO_2 network will improve the dielectric and spectroscopic properties [18–20]. The metal oxide NiO is a good nucleation agent with a divalent oxidation state in the SiO_2 glass matrix, and it is used to enhance the photo-electronic properties of SiO_2 glasses. The Ni^{2+} ions typically have substantial effects on the spectroscopic properties of the glasses [21,22]. Silicate materials containing Ni^{2+} ions with mixed valence states are of interest as cathode materials in rechargeable batteries because of their good energy density and capacitance [23. In addition, they exhibit good thermoluminescent intensities under gamma irradiation[24,25]. Potential elastic, thermoluminescent, and photoelectric functions can be achieved by improving solid-state glass materials with transition (or) rare earth metals dopants [26,27]. Thus, in the present study, NiO and CaO functional alumina silicate glasses were synthesized, and we assessed their suitability for gamma irradiation, thermoluminescent, and photo-electronic applications. Due to the need to develop mechanically flexible, thermoluminescent, and photoluminescent materials for thermoluminescent and photoelectronic applications, we prepared solid-state glass materials with a chemical composition of $Ca_{(10-x)}Al_{30}Si_{60}Ni_x$ and studied the effects of Ni^{2+} ions on their structural, mechanical, spectroscopic, and irradiative thermoluminescence properties.

2. Experimental methods

Samples with the formula $Ca_{(10-x)}Al_{30}Si_{60}Ni_x$, where $0.0 = x \leq 1.0$ (step size = 0.2 mol%), were synthesized using the melt quenching technique. Based on this composition, the test samples were designated as Ni-0.0, Ni-0.2, Ni-0.4, Ni-0.6, Ni-0.8, and Ni-1.0. Pure analytical reagent grade (99.9%) chemicals comprising NiO, CaO, Al_2O_3, and SiO_2 were ground in an agate mortar before use, and the required mixture (mol%) was placed in a crucible with a volume of 25 mL to prepare the glass. The furnace operated at a temperature up to 1485 °C. Each finely ground test sample was heated for 30 min in the crucible and efforts were made to avoid contamination in the furnace. Finally, the melt obtained was allowed to cool in a brass cast to yield the test glass.

The test glass was then annealed at 500 °C in another furnace. The test samples were prepared with appropriate dimensions

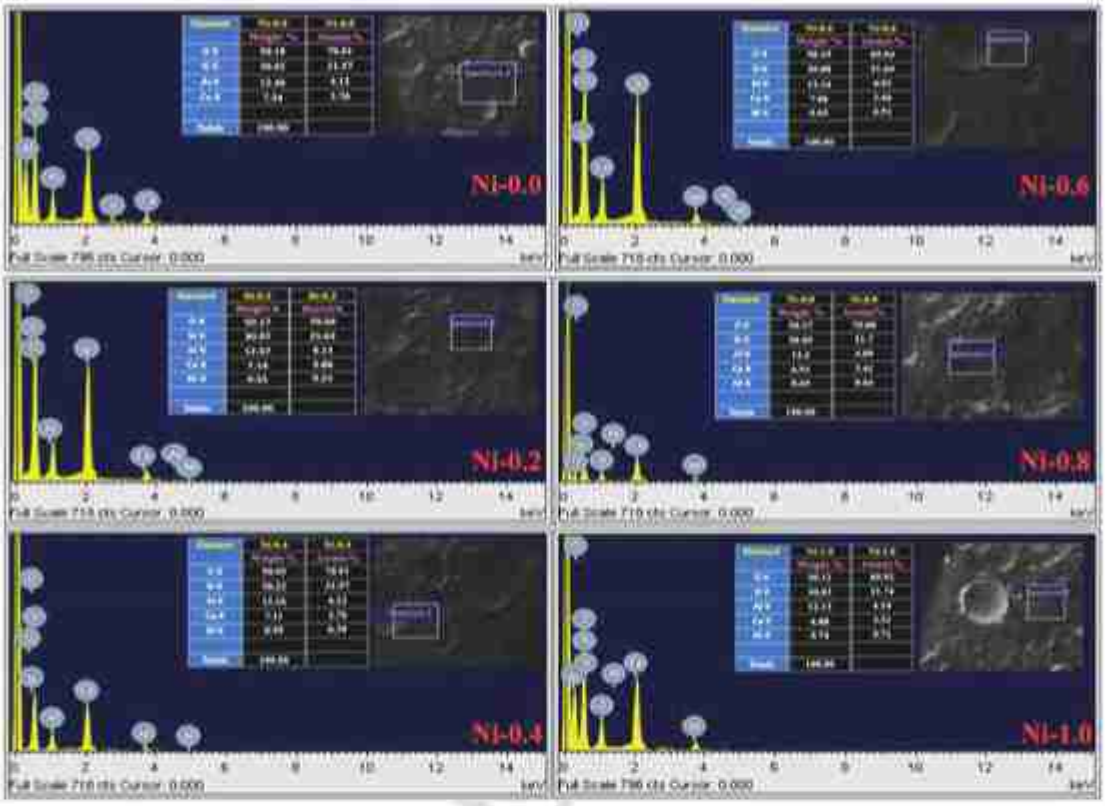

Fig. 3. Chemical analysis of $Ca_{10-x}Al_{30}Si_{60}Ni_x$ glasses recorded at room temperature.

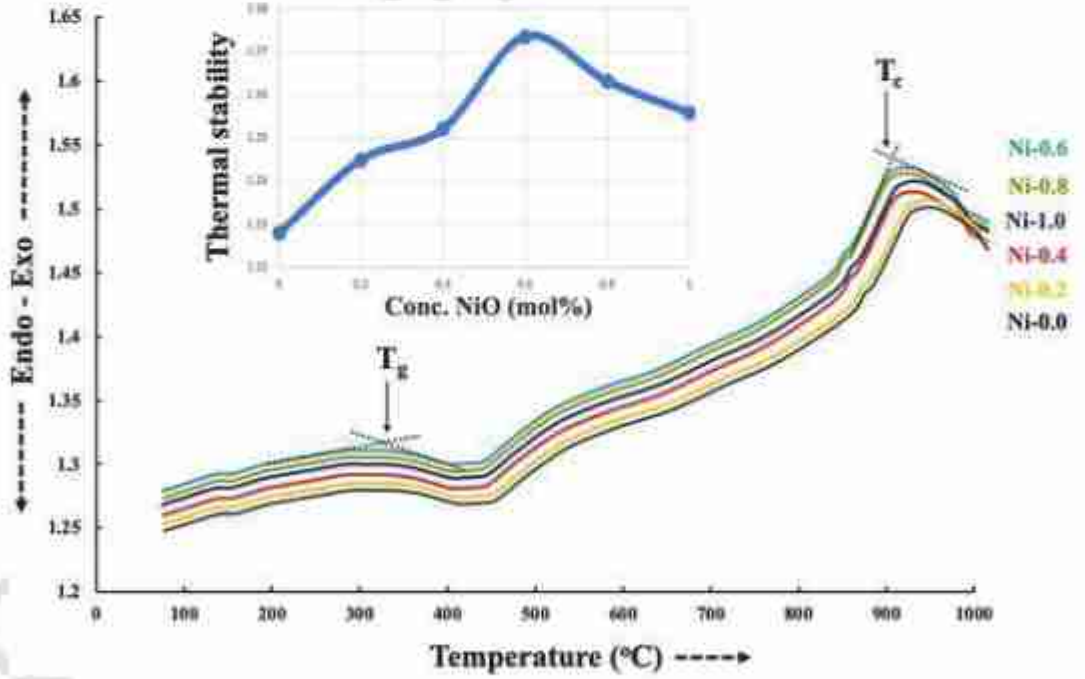

Fig. 4. DTA thermograms of $Ca_{10-x}Al_{30}Si_{60}Ni_x$ glasses, where 'x' varies 0–1 mol% with a step size of 0.2 mol%. Inset (a) shows the variation in thermal stability with increasing concentration of NiO. The temperatures are taken up to an accuracy of ± 1 °C.

(length = 1 cm, width = 1 cm, thickness = 0.2 cm) and used for spectroscopic and DC conductivity analyses. The finely ground powdered test samples were used for X-ray diffraction (XRD), surface morphology, energy dispersion spectra, differential thermal analysis (DTA), Fourier transform-infrared (FT-IR), photoluminescence, and thermoluminescence analyses. Samples with a length of 2 cm, width of 2 cm, and thickness of 1 cm were used for ultrasonic longitudinal velocity measurements. Cylindrical test samples with a length of 2 cm and radius of 1 cm were used for ultrasonic shear velocity measurements.

A Scaletec weighing balance (range = 0.0001–250 g, and precision = 10^{-4} g) was used to record the mass of each test sample. A Shimadzu XRD-7000 (diffraction angle range = 10°–80°, and precision = 0.1°) was used to record XRD patterns for the test samples. A Hi-

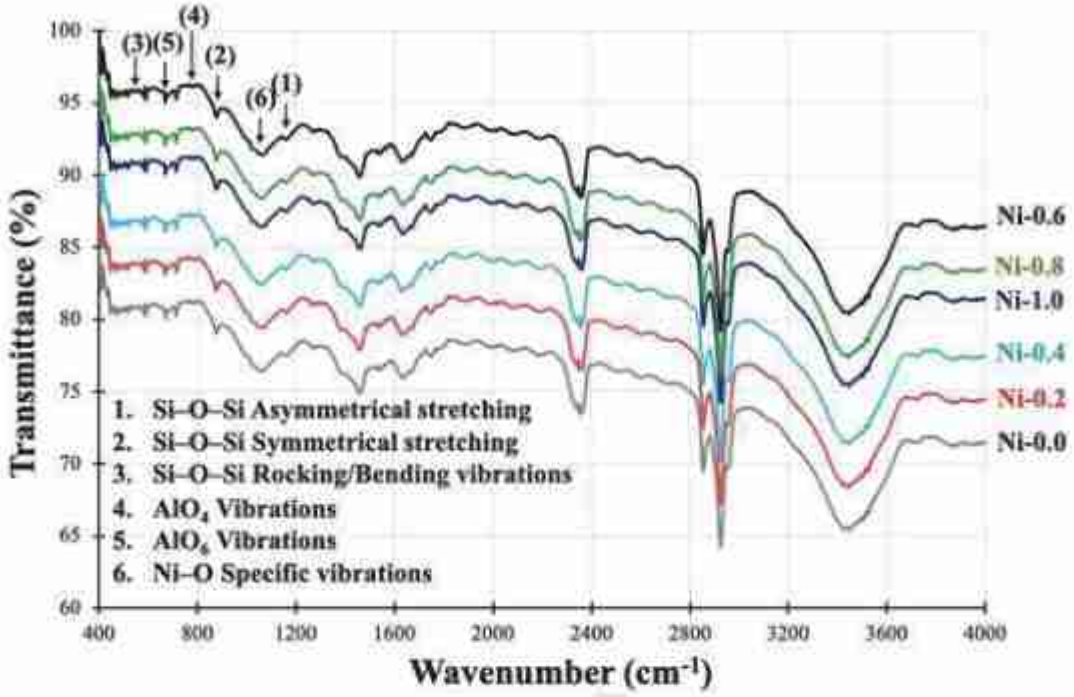

Fig. 5. FT-IR spectra of $Ca_{35-x}Al_{30}Si_{40}Ni_x$ glasses recorded at room temperature with in the wave number range of 400–1400 cm^{-1}. The wave number are taken up to an accuracy of ±1 cm^{-1}. The lines drawn background of the image only for guiding better the eye view.

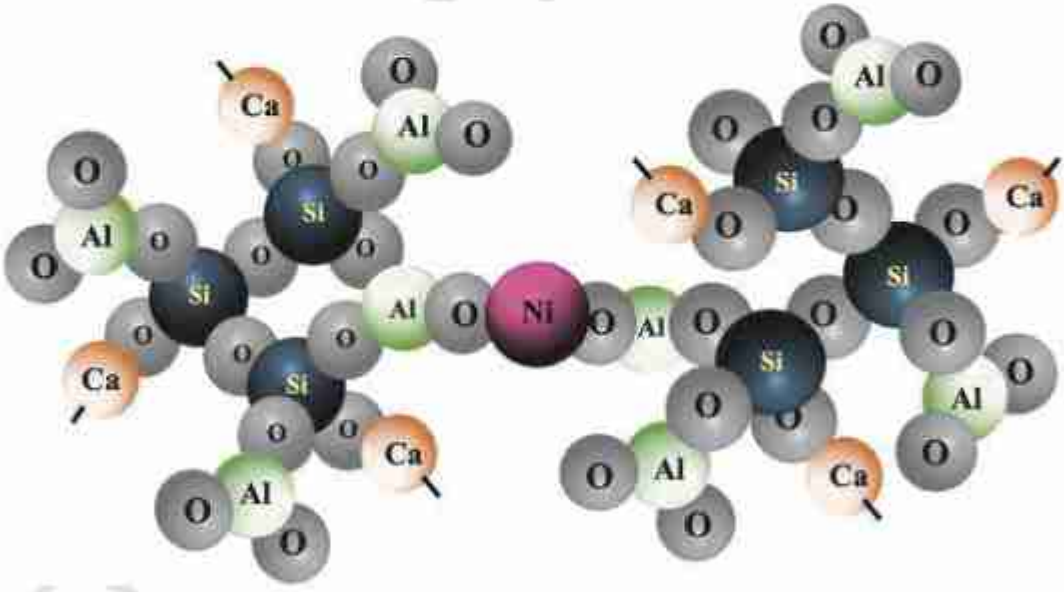

Fig. 6. Proposed lattice of the $Ca_{35-x}Al_{30}Si_{40}Ni_x$ glasses. Mac based Chem Draw Ultra version 12.0 was used to plot the figure.

tachi S–3700 N (range = 1 nm to 500 μm, and precision = 0.1 nm) was used to record the surface morphology and chemical properties of the test samples. A Hitachi-DTG-60-H thermal analyzer (range = 30 °C–1000 °C, and precision = 0.1 °C) was utilized to obtain DTA thermograms for the test samples. A Shimadzu 8400 S FT-IR (range = 400 cm^{-1} to 4000 cm^{-1}, and precision = 1 cm^{-1}) spectrometer was used for FT-IR analysis. A WT-311D flaw detector (range = 0–10^4 m s^{-1}, and precision = 1 m s^{-1}) was used to record the ultrasonic velocities of samples in order to calculate their elastic properties. A Keithley 6514 electrometer (range = 30 °C–300 °C, potential = 2 V, and precision = 1 °C m s^{-1}) was used to obtain DC conductivity measurements. A Nucleonix TL/OSL reader (temperature range = 30 °C–550 °C, and precision = 0.1 °C) and caesium-137 radionuclides (range = 0–75 kGy, and precision = 0.1 kGy) were used to determine the thermoluminescence properties of the test samples. A V670 UV–Vis–NIR spectrometer (range = 200–2200 nm, and precision = 0.1 nm) was used to record optical absorption spectra for the test samples. A JASCO FP 6300 spectrometer (range = 200–900 nm, and precision = 0.1 nm) was used to obtain photoluminescence spectra for the test samples. MAC Office 2021, ChemDraw ultra 12.0, and Matlab 2.3 software were used to analyze the test results.

Table 1
Summary on structure, elasticity and luminescence properties of the $Ca_{(10-x)}Al_{30}Si_{60}Ni_x$ glasses, where 'x' varies 0–1 mol% with a step size of 0.2 mol%.

Glass	Ni-0.0	Ni-0.2	Ni-0.4	Ni-0.6	Ni-0.8	Ni-1.0
Structure, and Elasticity						
Density (gm/cm³)	2.689	2.787	2.834	3.1951	3.01	2.9151
Ionic radius (Å)	....	12.7	10.0	8.44	7.83	7.34
Polaron radius (Å)	....	5.18	4.06	3.40	3.15	2.96
Molar volume (x 10^{24} cm³ mol⁻¹)	27.026	26.09	25.67	22.78	24.19	24.99
Field strength (x 10^{16} cm⁻²)	....	3.79	6.0	8.63	10.0	11.4
Oxygen Packing Density	94.11	94.26	94.42	94.57	94.72	94.87
Optical Basicity	7.72	7.7162	7.7164	7.7146	7.7128	7.695
Refractive index	1.655	1.665	1.671	1.692	1.686	1.678
Glass transition temp. (°C)	551	547	545	540	542	544
Forming ability (%)	1.2279	1.2449	1.2521	1.2735	1.2631	1.2559
Young's modulus (GPa)	26.175	27.71	28.49	32.90	30.74	29.52
Shear modulus (GPa)	12.06	12.69	13.09	15.45	14.37	13.75
Bulk modulus (GPa)	27.17	28.32	28.99	33.21	31.07	29.86
Poison Ratio (GPa)	0.1009	0.0969	0.0953	0.0650	0.0696	0.0733
Micro-hardness (GPa)	3.209	3.371	3.592	4.490	4.121	3.911
DC Conductivity (x 10^{-6}, ohm⁻¹ cm⁻¹)	0.7551	0.891	1.117	1.956	1.751	
Avg. A.E. (eV)		0.721	0.551	0.432	0.364	0.426
Thermoluminiescence, under 30 kGy gamma Irradiation						
Peak Temperature Max (K)		438	436	428	430	433
Frequency factor (x 10^{12}, S^{-1})		2.379	2.491	2.717	2.661	2.574
Shape Symmetry		438	436	428	430	433
A.E. E_a (eV)		1.255	1.183	0.797	0.856	0.93
Optical Absorption, and Photoluminescence						
Band edge		283	286	293	296	305
Indirect optical band gap (eV)		2.2	2.11	1.6	1.5	1.92
Direct optical band gap (eV)		3.72	3.75	3.49	3.58	3.63
Crystal field separation energy (D_q) (cm^{-1})		764	767	779	776	773
Racah parameter (B) (cm^{-1})		851.7	854	865.8	861.2	856.1
nephelauxetic ratio (β)		0.715	0.727	0.799	0.774	0.742
Emission transitions (nm) $^2T_1(P) \rightarrow {}^3A_2(F)$, and $^2T_1(P) \rightarrow {}^3T_1(F)$		582	584	591	589	587
		680	683	692	696	694
Transition probability (x 10^{24}) $^2T_1(P) \rightarrow {}^3A_2(F)$ and $^2T_1(P) \rightarrow {}^3T_1(F)$		1.57	1.68	1.85	1.77	1.69
		0.991	0.919	0.975	0.963	0.944
Emission cross section (x 10^2, cm^2) $^2T_1(P) \rightarrow {}^3A_2(F)$, and $^2T_1(P) \rightarrow {}^3T_1(F)$		0.919	0.824	0.869	0.845	0.839
		1.13	1.16	1.34	1.25	1.21

3. Results and discussion

3.1. Structure

Fig. 1 shows images of the $Ca_{(10-x)}Al_{30}Si_{60}Ni_x$ glasses (where $0.0 = x \leq 1.0$, step size = 0.2 mol%). Fig. 2 shows the XRD spectra obtained for the $Ca_{(10-x)}Al_{30}Si_{60}Ni_x$ glasses. The results indicated no crystallinity and sharp peaks, thereby demonstrating the glassy behavior of the samples. Fig. 3 shows the chemical properties of the $Ca_{(10-x)}Al_{30}Si_{60}Ni_x$ glasses, with different Al, Ni, Si, O, and Ca compositions in terms of the atomic weight (%). Analysis of the physical properties showed that Ni-0.6 had the best physical properties of all the glasses examined. Fig. 4 shows the DTA spectra obtained for the $Ca_{(10-x)}Al_{30}Si_{60}Ni_x$ glasses. The glass transition (T_g), and crystallization (T_c) temperature positions were identified based on the spectra. The thermal stabilities of the glasses were calculated based on the glass transition (T_g), and crystallization (T_c) temperatures. The thermal stabilities of the glasses are shown in the inset in Fig. 4. The results demonstrated that the glass with a NiO concentration of 0.6 mol% had the highest thermal stability. All of the changes in the exothermic and endothermic thermograms were due to enthalpy changes in the $Ca_{(10-x)}Al_{30}Si_{60}Ni_x$ glasses [28,29]. Structural characterization based on XRD, morphological, chemical, and thermal analyses demonstrated the glassy behavior of the samples. Fig. 5 shows the FT-IR spectra obtained for the $Ca_{(10-x)}Al_{30}Si_{60}Ni_x$ glasses. The spectra were resolved into the following bands due to silicate, aluminum, and nickel units in different wavenumber regions [30–36]: Si–O–Si asymmetrical stretching (~1025–1043 cm^{-1}), Si–O–Si symmetrical stretching (~843–858 cm^{-1}), Si–O–Si rocking/bending vibrations (~474–462 cm^{-1}), Al–O linkages (~640–645 cm^{-1}), and Ni–O–Ni specific stretching vibrations (~534–539 cm^{-1}). Among the $Ca_{(10-x)}Al_{30}Si_{60}Ni_x$ glasses, the glass with a NiO concentration of 0.6% exhibited the highest shifts in the wavenumber positions for the silicate, aluminum, calcium, and nickel structural units. SiO_2 is a regular class glass former that is widely available in amorphous form, and pure class form silica is observed in nature as quartz. The tetrahedrons in the geometry of SiO_2 are interconnected with mutually shared corners. Adding Al_2O_3 to SiO_2 optical glasses improves the hardness, refractive index, and density. It can also improve the thermoelectric and piezoelectric characteristics of SiO_2 glasses. SiO_2 glass phosphors, conductive ceramics, and dielectrics containing Al_2O_3 are valuable photoelectronic materials. The addition of CaO provides highly active Ca^{2+} ions, which improve Ca–O–Ca linkages by breaking Si–O–Si and Al–O–Si linkages, thereby increasing the number of non-bridging oxygens within the glass network. Fig. 6 shows the probable structural changes in the calcium aluminum silicate glasses after the addition of NiO. The addition of NiO provided active Ni^{2+} ions in the silicate glass network to produce Ni–O–Si linkages, which further influenced Si^{4+}, Al^{3+}, and Ca^{2+} ions within the glass network to increase the number of non-bridging oxygens. XRD analysis indicated the amorphous nature of the glasses, which was also supported by the surface morphology and DTA results. Chemical analysis indicated the presence of all chemicals at the appropriate weight percentages selected for synthesis. FT-IR analysis indicated the presence of various bonds, such as Si–O–Si asymmetrical stretching (~1025–1043 cm^{-1}), Si–O–Si symmetrical stretching (~843–858 cm^{-1}), Si–O–Si bending (~474–462 cm^{-1}), Al–O (~645 cm^{-1}) distorted octahedral, and Ni–O–Ni specific stretching (~534–539 cm^{-1}) vibrational units. Among the $Ca_{(10-x)}Al_{30}Si_{60}Ni_x$ glasses, the glass with a NiO concentration of 0.6% exhibited the highest shifts in the wavenumber positions for the silicate, aluminum, calcium, and nickel structural units due to the steady inter-ionic forces between Ni^{2+} ions and Si^{4+}, Al^{3+}, and Ca^{2+} ions. Uncertainties in the magnitudes of the interstitial holes and dissimilarity in the coordination of Ni^{2+} ions with Si^{4+}, Al^{3+}, and Ca^{2+} ions explained the variations in the density, molar volume, field strength, refractive index, and polarizability of the different $Ca_{(10-x)}Al_{30}Si_{60}Ni_x$ glasses. The steady inter-ionic forces between Ni^{2+} ions and Si^{4+}, Al^{3+}, and Ca^{2+} ions led to the thermal stability of the materials, with the highest thermal stability for the glass with a NiO concentration of 0.6%. Change in enthalpy within the glass network explained the differences in the peak intensities in the DTA thermograms.

3.2. Physical and elastic properties

Archimedes' equation was used to estimate the densities of the samples, and the following equations were used to evaluate the physical and elastic properties of the glasses. The following mathematical equations were used to calculate all of the parameters [37–40]. The glass with a NiO concentration of 0.6 mol% had the best mechanical properties among the glasses.

$$\text{Density of a glass (D)} = \{(S_a)/(S_a - S_b)\} \times D_{ortho} \quad (1)$$

where S_a - weight of a glass measured in air;
S_b - weight of glass measured in liquid ortho-xylene;
D_{ortho} - density of ortho-xylene.

The following equations were used to evaluate all of the physical properties of the glasses.

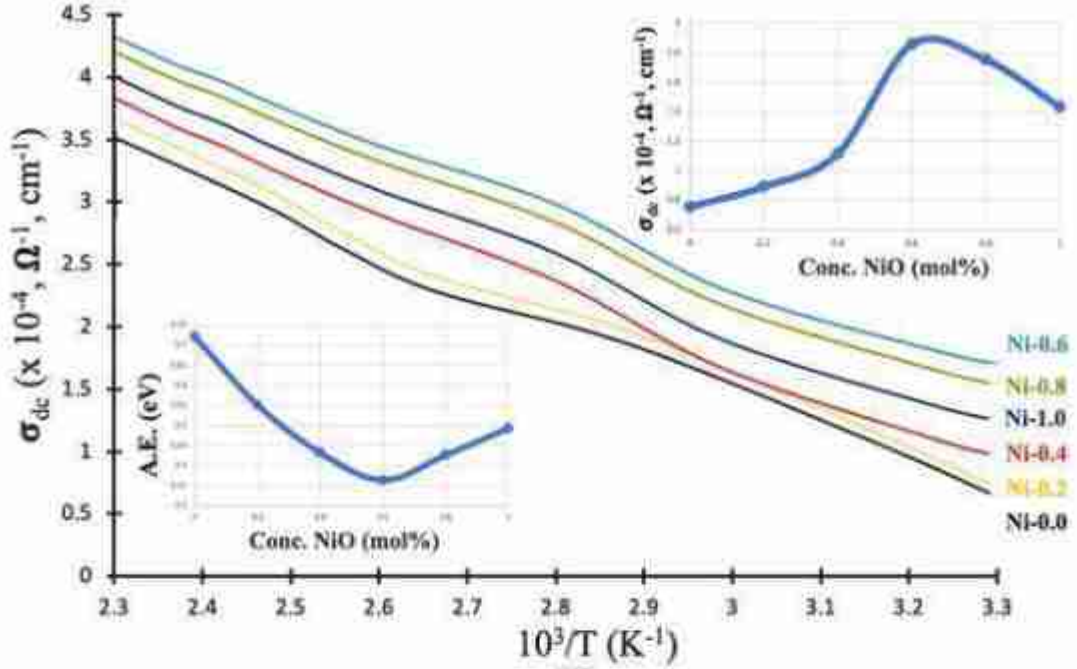

Fig. 7. Variation of DC Conductivity with 1/T for $Ca_{(10-x)}Al_{30}Si_{60}Ni_x$ glasses, where 'x' varies 0–1 mol% with a step size of 0.2 mol%. The inset 8(a) represents variation in activation energy with concentration, and inset 8(b) variation in DC conductivity with concentration of NiO. The temperatures are taken up to an accuracy of ± 1 °C.

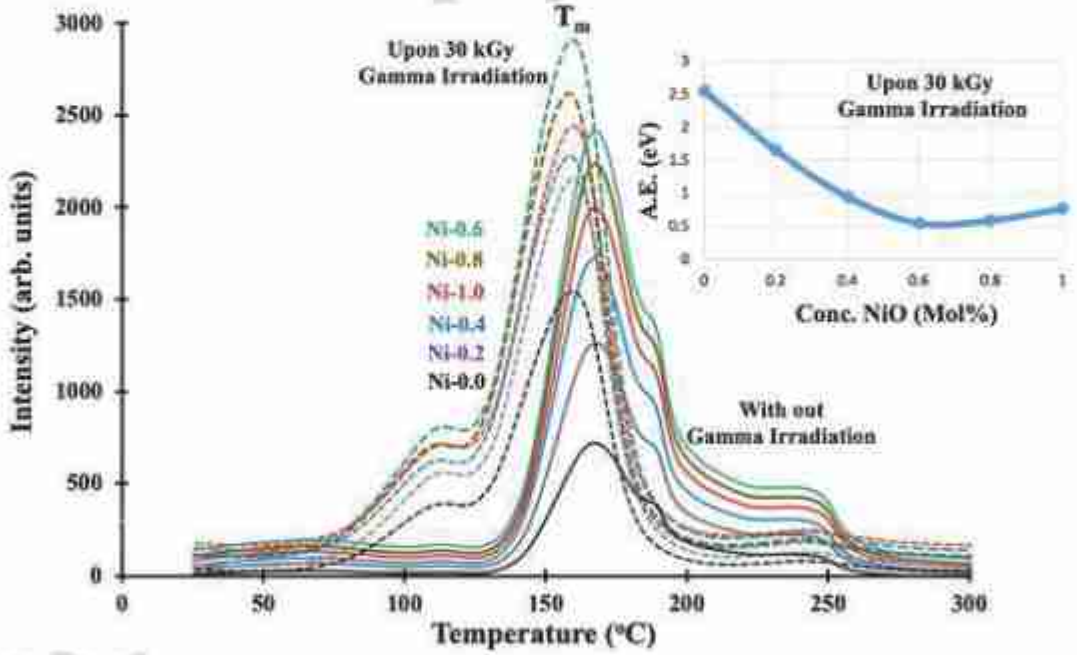

Fig. 8. Thermoluminiscence analysis of $Ca_{(10-x)}Al_{30}Si_{60}Ni_x$ glasses, where 'x' varies 0 -1 mol% with a step size of 0.2 mol%. The temperatures are taken up to an accuracy of ± 0.1 °C. Inset of the figure represents variation in A.E. with increasing NiO concentration.

Molar volume (V_m) = M/D (2)

Ion concentration (N_i) = $N_A C(\rho)/M_w$ (3)

Ionic radius (R_i) = $1/(N_i)^{1/3}$ (4)

Polaron radius (R_p) = $1/2\ \{\pi/(6\ N_i)\}^{1/3}$ (5)

Field strength (F_i) = (Z/R^2_p) (6)

Electronegativity (χ_{th}) = $\Sigma_k A^k B^k$ (7)

Optical basicity (Λ_{th}) = $\chi_{th}/(\chi_{th}-1.36)$ (8)

Oxygen packing density = $[(1000 \times Z)/(V_m)]$ (9)

where M_w - weight of a glass measured in air; Z - atomic number;
A^k - concentration of oxide compounds; B^k - Pauling electronegativity of oxide compounds;

Longitudinal elastic coefficient (L) = $D(Z_p)^2$ (10)

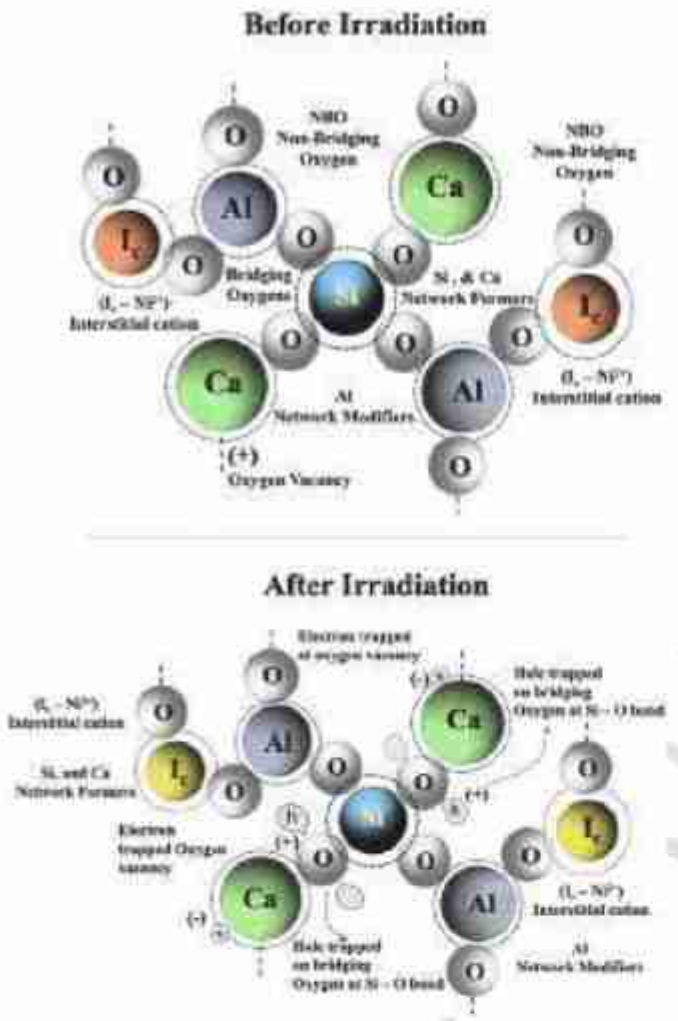

Fig. 9. Thermoluminiscence defect centers with and without irradiation of $Ca_{(10-x)}Al_{20}Si_{60}Ni_x$ glasses, where 'x' varies 0.1 mol% with a step size of 0.2 mol%.

$$\text{Shear modulus (B)} = D(Z_y)^2 \quad (11)$$

$$\text{Bulk modulus (C)} = L - (4/3B) \quad (12)$$

$$\text{Young's modulus (A)} = 2(1 + P)B \quad (13)$$

$$\text{Poisson's ratio (P)} = \tfrac{1}{2}[(L - 2B)/(L - B)] \quad (14)$$

$$\text{Elastic microhardness} = (A/6)[(1-2P)/(1 + P)] \quad (15)$$

where Z_X – longitudinal velocity, and Z_y – shear velocity.

The mechanical properties calculated for the $Ca_{(10-x)}Al_{20}Si_{60}Ni_x$ glasses are presented in Table 1. All of the glasses considered exhibited extreme elastic behavior. The elastic moduli of the glass materials were interdependent of intermolecular control. In some glass (or) glass-ceramic materials, the elastic modulus can be improved in a predictable manner according to the molecular density. Replacement of Ca^{2+} ions by divalent Ni^{2+} ions within the materials led to great variations in the elastic moduli (bulk, shear, and Young's moduli). Furthermore, the high degree of covalent bonding in the glass with a NiO concentration of 0.6 mol% increased the atomic density and variations in interstitial defects, which could explain the increases in the bulk, shear, and Young's moduli [41–43]. The microhardness of the glasses was related to their covalently interlinked structures.

3.3. DC conductivity properties

Fig. 7 shows the variations in the DC conductivity as the temperature increased, where the relationship was almost linear. Fig. 7(a) and (b) show the variations in the DC conductivity and activation energy as the concentration of added NiO increased. The DC conductivity increased as the added NiO concentration increased up to 0.6 mol%. By contrast, the activation energy decreased as the added NiO concentration increased to 0.6 mol% [44,45]. The DC conductivity measurements showed that the best results were obtained for the glass with an added NiO concentration of 0.6 mol%. The linear relationship between the DC conductivity and the increase in the temperature for the $Ca_{(10-x)}Al_{20}Si_{60}Ni_x$ materials indicated the linear thermal excitement of charge carrier movements for conduction [46,47]. The decrease in the activation energy as the DC conductivity increased up to an added NiO concentration 0.6 mol% suggested a higher rate of polaron hopping and ionic transport phenomenon within the $Ca_{(10-x)}Al_{20}Si_{60}Ni_x$ materials. Mixed ionic and electronic conduction effects increased the DC conductivity and decreased the activation energy up to an added NiO concentration of 0.6 mol%, but the DC conductivity decreased and the activation energy decreased above this concentration. These findings suggest the occurrence of dissimilar conduction phenomena above and below this added NiO concentration. These variations in the DC conductivity and activation energy in the $Ca_{(10-x)}Al_{20}Si_{60}Ni_x$ materials were due to the mobility of both Ca^{2+} and Ni^{2+} ions. The larger atomic radius of Ni^{2+} ions, trivalent coordination of aluminum ions, octahedral tendency of Ni^{2+} ions, maximum intermolecular force between the ions, and short range periodic order within the glass with an added NiO concentration of 0.6 mol% explained the enhanced properties.

3.4. Thermoluminescence properties

The thermoluminescence was recorded for the $Ca_{(10-x)}Al_{20}Si_{60}Ni_x$ glasses from room temperature to 300 °C without gamma irradiation and under gamma irradiation for 30 min (~30 kGy), and the results are shown in Fig. 8. In both cases, the luminescence intensity increased as the concentration of added NiO increased and the concentration of CaO decreased in the host glass, i.e., up to 0.6 mol% for NiO and 9.4 mol% for CaO, before the intensity decreased. Thus, Ni-0.6 exhibited the highest thermoluminescence compared with the other test samples. The luminescence plot for each glass sample contained two intensity peaks, with one at a low temperature and another at a high temperature. The intensity peak at a low temperature disappeared rapidly compared with that at a high temperature. The trap depth factors were calculated for the glass samples using the following equations [48,49].

$$E_x = C_x\left(\frac{KT_m^2}{x}\right) - b_x\left(2KT_m\right) \quad (16)$$

$$E_y = C_y\left(\frac{KT_m^2}{y}\right) \quad (17)$$

$$E_z = C_z\left(\frac{KT_m^2}{z}\right) \quad (18)$$

where T_m is the temperature at peak intensity, $T_1 = \frac{Tm}{\sqrt{2}}$ intercept of temperature on the left-hand side of the curve, $T_2 = \frac{Tm}{\sqrt{2}}$ intercept of temperature on the right-hand side of the curve, and K is the Boltzmann constant.

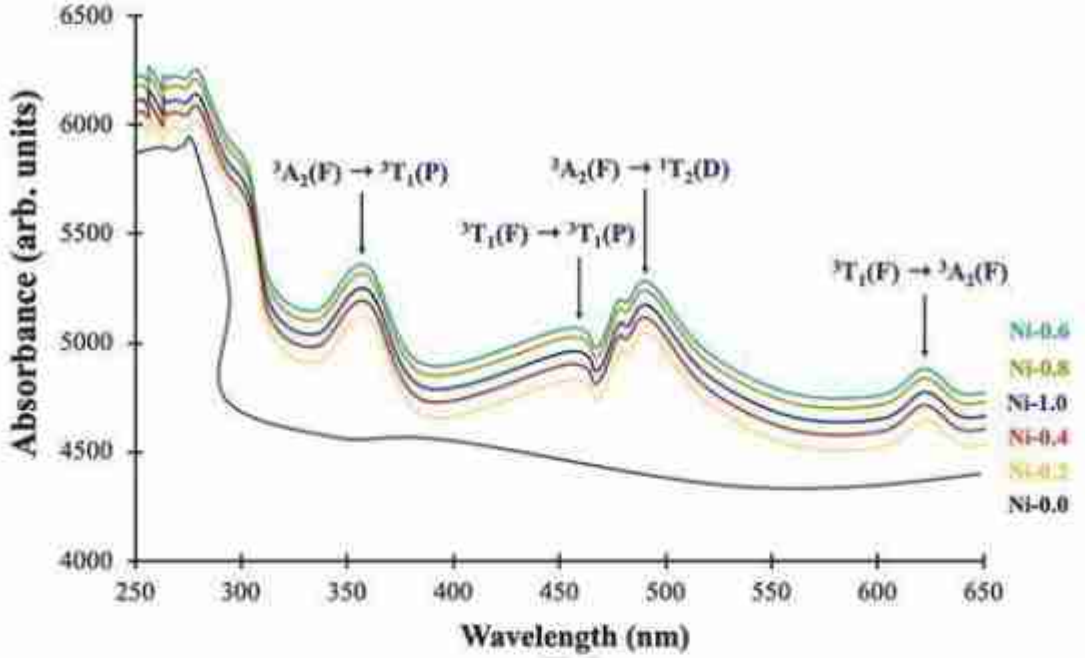

Fig. 10a. Optical absorption spectra of $Ca_{(10-x)}Al_{20}Si_{62}Ni_x$ glasses recorded at room temperature with in the wavelength range of 200–2200 nm range. The wavelengths are taken up to an accuracy of ±0.1 nm.

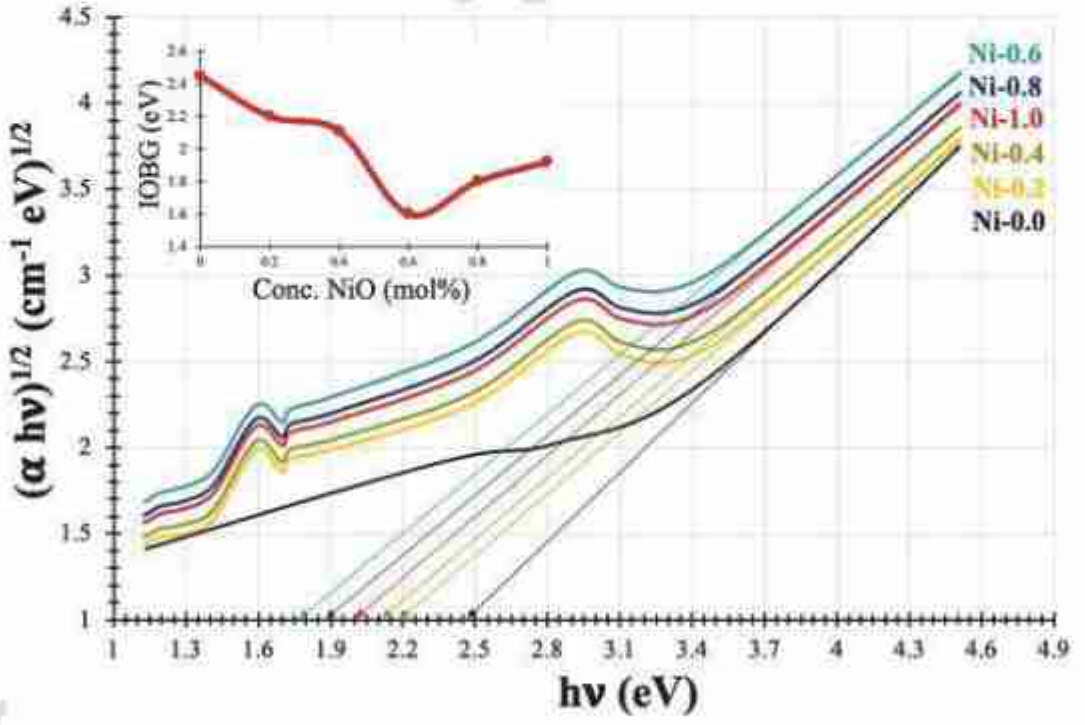

Fig. 10b. Tauc plot – Indirect optical band gap of $Ca_{(10-x)}Al_{20}Si_{62}Ni_x$ glasses, where 'x' varies 0–1 mol% with a step size of 0.2 mol%. Wavelengths are taken up to an accuracy of ±0.1 nm. Inset of the figure represents variation in indirect optical band gap values with NiO increasing concentration.

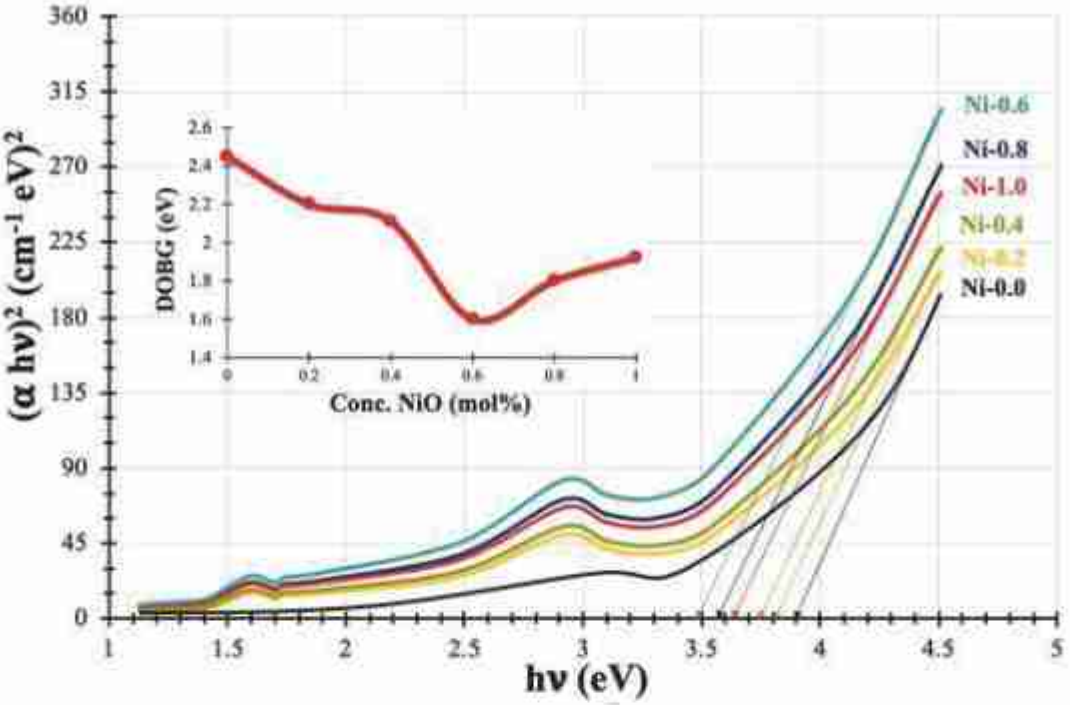

Fig. 10c. Tauc plot of $Ca_{(10-x)}Al_{20}Si_{40}Ni_x$ glasses, where 'x' varies 0–1 mol% with a step size of 0.2 mol%. Wavelengths are taken up to an accuracy of ±0.1 nm. Inset of the figure represents variation in direct optical band gap values with NiO increasing concentration.

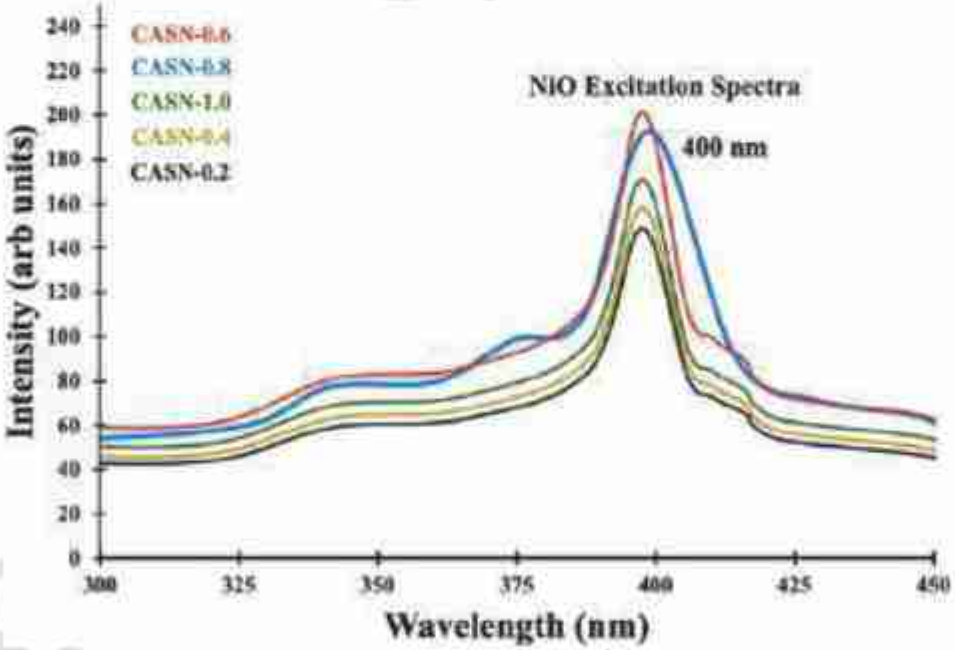

Fig. 11a. Excitation spectra of $Ca_{(10-x)}Al_{20}Si_{40}Ni_x$ glasses, recorded at room temperature. The wavelengths are taken up to an accuracy of ±0.1 nm.

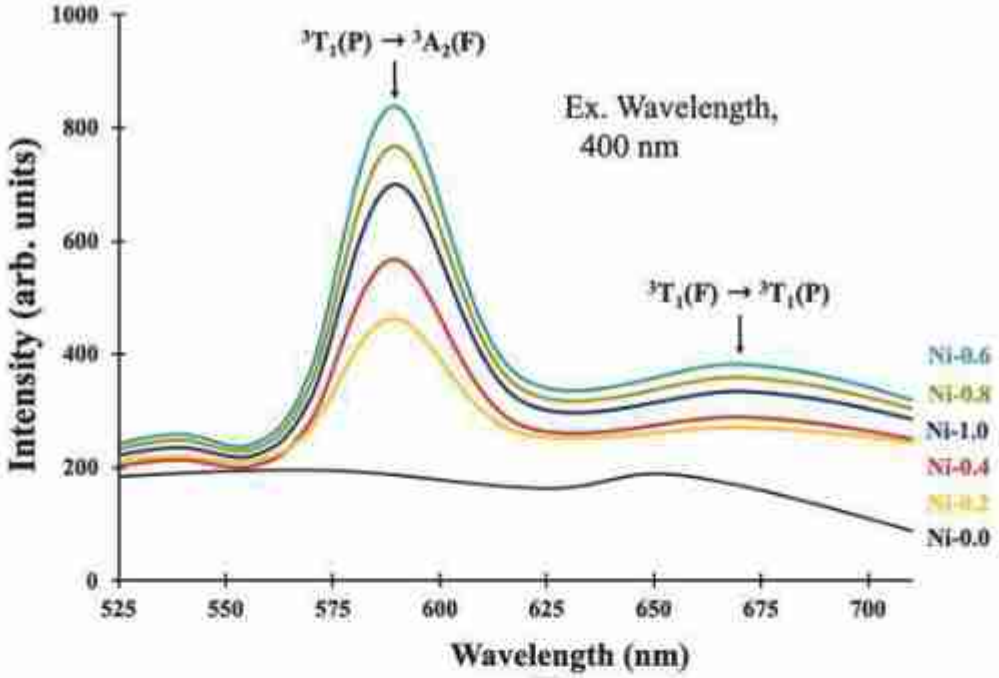

Fig. 11b. Photoluminescence spectra of $Ca_{(10-x)}Al_{30}Si_{60}Ni_x$ glasses, recorded at room temperature with in the wavelength range of 370–800 nm and with an excitation wavelengths of both 400 nm. The wavelengths are taken up to an accuracy of ±0.1 nm.

$x = T_m - T_1, y = T_2 - T_m, z = T_2 - T_1$ and Symmetry ratio (η) $= \frac{y}{z}$,

$C_x = 1.510 + 3(\eta - 0.42)$, $C_y = 0.976 + 7.3(\eta - 0.42)$ and $C_z = 2.52 + 10.2(\eta - 0.42)$, $b_\alpha = 1.58 + 4.2(\eta - 0.42)$

The trap depth factors comprising the activation energies (E_α, E_γ, and E_ω) and shape symmetry ratios without gamma irradiation and under gamma irradiation for 30 min calculated based on the thermoluminescence results indicated that Ni-0.6 obtained the best performance, as shown in Table 1.

In general, Al_2O_3 exhibits (Al/Si)–O tri-clusters. Ca^{2+} ions and octahedral (Al/Si)–O_6 tri-clusters dislocate silicate linkages and induce binding defects. The addition of Al_2O_3 improved the structural defects within the glass network. The application of external heat or thermal energy led to the liberation of electrons, which also increased the activities of Al^{3+}, Si^{4+}, Ca^{2+}, and Ni^{2+} ions within the samples. Irradiation of the surfaces of the sample induced trap centers and the number increased with the irradiation dose. Subsequently, thermal movements within the samples led to electron trapping in the trap centers within the materials [50,51]. The sample with an added concentration of 0.6 NiO mol% exhibited the highest thermoluminescence. The trap centers and the outermost orbital (3d) degeneracy of Ni^{2+} ions led to a lower nephelauxetic ratio, which also increased the thermoluminescence of the samples [52–54]. The thermoluminescent intensities were dependent on the site symmetry of Al^{3+}, Si^{4+}, Ca^{2+}, and Ni^{2+} ions, as well as the order of Ca–O, Al–O, Ni–O, and Si–O bond linkages, and interatomic forces. The octahedral SbO_6 units acted as modifiers and induced bonding defects. The increased number of Al–O–Si, Ca–O–Si, and Ni–O–Si linkages as the NiO concentration increased also led to enhanced thermoluminescent emissions, which induced interstitial and volume defects to cause disorder within the samples. Increasing the added NiO concentration from 0 mol% to 0.6 mol% enhanced the octahedral tendency of the samples, which led to variations in the intensity of the thermoluminescence glow curves. The opposite trend was found in the thermoluminescence above this concentration. The decreased concentration of Ca^{2+} ions within the samples also explained the greater thermoluminescence of the samples. The nephelauxetic effect within the valence orbitals of Ca^{2+} ions enhanced the thermoluminescent emissions. Fig. 9 show the thermoluminescence defect centers before and after irradiation of the glasses. The larger atomic radius of Al^{3+} ions, trivalent coordination of Al^{3+} ions, octahedral tendency of Ni^{2+} ions, maximum intermolecular force between the ions, and short range periodic order within the glasses explained their enhanced properties [55–58].

3.5. Spectroscopic properties

3.5.1. Optical absorption properties

Fig. 10(a) shows the optical absorption properties of the glasses. The optical band gap was determined for the glasses as ~307.5 nm. The glass with an added NiO concentration 0.6 mol% had the highest optical absorption properties among the glasses. The NiO absorption bands for $^3A_2$ (F) → $^3T_1$(P), $^3T_1$ (F) → $^3T_2$(P), $^3A_2$ (F) → $^1T_2$(D), and $^3T_1$ (F) → $^3A_2$(F) were detected around wavelengths of 470, 685, 740, and 1045 nm, respectively [59,60]. Fig. 10(b) and (c) show the indirect and direct Tauc plots calculated for the glasses to identify the bandgap values. The glass with an added NiO concentration of 0.6 mol% had the highest bandgap among all of the glasses. Urbach energy evaluations were also conducted for the glasses [61,62]. Absorption spectra, identifications, and other results for the $Ca_{(10-x)}Al_{30}Si_{60}Ni_x$ glasses are shown in Table 1. Ca^{2+} and Ni^{2+} ions improved the bonding defects and the number of non-bridging oxygens, which could have induced depolymerization within the glass host. Ni^{2+} ions provided donor ions, which overlapped with the excited states of electrons trapped mainly by Ni^{2+} ionic sites, thereby leading to the impurity energy band entering the actual optical bandgap. The absorption edge shifted toward a longer wavelength due to the decrease in the optical bandgap value. When the added NiO concentration exceeded 0.6 mol%, the width of the impurity band decreased and the optical absorption edge shifted to a higher wavelength due to the increase the optical bandgap. Well resolved bands such as $^3A_2$(F) → $^3T_1$(P) and $^3A_2$(F) → $^1T_2$(D) indicated oc-

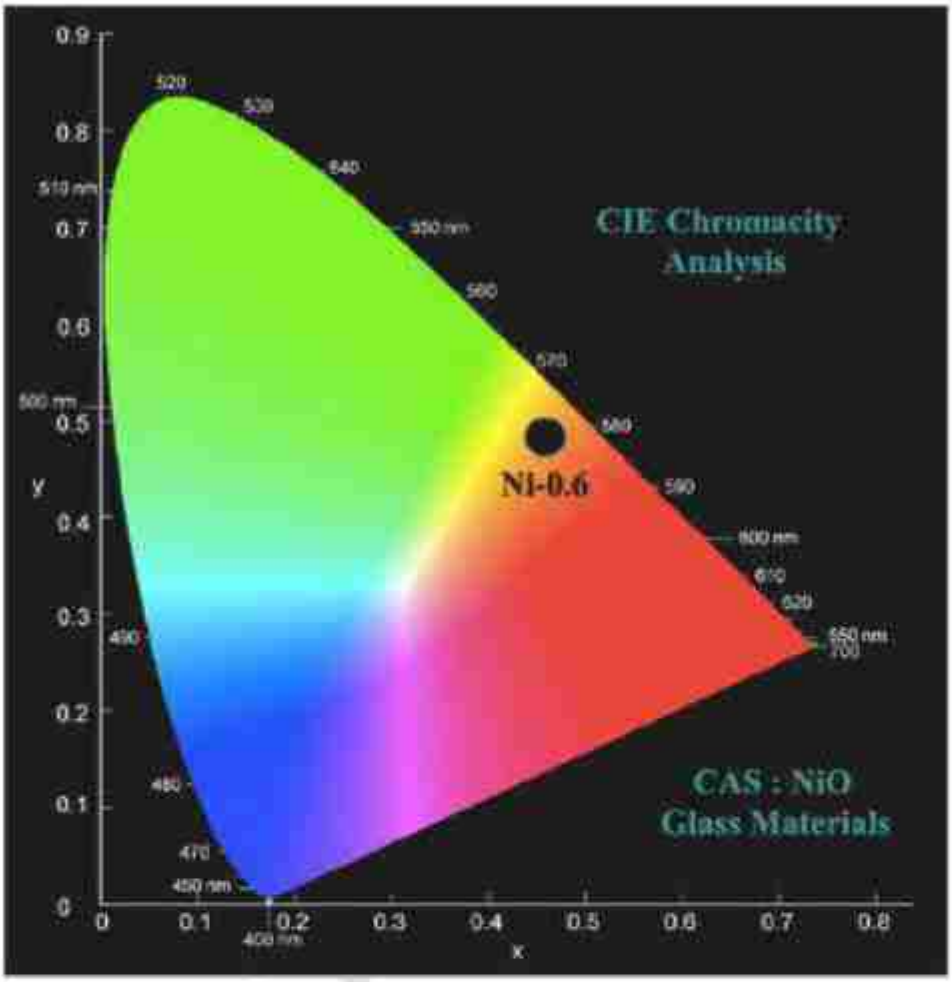

Fig. 12. Chromacity analysis of $Ca_{(10-x)}Al_{30}Si_{60}Ni_x$ glasses, where 'x' varies 0–1 mol% with a step size of 0.2 mol%. The wavelengths are taken up to an accuracy of ±0.1 nm.

tahedral sites, whereas the other spectral bands such as $^3T_1(F) \rightarrow {}^3T_1(P)$ and $^3T_1(F) \rightarrow {}^3A_2(F)$ were due to tetrahedral sites. The optical absorption spectra indicated the presence of Ni^{2+} ions in both octahedral and tetrahedral sites in the $Ca_{(10-x)}Al_{30}Si_{60}Ni_x$ materials. The increase in the intensity of the absorption bands showed that the Ni^{2+} ions mainly occupied octahedral sites, and the less intense bands were related to tetrahedral sites. The results suggest improved ionic environment was due to the covalent nature of the glassy materials, and the best results were obtained for the glass with an added NiO concentration of 0.6 mol%.

In the $Ca_{(10-x)}Al_{30}Si_{60}Ni_x$ materials, Ni^{2+} ions mainly occupied tetrahedral sites with NiO_4 structural units in the glass network as well as octahedral sites, but the number of occupied octahedral sites was less than that of tetrahedral sites. The bandgap values for the glass materials decreased up to an added NiO concentration of 0.6 mol%. Unsteady interionic forces between Al^{3+} ions and Ni^{2+} ions led to depolymerization within the glassy network, which further induced additional bonding defects and natural bond orbitals. Enlargement of ionized donors influenced the overlapped conduction states, including electrons trapped mainly within Ni^{2+} ions and 3d orbitals to decrease the optical bandgap [63,64]. The absorption edges of the glasses shifted as the added NiO concentration increased due to uncertain interionic forces between Al^{3+} and Ni^{2+} ions within the glass host. However, the decrease in the width of the impurity band above 0.6 mol% NiO led to an increase in the bandgap value.

3.5.2. Excitation spectra and photoluminescence

Fig. 11(a) shows the excitation spectra obtained for the $Ca_{(10-x)}Al_{30}Si_{60}Ni_x$ glasses. Fig. 11(b) shows the photoluminescence spectra for the $Ca_{(10-x)}Al_{30}Si_{60}Ni_x$ glasses. Luminescence parameters comprising the stimulated emission cross section and transition probability analogous to the emissive bands of $^3T_1(P) \rightarrow {}^3A_2(F)$ and $^3T_1(P) \rightarrow {}^3T_2(F)$ at wavelengths of 565 and 695 nm, respectively [65], were analyzed. The glass with an added NiO concentration of 0.6 mol% had the highest luminescence values. The equations used to determine the luminescence values are as follows:

$$A = [8\nu^2 \times 10^6]/(e)^2 \quad (19)$$

$$\delta = [(\lambda)^4 A] / [8\pi \Delta\lambda\, c\, (\mu)^2] \quad (20)$$

where λ-wavelength; Δλ - peak half width; A-transition probability; μ-refractive index; δ - cross section; ν - frequency; c - velocity of light; and e – electron charge;

The glasses had CIE coordinates of ($X_{0.2}$–0.396, $Y_{0.2}$–0.462) ($X_{0.4}$–0.399, $Y_{0.4}$–0.467) ($X_{0.6}$–0.415, $Y_{0.6}$–0.48), ($X_{0.8}$–0.411, $Y_{0.8}$–0.472), and ($X_{1.0}$–0.415, $Y_{1.0}$–0.469). The color purities of the samples were evaluated using the formula: $([(X - X_i) - (Y - Y_i)]/[(X_d - X_i) - (Y_d - Y_i)])^{1/2}$, where (X, Y), ($X_i$, Y_i), and (X_d, Y_d) are the CIE chromaticity coordinates of the sample, white illumination, and dominant wavelength, respectively. The glass with an added NiO concentration of 0.6 mol% had the highest color purity grade (96.61%). Fig. 12 shows the color chromaticity values for the glass with an added NiO concentration of 0.6 mol%. Chromaticity analysis based on the transitions

comprising $^3T_1(P) \rightarrow {}^3A_2(F)$ and $^3T_1(P) \rightarrow {}^3T_2(F)$ indicated orange emissions, which changed with the NiO concentration. The glass with an added NiO concentration of 0.6 mol% exhibited the highest shift toward the red region among all of the materials. The improved efficiency up to an added NiO concentration of 0.6 mol% was due to the enlarged number of octahedral Ni^{2+} ions within the glasses [66]. Ni^{2+} ions at octahedral sites explained the enhanced luminescence of the materials. The glass with an added NiO concentration of 0.6 mol% had the highest luminescence output and the highest octahedral tendency. The intensities of the luminescence bands for $^3T_1(P) \rightarrow {}^3A_2(F)$ and $^3T_1(P) \rightarrow {}^3T_2(F)$ red shifted as the added NiO concentration increased to 0.6 mol% due to the octahedral tendency. Details of the structure, elasticity, electrical, and luminescence data are presented in Table 1. Blue shifting occurred due to the Ni^{2+} ions when the added NiO concentration exceeded 0.6 mol%. The red shift with an added NiO concentration up to 0.6 mol% was due to the decreased strength of the crystal field stabilization energy around Ni^{2+} octahedral ions, which decreased the separation between ground to excited states. The blue shift above an added NiO concentration of 0.6 mol% was due to the increased strength of the crystal field stabilization energy around Ni^{2+} octahedral ions, which increased the separation between ground to excited states [67]. The probability transition and cross-section values for the emissions by the materials the highest values were obtained for the glass with an added NiO concentration of 0.6 mol% due to the highest interionic balance and resultant forces between Ni^{2+} ions and Ca^{2+}, Al^{3+}, and Si^{4+} ions. The larger atomic radius of Ni^{2+} ions, trivalent coordination of aluminum ions, octahedral tendency of Ni^{2+} ions, maximum intermolecular force between ions, and short range periodic order within the glasses explained their enhanced properties.

4. Conclusion

In this study, we prepared glasses with the chemical compositions of $Ca_{(1-x)}Al_{20}Si_{80}Ni_x$, where $0.0 = x \leq 1.0$ (step size = 0.2 mol%), determined their structural, elastic, thermoluminescence, and photoluminescence properties. The results obtained can be summarized as follows.

- The XRD results indicated the glassy structure of the samples. DTA plots were used to obtain the glass transition values and thermal stabilities of the glasses. The glass with an added NiO concentration of 0.6 mol% had the highest stability value, which indicated the higher order of intermolecular force and density value in this glass. FT-IR spectra were used to investigate the structural vibrational modes in the glasses. The asymmetric band around Si–O–Si involving bridging molecules shifted and the vibration mode of Si–O–Si also shifted as the concentration of NiO increased in the glasses. The FT-IR results demonstrated that NiO entered the calcium aluminosilicate glass network.
- Analyses of the physical properties of the glasses, including the density, molar volume, optical basicity, interionic distance, polaronic radius, refractive index, and optical basicity, suggested that the glass with an added NiO concentration of 0.6 mol% had the best properties due to the higher order intermolecular force and covalent behavior within the glass. The ultrasonic velocities of the glasses were calculated. The calculated microhardness values (~4.48 GPa) demonstrated the high rigidity and elastic strength of the glasses, where the glass with an added NiO concentration of 0.6 mol% had the best results due to the higher order density, interatomic distance, and covalently interlinked structure in the glass.
- The electrical properties of the glasses were determined. The observed DC conductivity of $1.856 \times 10^{-4}\ \Omega^{-1}\ cm^{-1}$ and the activation energy values determined for the glasses suggested that the glass with an added NiO concentration of 0.6 mol% is a valuable electrically conductive glass material. Due to the higher polaronic radius, interstitial defects, and octahedral tendency of Ni^{2+} ions, the glass with an added NiO concentration of 0.6 mol% had the best electrical properties.
- The thermoluminescence under gamma irradiation was investigated for the glasses. The shape symmetry factor value (~0.535) and low activation energies (E_1 = 0.619, eV, E_2 = 0.466 eV, and E_m = 0.568 eV) for the glass with an added NiO concentration of 0.6 mol% according to thermoluminescence analysis indicated that this glass had the best thermoluminescent properties. Due to the higher ionic radius, greater number of trap centers, and octahedral tendency of Ni^{2+} ions, the glass with an added NiO concentration of 0.6 mol% exhibited good thermoluminescence properties.
- Spectroscopic analysis of the glasses determined the optical bandgap (~1.78 eV), transition probability ($\sim 1.85 \times 10^{34}\ S^{-1}$), and cross-section ($\sim 0.869 \times 10^{11}\ cm^2$) corresponding to the transition of $^4T_{2g}(F) \rightarrow {}^4A_{2g}(F)$ for the glass with an added NiO concentration of 0.6 mol%, and thus it is appropriate for photonic applications. Due to the higher refractive index, octahedral tendency of Ni^{2+} ions, and nephelauxetic ratio, the glass with an added NiO concentration of 0.6 mol% exhibited better spectroscopic properties.

Overall, the results obtained in this study suggest that the glass with an added NiO concentration of 0.6 mol% is suitable for thermoluminescence and photoluminescence applications.

Authors contribution statement

- Mr. K. Veerabhadra Rao – methodology, characterization, results, analysis, and report drafting.
- Dr. Ch. Ramesh – helped with the characterization of test samples.
- Dr. S. Shesha Devi - helped with the characterization of test samples.
- Mr. P. Ashok - helped with the results and analysis.
- Dr. Ravi Kumar Guntu – helped with the results, analysis, report correction, and communication.
- Prof. G. Bhikshamaiah – suggestions for improving the paper.
- Prof. B. Appa Rao – report correction and suggestions.

Uncited reference

[24].

Declaration of competing interest

The authors declare that they have no known competing financial interests or personal relationships that could have appeared to influence the work reported in this paper.

Data availability

Data will be made available on request.

Acknowledgments

The corresponding author Dr. RK Guntu thanks Dr. KT Mabee (Secretary, Sree Group of Institutions), Mr. K. Abijith Rao (CEO, Sree Group of Institutions), and Prof. CV Tomy (Director, Sreenidhi Institute of Science and Technology, JNT University, Hyderabad) for continuous moral support during the overall task. The authors thank the Management of Methodist College of Engineering and Technology, ABIDS, Hyderabad – 500 001, Telangana, India for continuous moral support during the overall task.

References

[1] C. Martinet, M. Heili, V. Martinez, G. Kermouche, G. Molnar, N. Shcheblanov, B. Barthel, A. Tanguy, Highlighting the impact of shear strain on the SiO_2 glass structure: from experiments to atomistic simulations, J. Non-Cryst. Solids 533 (2020) https://doi.org/10.1016/j.jnoncrysol.2020.119998, 119998.

[2] M. Picheon, E. Burov, G. Aquilanti, N. Tyoera, V. Montouillout, L. Cormier, Structural evolution of high zirconia aluminosilicate glasses, J. Non-Cryst. Solids 539 (2020) 120050, https://doi.org/10.1016/j.jnoncrysol.2020.120050.

[3] Rehab M. El-Sharkawy, Kh S. Shaaban, Reda Elsaman, Elhassan A. Allam, Atef El-Taher, Mohamed E. Mahmoud, Investigation of mechanical and radiation shielding characteristics of novel glass systems with the composition xNiO-20ZnO-60B2O3-(20-x) CdO based on nanometal oxides, J. Non-Cryst. Solids 528 (2020) https://doi.org/10.1016/j.jnoncrysol.2019.119754, 119754.

[4] A. Venkata Sekhar, L. Pavić, A. Moguš-Milanković, Valluri Ravi Kumar, A. Siva Sesha Reddy, G. Naga Raju, N. Veeraiah, Dielectric dispersion and impedance spectroscopy of NiO doped Li2SO4 MgO P2O5 glass system, J. Alloys Compd. 824 (2020) https://doi.org/10.1016/j.jallcom.2020.153907, 153907.

[5] M.S. Al-Buriahi, A.S. Abouhaswa, H.O. Tekin, C. Srivunkum, P.I. El-Agawany, T. Nutaro, Esra Kavaz, Y.S. Rammah, Structure, optical, gamma-ray and neutron shielding properties of NiO doped B2O3-BaCO3-Li2O3 glass systems, Ceram. Int. 46 (Issue 2) (2020) 1711–1721, https://doi.org/10.1016/j.ceramint.2019.09.144.

[6] O.A. Zamyatin, M.F. Churbanov, J.A. Medvedeva, S.A. Gavrin, E.V. Zamyatina, A.D. Plekhovich, Glass-forming region and optical properties of the TeO2 – ZnO – NiO system, J. Non-Cryst. Solids 479 (2018) 29–41, https://doi.org/10.1016/j.jnoncrysol.2017.10.005.

[7] A. Padmanabham, Y. Gandhi, T. Satyanarayana, N. Veeraiah, Spectroscopic and dielectric properties of crystallized PbO–Sb2O3–Al2O3:NiO glass system, J. Alloys Compd. 488 (Issue 1) (2009) https://doi.org/10.1016/j.jallcom.2009.08.145, 400–408, ISSN 0925-8388.

[8] Botao Wu, Shifeng Zhou, Jinjun Ren, Yanbo Qiao, Danping Chen, Congshan Zhu, Jianrong Qiu, Enhanced luminescence from transparent Ni2+-doped MgO–Al2O3–SiO2 glass ceramics by Ge2O3 addition, J. Phys. Chem. Solid. 69 (Issue 4) (2008) 991–994, https://doi.org/10.1016/j.jpcs.2007.10.001.

[9] Botao Wu, Jianrong Qiu, Mingying Peng, Jinjun Ren, Xiongwei Jiang, Congshan Zhu, Transparent Ni2+-doped ZnO–Al2O3–SiO2 system glass-ceramics with broadband infrared luminescence, Mater. Res. Bull. 42 (Issue 4) (2007) 762–768, https://doi.org/10.1016/j.materresbull.2006.07.012.

[10] Ping Yang, Chun Peng Song, Kai Lü Meng, Jun Chang, Ying Zi Wang, Zhong Xi Yang, Guang Jun Zhou, Xu Dong, Duo Long Yuan, Zi Ping Ai, Defects and photoluminescence of Ni2+ and Mn2+-doped sol–gel SiO2 glass, J. Solid State Chem. 160 (Issue 1) (2001) 272–277, https://doi.org/10.1006/jssc.2001.9245.

[11] Chun Feng Song, Kai Lü Meng, Feng Gu, Su Wen Liu, Shu Fen Wang, Xu Dong, Duo Rong Yuan, Effect of Al3+ on the photoluminescence properties of Ni2+-doped sol–gel SiO2 glass, Inorg. Chem. Commun. 6 (Issue 5) (2003) 523–526, https://doi.org/10.1016/S1387-7003(03)00019-4.

[12] Jingxuan Wang, Siuwen Yu, Qing Guan, Effect of transition metal ions Mn3+, Co2+, Ni2+ on the color of mixed PrVd glasses, J. Non-Cryst. Solids 52 (Issues 1–3) (1992) 447–454 https://doi.org/10.1016/0022-3093(82)90619-2, ISSN 0022-3093.

[13] M. Shibata, M. Ookawa, T. Yokokawa, Studies of NiO dissolved in alkali silicate melts based on redox potential and visible absorption spectra, J. Non-Cryst. Solids 190 (3) (1995) 226–232 https://doi.org/10.1016/0022-3093(95)00250-2, ISSN 0022-3093.

[14] A.S. Grabtchikov, I.A. Khodasevich, N.V. Golubev, E.S. Ignat'eva, V.M. Mashinsky, E.O. Koclova, G.E. Malashkevich, V.N. Sigaev, Optical amplification in Ni2+-doped gallium germanosilicate glass-ceramics, Opt Commun. 491 (2021) 126965, https://doi.org/10.1016/j.optcom.2021.126965.

[15] B. Cochain, L. Cormier, A. Novikova, G. Lelong, S. Selin, X.H. Zhang, In situ local environment and partitioning of Ni2+ ions during crystallization of an oxyfluoride glass, J. Non-Cryst. Solids 405 (2015) https://doi.org/10.1016/j.jnoncrysol.2014.09.051, 7–12, ISSN 0022-3093.

[16] Sarah M. Kamil, AshrafA. Abul-Magd, W. El-Gammal, H.A. Saudi, Enhanced optical and structural features of Ni2+/La3+ hybrid borate glasses, Spectrochim. Acta Mol. Biomol. Spectrosc. 267 (2022) https://doi.org/10.1016/j.saa.2021.120569, Part 2, 120569.

[17] R. Nevgi, Gangadhar Das, M. Aset, K.R. Priolkar, Importance of site occupancy and absence of strain glassy phase in Ni2−xFexMn1.5Sn0.5, J. Alloys Compd. 797 (2019) 995–1001, https://doi.org/10.1016/j.jallcom.2019.05.172.

[18] T. Raghavendra Rao, Ch Rama Krishna, Ch Venkata Reddy, U.S. Udayachandran Thampy, Y.P. Reddy, P.S. Rao, R.V.S.S.N. Ravikumar, Mixed alkali effect and optical properties of Ni2+ doped 20ZnO+xLi2O+(30−x)Na2O+50B2O3 glasses, Spectrochim. Acta Mol. Biomol. Spectrosc. 79 (Issue 5) (2011) 1116–1122, https://doi.org/10.1016/j.saa.2011.04.030.

[19] Sutapa Roy, Dibyendu Ganguli, Optical properties of Ni2+-doped silica and silicate gel monoliths, J. Non-Cryst. Solids 151 (Issue 3) (1992) 205–208, https://doi.org/10.1016/0022-3093(92)90030-N.

[20] Shahriar Iftekhar, Jekabs Grins, Mattias Edén, Composition–property relationships of the La_2O_3–Al_2O_3–SiO_2 glass system, J. Non-Cryst. Solids 356 (20) (2010) 1043–1049, https://doi.org/10.1016/j.jnoncrysol.2010.01.017.

[21] Jianzheng Xie, Minghui Zhang, Rongting Guo, Ying Shi, Xuezhao Liu, Xiufeng Pan, Kun Chen, Weijie Deng, Investigation of optical and thermal properties in Bi^{3+}-doped Ga_2O_3-La_2O_3-Ta_2O_5 glasses fabricated by container less solidification, J. Alloys Compd. 872 (2021) 159651, https://doi.org/10.1016/j.jallcom.2021.159651.

[22] Liliya Vladislavova, Christian Thieme, Tilman Taubeckel, Thomas Hoche, Christian Rüssel, Crystallization of $Ba_{1-x}Sr_xZrSi_2O_7$ from the BaO–SrO/ZnO–SiO_2 glass system: effect of platinum and Sb_2O_3 on nucleation, J. Alloys Compd. 795 (2019) 705–714, https://doi.org/10.1016/j.jallcom.2019.04.034.

[23] En-Lai Zhao, Shi-Xi Zhao, Xia Wu, Jing-Wei Li, Ge-Wen Nan, Guozhong Cao, Lü-Qiang Yu, Electrochemical performance of Li_2O-V_2O_5-SiO_2-B_2O_3 glass as cathode material for lithium ion batteries, J. Materi S 4 (2019) 663–669, https://doi.org/10.1016/j.jmat.2019.05.002.

[24] Sea-Fue Wang, Yung-Fu Hsu, Yueh-Chi Hsieh, Effects of La_2O_3, Nd_2O_3, NiO and CoO additions on the characteristics of SiO_2–Al_2O_3–Y_2O_3–ZnO glass seals for intermediate temperature solid oxide fuel cells, Int. J. Hydrogen Energy 40 (8) (2015) 3338–3347, https://doi.org/10.1016/j.ijhydene.2015.01.045.

[25] B. Suresh, M. Srinivasa Reddy, A. Siva Sesha Reddy, Y. Gandhi, V. Ravi Kumar, N. Veeraiah, Spectroscopic features of Ni^{2+} ion in PbO–Bi_2O_3–SiO_2 glass system, Spectrochim. Acta Mol. Biomol. Spectrosc. 141 (2015) 263–271, https://doi.org/10.1016/j.saa.2015.01.052.

[26] Christian Thieme, Christian Rüssel, High thermal expansion of crystallized glasses in the system BaO–ZnO–NiO–SiO2, Ceram. Int. 41 (10) (2015) 13310–13319 https://doi.org/10.1016/j.ceramint.2015.07.114, Part A.

[27] Sea-Fue Wang, Yung-Fu Hsu, Yueh-Chi Hsieh, Effects of La_2O_3, Nd_2O_3, NiO and CoO additions on the characteristics of SiO_2–Al_2O_3–Y_2O_3–ZnO glass seals for intermediate temperature solid oxide fuel cells, Int. J. Hydrogen Energy 40 (8) (2015) 3338–3347, https://doi.org/10.1016/j.ijhydene.2015.01.045.

[28] Padala Ashok, et al., [Sb2O3]x [Al2O3]y – x composite influence on Ho2O3 doped PbO - SiO2 glasses for optical use, Optik 206 (2020) 164567, https://doi.org/10.1016/j.ijleo.2020.164567.

[29] Y. Al-Hadeethi, M.I. Sayyed, J. Kaewkhao, Bahaaudin M. Raffah, Rahma Almalki, R. Rajaramakrishna, Mahmoud A. Hussein, Physical, optical properties and radiation shielding studies of xLa_2O_3–$(100-x)B_2O_3$ glass system, Ceram. Int. 46 4 (2020) 5390–5396, https://doi.org/10.1016/j.ceramint.2019.10.293.

[30] J.L. Amorós, E. Blasco, A. Moreno, N. Marín, C. Feliu, Sinter-crystallisation kinetics of a SiO_2–Al_2O_3–CaO–MgO–SrO glass-ceramic glaze, J. Non-Cryst. Solids 532 (2020) 119900, https://doi.org/10.1016/j.jnoncrysol.2020.119900.

[31] K.V. Rao, M. Madhu, P. Ashok, et al., Radiation Shielding, EPR, and TL Mechanism in Cr_2O_3 Doped $Ba[La]_2SiO_5$ Glass Ceramics, Silicon, 2022. https://link.springer.com/article/10.1007/s12633-022-01751-6.

[32] Bikram Konar, Dong-Geun Kim, In-Ho Jung, Critical thermodynamic optimization of the Li_2O–Al_2O_3–SiO_2 system and its application for the thermodynamic analysis of the glass-ceramics, J. Eur. Ceram. Soc. 36 11 (2016) 3891–3904, https://doi.org/10.1016/j.jeurceramsoc.2016.04.031.

[33] Q.Y. Zhang, W.J. Zhang, W.C. Wang, Z.H. Jiang, Calculation of physical properties of glass via the phase diagram approach, J. Non-Cryst. Solids 457 (2017) 36–43, https://doi.org/10.1016/j.jnoncrysol.2016.11.005.

[34] Ravi Kumar Guntu, V. Venkatramu, Ch Srinivasa Rao, V. Ravi Kumar, Structure, and opto-dielectric investigations of Cu^{2+}-doped calcium bismuth silicate glass ceramics, Opt. Mater. 113 (2021) https://doi.org/10.1016/j.optmat.2021.110876, 110876.

[35] Padala Ashok, et al., Influence of Al^{3+} and Sb^{3+} ions on thermo and photoluminescence properties of Pr_2O_3 doped PbO – SiO_2 glasses for optical use, J. Lumin. 227 (2020) 117473, https://doi.org/10.1016/j.jlumin.2020.117473.

[36] I. Alekseeva, O. Dymshits, M. Tsenter, A. Zhilin, Influence of various alkali and divalent metal oxides on phase transformations in NiO-doped glasses of the Li_2O–Al_2O_3–SiO_2–TiO_2 system, J. Non-Cryst. Solids 357 (2011) 2209–2214, https://doi.org/10.1016/j.jnoncrysol.2010.12.065.

[37] Prathana Imsavin, Surapong Pinyata, Arnon Kraipok, Tawee Tunkasiri, Sukum Eitssayeam, Kamonpan Pengpat, Effects of TiO_2 content and thermal parameters on crystallization kinetics and mechanical properties of phosphate based glass system, Thermochim. Acta (2020) 179699, https://doi.org/10.1016/j.tca.2020.179699.

[38] Jianlei Liu, Lei Han, Zhitwei Luo, Qianning Huang, Xi He, Changwei Lin, Taoyong Liu, Li Cui, Anxian Lu, Non-alkali glass substrate with improved mechanical properties for display devices, J. Non-Cryst. Solids 524 (2019) 119610, https://doi.org/10.1016/j.jnoncrysol.2019.119610.

[39] Zahra Jamili-Shirvan, Mohsen Haddad-Sabzevar, Jalil Vahdati-Khaki, Ke-Fu Yao, Mechanical and thermal properties of identified zones at a Ti-based bulk metallic glass weld spot jointed by friction stir spot welding (FSSW), J. Non-Cryst. Solids 544 (2020) 120188, https://doi.org/10.1016/j.jnoncrysol.2020.120188.

[40] M.S. Al-Buriahi, A.S. Abouhaswa, H.O. Tekin, C. Srivunkum, P.I. El-Agawany, T. Nutaro, Esra Kavaz, Y.S. Rammah, Structure, optical, gamma-ray and neutron shielding properties of NiO doped B_2O_3–BaCO2–Li_2O_3 glass systems, Ceram. Int. 46 2 (2020) 1711–1721, https://doi.org/10.1016/j.ceramint.2019.09.144.

[41] Zhuo-hao Xiao, Xin-yuan Sun, Kun Liu, Wen-yan Luo, Yun-zhi Wang, Min-Hua Luo, Run-Lin Han, Yan Liu, Crystallization behaviors, thermo-physical properties and seal application of Li_2O–ZnO–MgO–SiO_2 glass-ceramics, J. Alloys Compd. 657 (2016) 231–236, https://doi.org/10.1016/j.jallcom.2015.10.106.

[42] Eren Şahiner, TL and OSL dose response and stability properties of various commercially glass samples obtained from Turkey for dosimetric purposes in the UV emission spectral region, Appl. Radiat. Isot. 128 (2017) 68–74, https://doi.org/10.1016/j.apradiso.2017.06.030.

[43] Ravi Kumar Guntu, Nd_2O_3 influenced Al_2O_3 & Sb_2O_3 functional PbO-SiO2 glass materials, 1.06 μm photonic resource, Mater. Sci. Eng., B 262 (2020) https://doi.org/10.1016/j.mseb.2020.114784, 114784.

[44] Christian Thieme, Christian Rüssel, High thermal expansion of crystallized glasses in the system BaO–ZnO–NiO–SiO2, Ceram. Int. 41 (10) (2015) 13310–13319 https://doi.org/10.1016/j.ceramint.2015.07.114, Part A.

[45] I. Alekseeva, O. Dymshits, M. Tsenter, A. Zhilin, Influence of various alkali and divalent metal oxides on phase transformations in NiO-doped glasses of the

Li_2O-Al_2O_3-SiO_2-TiO_2 system, J. Non-Cryst. Solids 357 (2011) 2209–2214, https://doi.org/10.1016/j.jnoncrysol.2010.12.065.

[46] Jianlei Liu, Lei Han, Zhiwei Luo, Qianning Huang, Xi He, Changwei Lin, Taoyong Liu, Li Cai, Anxian Lu, Non-alkali glass substrate with improved mechanical properties for display devices, J. Non-Cryst. Solids 524 (2019) 119610, https://doi.org/10.1016/j.jnoncrysol.2019.119610.

[47] Ravi Kumar Guntu, EPR - TL correlation, in radiation shielding Ba(10-x) MnxLa30Si60 glasses, J. Mol. Struct. 1248 (2021) 131588, https://doi.org/10.1016/j.molstruc.2021.131588.

[48] Yuya Isokawa, Daisuke Nakauchi, Go Okada, Noriaki Kawaguchi, Takayuki Yanagida, Radiation induced luminescence properties of Ce-doped Y_2O_3-Al_2O_3-SiO_2 glass prepared using floating zone furnace, J. Alloys Compd. 792 (2019) 859–864, https://doi.org/10.1016/j.jallcom.2018.12.245.

[49] Y. Al-Hadeethi, M.I. Sayyed, J. Kaewkhao, Bahaaudin M. Raffah, Rahma Almalki, R. Rajaramakrishna, Mahmoud A. Hussein, Physical, optical properties and radiation shielding studies of xLa_2O_3-(100-x)B_2O_3 glass system, Ceram. Int. 46 4 (2020) 5580–5586, https://doi.org/10.1016/j.ceramint.2019.10.293.

[50] J.L. Amorós, E. Blasco, A. Moreno, N. Marín, C. Feliu, Sinter-crystallisation kinetics of a SiO_2-Al_2O_3-CaO-MgO-SrO glass-ceramic glaze, J. Non-Cryst. Solids 532 (2020) 119900, https://doi.org/10.1016/j.jnoncrysol.2020.119900.

[51] Ho Kim Dan, Nguyen Minh Ty, Tran Duy Tap, Ha Xuan Vinh, L.T. Vinh, Qing Jiao, Desheng Zhou, Jianbei Qiu, Effects of Al^{3+}/La^{3+} ratio on the DSC/DTA and luminescence properties of Bi-doped lanthanum aluminosilicate glasses, Infrared Phys. Technol. 105 (2019) 103072, https://doi.org/10.1016/j.infrared.2019.103072.

[52] Zhuo-hao Xiao, Xin-yuan Sun, Kun Liu, Wen-yan Luo, Yun-shi Wang, Min-hua Luo, run-lin han, yan liu, crystallization behaviours, thermo-physical properties and seal application of Li2O–ZnO–MgO–SiO_2 glass-ceramics, J. Alloys Compd. 657 (2016) 231–236, https://doi.org/10.1016/j.jallcom.2015.10.106.

[53] J.M. Stencel, L.E. Makovsky, J.R. Diehl, T.A. Sarkus, A spectroscopic study of the effect of H2O and NiO on the surface structure of NiO-MoO3-Al2O3, J. Catal. 95 (Issue 2) (1985) https://doi.org/10.1016/0021-9517(85)90119-6, 414-422, ISSN 0021-9517.

[54] G. Anil Kumar, Y. Rambabu, K. Sivaram, M. Sreenath Reddy, Ch Srinivasa Rao, V. Venkataramu, V. Ravi Kumar, N. Ch Sriman Narayana Iyengar, Ravi Kumar Guntu*, ZnxCa80-xP70 thermoluminescent bio glass, structure, and elasticity, J. Mech. Behav. Biomed. Mater. 119 (2021) https://doi.org/10.1016/j.jmbbm.2021.104517, 104517.

[55] A. Padmanabham, Y. Gandhi, T. Satyanarayana, N. Veeraiah, Spectroscopic and dielectric properties of crystallized PbO–Sb_2O_3–As_2O_3:NiO glass system, J. Alloys Compd. 488 (Issue 1) (2009) https://doi.org/10.1016/j.jallcom.2009.08.148, 400-408, ISSN 0925-8388.

[56] Venkata Sekhar, L. Pavić, A. Moguš-Milanković, Valluri Ravi Kumar, A. Siva Sesha Reddy, G. Naga Raju, N. Veeraiah, Dielectric dispersion and impedance spectroscopy of NiO doped Li_2SO_4–MgO–P_2O_5 glass system, J. Alloys Compd. 824 (2020) 153907, https://doi.org/10.1016/j.jallcom.2020.153907.

[57] Shams A.M. Issa, G. Susoy, H.O. Tekin, Yasser B. Saddeek, Reda Elsaman, H.H. Somaily, H. Algarni, Atif Mossad Ali, Mechanical, physical and gamma ray shielding properties of xPbO-(50-x) MoO_3–$50V_2O_5$ ($25 \leq x \leq 45$ mol %) glass system, Ceram. Int. 46 12 (2020) 20251–20263, https://doi.org/10.1016/j.ceramint.2020.05.107.

[58] G. Ravi Kumar, M. Kotesvara Rao, T. Srikumar, M.C. Rao, V. Ravi Kumar, N. Veeraiah, Ch Srinivasa Rao, Spectroscopic, dielectric dispersion and dc conductivity studies of Sb_2O_3 doped lithium fluoro borophosphate glasses mixed with small concentrations of NiO, J. Alloys Compd. 752 (2018) 179–190, https://doi.org/10.1016/j.jallcom.2018.04.165.

[59] Ravi Kumar Guntu, Luminescence and dielectric properties of Ni^{2+} ions added to calcio yttria borophosphate glasses for optoelectronic uses, J. Lumin. 209 (2019) 259–266, https://doi.org/10.1016/j.jlumin.2019.01.051.

[60] Y. Gandhi Padmanabham T Satyanarayana, N Veeraiah, Spectroscopic and dielectric properties of crystallized PbO–Sb_2O_3–As_2O_3:NiO glass system, J. Alloys Compd. 488 1 (2009) 400–408, https://doi.org/10.1016/j.jallcom.2009.08.148.

[61] N. Rama Krishna Chand, B.K. Sudhakar, G. Ravikumar, G. Srinivasa Rao, Ch Srinivasa Rao, Influence of manganese ions on elastic and spectroscopic properties of ZnO doped novel calcium fluorophosphate bio active glasses, Phys. Scripta 96 (2021) 125020, https://doi.org/10.1088/1402-4896/abd202.

[62] O.A. Zamyatin, M.F. Churbanov, J.A. Medvedeva, S.A. Gavrin, E.V. Zamyatina, A.D. Plekhovich, Glass-forming region and optical properties of the TeO_2 – ZnO – NiO system, Journal of Non-Crystalline https://doi.org/10.1016/j.jnoncrysol.2017.10.005.

[63] M.S. Al-Buriahi, A.S. Abouhaswa, H.O. Tekin, C. Sriwunkum, F.I. El-Agawany, T. Nutaro, Esra Kavaz, Y.S. Rammah, Structure, optical, gamma-ray and neutron shielding properties of NiO doped B_2O_3–$BaCO_3$–Li_2O_3 glass systems, Ceram. Int. 46 2 (2020) 1711–1721, https://doi.org/10.1016/j.ceramint.2019.09.144.

[64] G. Ravi Kumar, T. Srikumar, G. Murali Krishna, G. Sahaya Baskaran, A. Siva Sesha Reddy, V. Ravi Kumar, Ch Srinivasa Rao, The role of Ni^{2+} ions on structural and spectroscopic properties of Li2O–ZrO2–Y2O3–SiO2 glass system, J. Non-Cryst. Solids 498 (2018) https://doi.org/10.1016/j.jnoncrysol.2018.05.025, 372-379, ISSN 0022-3093.

[65] N. Rama Krishna Chand, B.K. Sudhakar, G. Ravi kumar, V. Gayathri, P. Devika, T. Vennela, G. Srinivasa Rao, Ch Srinivasa Rao, Influence of multi valent states of vanadium ions in ZnO doped novel calcium fluoro phosphate bio glasses, J. Mech. Behav. Biomed. Mater. 131 (2022) https://doi.org/10.1016/j.jmbbm.2022.105230, 105230.

[66] W.C. Wang, R. Zhou, H.Q. Le, Q.Y. Zhang, L. Wondraczek, Ni-doped fluoro sulfates with broad NIR luminescence, J. Lumin. 210 (2019) 457–463, https://doi.org/10.1016/j.jlumin.2019.03.007.

[67] Jian Zheng, Yin Cheng, Ni^{2+}-doped new silicate glass-ceramics for broadband near infrared luminescence, Opt. Mater. 62 (2016) https://doi.org/10.1016/j.optmat.2016.10.007, 641-647, ISSN 0925-3467.

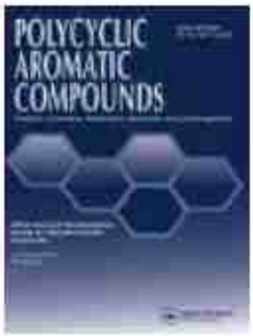

Polycyclic Aromatic Compounds

ISSN: (Print) (Online) Journal homepage: https://www.tandfonline.com/loi/gpol20

Impact of Protonation and Hydrogen Bonding Interactions on the Biological Properties of Antibacterial Compound 4-Dimethylaminopyridinium Salicylate Monohydrate: Correlation with Its Precursor Molecules

J. D. Deephlin Tarika, X. D. Divya Dexlin, A. Rathika, A. Arun kumar, D. Deva Jayanthi & T. Joselin Beaula

To cite this article: J. D. Deephlin Tarika, X. D. Divya Dexlin, A. Rathika, A. Arun kumar, D. Deva Jayanthi & T. Joselin Beaula (2022): Impact of Protonation and Hydrogen Bonding Interactions on the Biological Properties of Antibacterial Compound 4-Dimethylaminopyridinium Salicylate Monohydrate: Correlation with Its Precursor Molecules, Polycyclic Aromatic Compounds, DOI: 10.1080/10406638.2022.2110904

To link to this article: https://doi.org/10.1080/10406638.2022.2110904

POLYCYCLIC AROMATIC COMPOUNDS
https://doi.org/10.1080/10406638.2022.2110904

Taylor & Francis
Taylor & Francis Group

Impact of Protonation and Hydrogen Bonding Interactions on the Biological Properties of Antibacterial Compound 4-Dimethylaminopyridinium Salicylate Monohydrate: Correlation with Its Precursor Molecules

J. D. Deephlin Tarika[a], X. D. Divya Dexlin[a], A. Rathika[b], A. Arun kumar[c], D. Deva Jayanthi[d], and T. Joselin Beaula[a]

[a]Department of Physics and Research Centre, Malankara Catholic College, Mariagiri, India; [b]Department of Physics and Research Centre, Muslim Arts College, Tiruvithancode, India; [c]Department of Physics (H&Sc), Methodist College of Engineering and Technology (Autonomous), Hyderabad, India; [d]Department of Physics and Research Centre, Rani Anna Government College for Women, Tirunelveli, India

ABSTRACT

The hypothetical molecule 4-dimethylaminopyridinium salicylate monohydrate was synthesized and investigated leveraging FT-IR spectra, UV visible, NMR and quantum chemical calculations and also compared with its precursor molecules 4-dimethylamino pyridine and salicylic acid in the present work. To explore the impingement of hydrogen bonding on molecule the geometrical parameters, interaction energies, and vibrational spectra are employed. Natural Bond Orbital analysis indicated the existence of intermolecular hydrogen bonding N–H…O contact, which is mediated by a hyperconjugative interaction between the carbonyl oxygen atom donor and the pyridine ring N–H acceptor. The stretching wavenumber of hydrogen bond donor O–H and hydrogen bond acceptor C–O is red shifted due to elongation in respective bond lengths, according to vibrational analysis. The presence of intermolecular charge transfer from electron-rich pyridine to electron-deficient salicylate is revealed by FMO analysis, and this is corroborated by charge transfer due to excitation. A molecular docking simulation was also executed to better understand the structure-activity relation and further antibacterial tests confirmed that the compound inhibits the bacterial pathogens.

ARTICLE HISTORY
Received 30 March 2022
Accepted 26 July 2022

KEYWORDS
Charge transfer; interaction region; protonation; pneumococcal infections

1. Introduction

Antibacterial resistance is regarded as one of the most serious public health issues since it has a large economic impact over the world. Antibacterial resistance is limiting treatment choices for treating infections, which is increasing the morbidity and mortality associated with infectious illnesses caused by bacteria. Medicinal chemistry is concerned with the discovery, development, interpretation, and identification of the molecular mechanism of action of physiologically active molecules. Several physiologically active synthetic compounds incorporate a six-membered nitrogen containing heterocyclic ring in their structure. Structural frameworks have been defined as favored structures, and N-containing polycyclic structures, in particular, have been linked to a

CONTACT T. Joselin Beaula joselinbeaula@gmail.com Department of Physics and Research Centre, Malankara Catholic College, Mariagiri, 629153 Tamilnadu, India

Supplemental data for this article can be accessed online at https://doi.org/10.1080/10406638.2022.2110904

wide spectrum of biological activities. Pyridine derivative was chosen because of its antibacterial potential in the hunt for novel antibacterial agents. Pyridine moieties play an imperative role in medicinal chemistry ascribed to their antimicrobial, antiviral, antidiabetic, anticancer, antioxidant, antimalaric, anti-inflammatory and antibacterial properties.[1] Pyridine system functions as a proton acceptor by establishing bonds with proton donors through its lone pair electrons or electrons that are largely responsible for the biological enslavement of these compounds. Salicylic acid is a beta hydroxy acid that is naturally present in plants. Regardless of its propensity to stimulate exfoliation, it has direct anti-inflammatory effect and operates as a topical antibacterial agent. This hydrogen bonding interaction will alter the geometric structure, electronic properties, and vibrational spectra.[2] Screening of literature exposes that the structure and characterization was reported by Arunkumar et al.[3] and also the Weak and Covalent Interactions, Reactivity sites and Pharmacokinetic Studies of 4-Dimethylaminopyridinium Salicylate Monohydrate was reported by Deephlin et al.[4] but so far, there is no meticulous theoretical study on 4-dimethylaminopyridine salicylate monohydrate (DPSM) in comparison with its precursor molecule and antibacterial evaluation. So DPSM and its precursor molecules have been probed using Quantum chemical computations with the aid of spectroscopic techniques.

DFT calculations provide significant information on the stable geometry, vibrational tendency, interaction behavior, reactive nature, and possible local reactive sites of a molecular system.[5–7] Charge transportation is an indispensable factor in the stability of hydrogen bond complexes. Transfer of charge in molecules has been reflected through the exploration of the Highest Occupied Molecular Orbital (HOMO), Lowest Unoccupied Molecular Orbital (LUMO) and charge transfer excitation. The local reactivity descriptors help to understand the interaction of biologically privileged molecular systems and establish a link between biology and material science, which leads to the discovery of new pharmaceutical compounds and effective drug design applications.[8–11] The impact of protonation on the molecular structure, reactivity sites, vibrational frequencies were studied using the Density Functional Theory (DFT) method. Molecular docking is thought to be more useful in the design, evaluation, and comparison of new drugs because it allows for the examination of molecule interactions. Other techniques, such as in silico ADMET analysis, drug similarity prediction, and toxicity prediction, are also used to assess prospective medicines from various databases. These computationally mediated techniques reduce experimental costs and time in the drug development process.

2. Experimental section

2.1. Synthesis

Analytical grade 4-dimethylaminopyridine (DP) and salicylic acid (SA) were utilized in the synthesis of 4-dimethylaminopyridine salicylate monohydrate. Prior to adding 4-dimethylamino pyridine, a specified quantity of Salicylic acid was dissolved in deionized water (18.2 MΩ/cm). The reaction is agitated uninterruptedly at room temperature for 6 h, then the obtained solution is filtered and dried at room temperature. The dried filtrate was dissolved in a 1:1 methanol-water solution and filtered using Whatman filter paper. To facilitate crystal formation in a dust-free environment, the filtrate was laid aside without being disturbed. The crystals were extracted after 20 days and subjected to characterization studies. The grown crystal was depicted in Figure 1.

2.2. Characterization

The experimental details of the recorded single X-Ray Diffraction (XRD), Powder X-Ray Diffraction, Fourier Transform Infrared (FT-IR), Nuclear Magnetic Resonance (NMR) studies, Mass spectroscopy, Thermogravimetric (TG) and differential thermal analysis (DTA) of DPSM

were reported in our previous work.[3] Ultraviolet absorption spectrum was recorded using an ultraviolet visible (UV-vis) spectrophotometer, with spectral range of the instrument being 200–800 nm. Antibacterial activity was screened by agar well diffusion method.

2.3. Antibacterial testing

The Muller Hinton agar plate surface was inoculated with the microbial inoculum and then a 0.5 µL well is aseptically perforated with a micropipette tip, and DPSM sample at the desired concentration is injected into the well. The agar plates are then incubated under appropriate conditions based on the test microorganism. The antimicrobial ingredient diffuses across the agar medium, inhibiting the development of the tested microbiological strain. The inhibitory zone diameter measurements had been used to determine activity.

3. Computational details

DPSM was probed using Quantum chemical computational method with the B3LYP[12] functional using 6-311 G (d, p)[13] as a basis set employing the Gaussian'09 program package.[14] Natural Bond Orbital (NBO) analysis has been performed on the molecule at the same level using a second order Fock matrix.[15–18] Natural Coordinate Analysis (NCA) has been executed using the MOLVIB program version 7.0 written by Sundius in order to obtain a thorough interpretation of the fundamental modes.[19–21] The theoretical UV-Vis spectrum was simulated using the Time Dependent-Density Functional (TD-DFT) methodology with the DMSO as a solvent. Charge transfer excitation and Density of states analysis (DOS) were performed using Multiwfn[22]. Interaction region indicator (IRI) analysis was performed using Multiwfn program[22] and all isosurface maps were rendered by the VMD (Visual Molecular Dynamics) program. To model the ligand and protein mode of interactions for different active site proteins Auto dock tools 1.5.6 (ADT) software is employed.[23,24]

4. Results and discussions

4.1. Structural elucidations

Computed optimized geometrical parameters of DPSM were stacked up with XRD data (CCDC 876023) reported by Arun Kumar et al.[3] Table 1 depicts the bond length of DPSM and DP/SA molecules, while Table S1 and S2 depicts the bond angle and dihedral angle, and Figure 2 depicts the atomic numbering scheme of DPSM and DP/SA molecules obtained by DFT computation. When the estimated results were matched to the experimental observations, it was noted that the estimated values diverged marginally from the experimental values attributable to solid-state intermolecular interactions triggered by crystal packing effects.[25]

Due to low hydrogen atom scattering in the X-ray diffraction experiment the C–H and O–H bonds in the phenyl and pyridine rings contravene the observed values.[26] C_1–C_2 (1.416 Å), C_1–C_9 (1.401 Å), C_2–C_3 (1.403 Å) bonds in the phenyl ring are loftier than C_3–C_5 (1.385 Å), C_5–C_7 (1.399 Å) and C_7–C_9 (1.386 Å) bonds owing to the effect of substituents, and these substituents also induce attrition in endo angles C_1–C_2–C_3 (119.36°), C_2–C_1–C_9 (118.9°) from the typical trigonal angle. Imputable to the prevalence of an electronegative nitrogen atom in the pyridine ring, the C–C bond lengths were not equal. Attributable to the replacement of a dimethylamino group, the bond length of C_{20}–C_{21} (1.420 Å) and C_{18}–C_{20} (1.420 Å) is longer than other C–C bonds. When compared to bond lengths of C_{29}–N_{34} (1.359 Å), C_{16}–N_{33} (1.345 Å), and C_{23}–N_{33} (1.343 Å) the bond length of C_{25}–N_{34} (1.459 Å) and C_{29}–N_{34} (1.459 Å) gets contracted owing to the

Table 1. Experimental and Theoretical Bond length of DPSM, DP and SA.

Bond length	Theoretical (DPSM) (Å)	Theoretical (DP/SA) (Å)	Experimental (Å)	RMS	Bond length	Theoretical (DPSM) (Å)	Theoretical (DP/SA) (Å)	Experimental (Å)	RMS
C_1–C_2	1.416	1.412	1.398	0.0003	C_{16}–C_{18}	1.375	1.354	1.351	0.0005
C_1–C_9	1.401	1.405	1.388	0.0002	C_{16}–N_{33}	1.345	1.337	1.333	0.0001
C_1–C_{11}	1.492	1.455	1.491	0	H_{17}–O_{36}	2.284	–	2.408	0.0152
C_2–C_3	1.403	1.400	1.398	0.00002	C_{18}–H_{19}	1.079	1.083	0.930	0.0223
C_2–O_{14}	1.342	1.346	1.342	0	C_{18}–C_{20}	1.421	1.436	1.404	0.0002
C_3–H_4	1.083	1.082	0.930	0.0234	C_{20}–C_{21}	1.420	1.416	1.410	0.0001
C_3–C_5	1.385	1.385	1.363	0.0005	C_{20}–N_{34}	1.359	1.375	1.332	0.0007
C_5–H_6	1.085	1.084	0.929	0.0243	C_{21}–H_{22}	1.079	1.082	0.930	0.0223
C_5–C_7	1.399	1.402	1.379	0.0004	C_{21}–C_{23}	1.374	1.368	1.343	0.0010
C_7–H_8	1.084	1.082	0.930	0.0235	C_{23}–H_{24}	1.084	1.089	0.931	0.0235
C_7–C_9	1.386	1.381	1.365	0.0004	C_{23}–N_{33}	1.343	1.337	1.324	0.0003
C_9–H_{10}	1.082	1.084	0.930	0.0233	C_{25}–H_{26}	1.087	1.094	0.960	0.0163
C_{11}–O_{12}	1.282	1.346	1.263	0.0019	C_{25}–H_{27}	1.095	1.104	0.960	0.0182
C_{11}–O_{13}	1.258	1.225	1.238	0.00002	C_{25}–H_{28}	1.095	1.090	0.960	0.0182
O_{12}–H_{35}	1.404	–	1.534	0.0168	C_{25}–N_{34}	1.459	1.462	1.443	0.0002
O_{12}–H_{37}	1.867	–	1.876	0	C_{29}–H_{30}	1.087	1.093	0.960	0.0162
O_{13}–H_{15}	1.644	1.751	1.800	0.0241	C_{16}–C_{18}	1.375	1.354	1.351	0.0005
O_{14}–H_{15}	0.994	0.973	0.820	0.0303	H_{17}–O_{36}	2.284	–	2.408	0.0152
C_{16}–H_{17}	1.084	1.088	0.931	0.0241	N_{33}–H_{35}	1.132	–	0.941	0.0367
C_{29}–H_{31}	1.094	1.091	0.960	0.0181	O_{36}–H_{37}	0.973	–	0.911	0.0039
C_{29}–H_{32}	1.095	1.106	0.960	0.0182	O_{36}–H_{38}	0.962	–	0.911	0.0026
C_{29}–N_{34}	1.459	1.451	1.454	0.00003	–	–	–	–	–

subsistence of methyl groups which yields extra negative charges to the amino nitrogen atom, ensuing in contraction of respective bonds.[27]

Exo angles C_{18}–C_{20}–N_{34} (116.54°), C_{21}–C_{20}–N_{34} (121.72°), C_9–C_1–C_{11} (121.02°), C_2–C_1–C_{11} (121.22°), C_1–C_2–O_{14} (122.27°) and C_3–C_2–O_{14} (118.35°) swerved from the envisaged trigonal angle (120°) due to substituents replacing hydrogen atoms. The reduction in bond angles of H_{17}–C_{16}–N_{33} (115.05°) and H_{24}–C_{23}–N_{33} (114.38°) is attributable to the transfer of charge from the carboxylate anion to the Pyridinium cation, which further boosts the bioactivity of the compound.[26]

Bond length of C_1–C_{11} (1.492 Å) in DPSM, the site where the deprotonation takes place is increased by 0.037 Å when compared with SA (1.455 Å). Bond length of C_{20}–C_{21} tends to rise from standard value 1.34 Å to 1.42 Å, whereas C_{18}–C_{20} diminishes from 1.54 Å to 1.42 Å owing to the inclusion of dimethyl amino group, which imparts electrons to bonds surrounding the 4th position of the deficient pyridine ring. The substitution of dimethyl amino group in the fourth position of pyridine ring is responsible for the antibacterial activity of molecule. The hyperconjugation of the dimethyl amino group with the ring elevates the aromatic system's electron density.[28] Due to the obvious dimethyl amino group substitution, the heterocyclic ring resembles distorted, as evidenced by the bond angle of

C_{18}–C_{20}–C_{21} (116.54°), which is much less than conventional hexagonal angle of 120°. The O_{12} ... H_{35}–N_{33} (2.73 Å) distance, which is much shorter than van der Waals separation (3 Å), facilitate intermolecular hydrogen bonding interaction, which is crucial for designing molecules with enhanced biological profiles.[29] The hydrogen bonding interaction is liable for the elevation in bond length of O_{12}–H_{35} (1.402 Å), O_{36}–H_{17} (2.84 Å), and O_{12}–H_{37} (1.86 Å) over the standard O–H bond length (0.96 Å). The bond length of the hydroxyl group O_{14}–H_{15} in DPSM is increased by 0.0208 Å, whereas the bond length of the bond O_{13}–H_{15} formed as a result of hydrogen bonding interaction in DPSM is decreased by 0.107 Å when compared with DS. The optimal bond length of N_{33}–H_{35} is raised by 0.1918 Å when compared to its experimental bond length, and there is also an RMS error of 0.036 owing to this discrepancy in experimental and theoretical values ascribed to the hydrogen bonding formation. The bond length of C_{16}–H_{17} and C_{23}–H_{24} of DPSM is dropped by 0.004 Å and 0.005 Å, respectively when compared to DP, probably due to

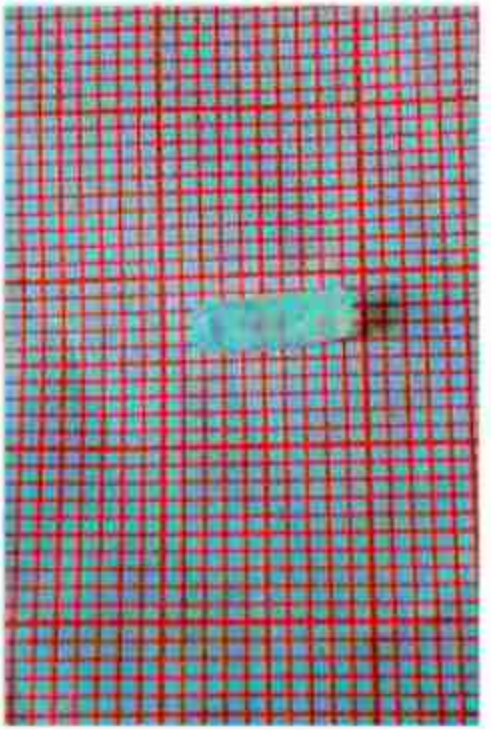

Figure 1. DPSM crystal.

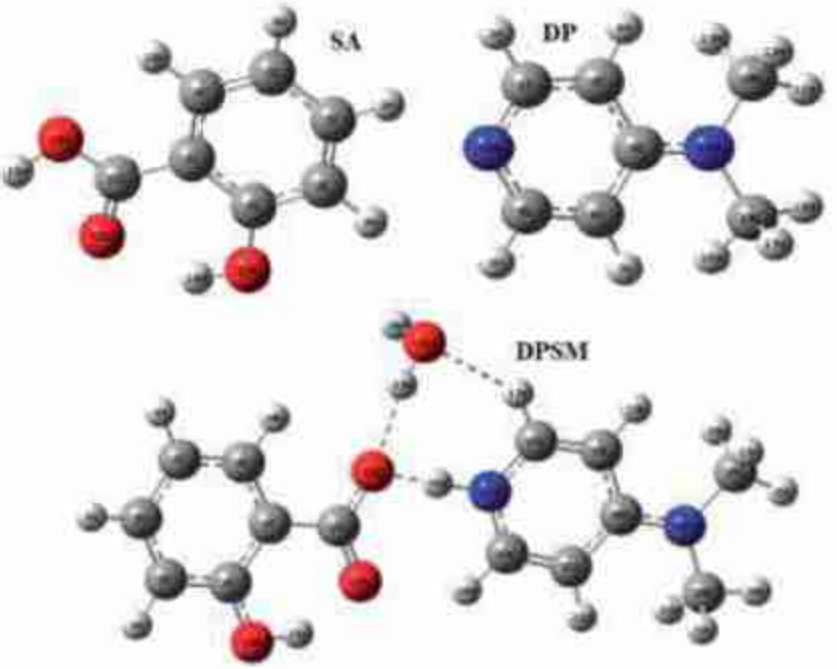

Figure 2. Optimized structures of DPSM, DP and SA.

hydrogen bonding interaction. The orbital contacts as well as charge distributions that transpire within the molecule enable bond length to elongate and contract

Bond distances of O_{36}–H_{37} and O_{14}–H_{15} which partake in hydrogen bonding interaction are elongated by 0.043 Å and 0.013 Å due to protonation effect. Protonation also induces the C_{16}–N_{33} (1.345 Å) and C_{23}–N_{33} (1.374 Å) bonds in DPSM to increase when compared to the C–N bond length of DP. In SA, the fully protonated Carboxylic acid have unequal bond length of C_{11}–O_{12} (1.346 Å) and C_{11}=O_{13} (1.225 Å) which slightly deviate from standard value of C–O (1.30 Å) and C=O (1.21 Å)[30] due to hydrogen bonding interactions. But in DPSM the carboxylic acid of SA gets deprotonated and becomes carboxylate. The C–O bond length of resonance deprotonated carboxylate is 1.26 Å, but in DPSM the bond length C_{11}–O_{12} (1.28 Å) and C_{11}–O_{13} (1.25 Å) is deviated from 1.26 Å ascribed to hydrogen bonding formation.[30] The estimated C_{20}–N_{34} bond length of 1.359 Å is less than the typical C–N bond length of 1.480 Å, and the shortening of this C–N bond length reveals the impact of resonance in the dimethylamino group.[31] Because of the steric effect of the lone-pair electron predicted by valence-shell electron-pair repulsion theory (VSEPR),[32] the internal C_{16}–N_{33}–C_{23} angle (119.77°) of the protonated N atom is significantly subservient than the nearby two angles C_{18}–C_{16}–N_{33} (121.41°) and C_{21}–C_{23}–N_{33} (121.51°) within the ring.

The planarity of Hydroxyl group and carboxylate group of phenyl ring is validated from the dihedral angles of C_3–C_2–H_{14}–O_{15} (179.91°), C_2–C_1–C_{11}–O_{13} (0.39°) and C_9–C_1–C_{11}–O_{12} (0.30°). Dimethylamino group is found to be out of plane with pyridine ring as indicated by dihedral angles H_{27}–C_{25}–N_{34}–C_{20} (60.29°), H_{28}–C_{25}–N_{34}–C_{20} (–61.22°), H_{31}–C_{29}–N_{34}–C_{20} (59.9°), H_{38}–O_{36}–H_{37}–O_{12} (–61.53°). Carboxylate groups C_2–C_1–C_{11}–O_{12} (–179.78°), C_9–C_1–C_{11}–O_{13} (–179.51°) and hydroxyl group C_1–C_2–H_{14}–O_{15} (–0.1349°) are oriented in salicylate with anti-periplanar (-ap) conformation whereas C_3–C_2–H_{14}–O_{15} (179.91°), C_2–C_1–C_{11}–O_{13} (0.39°) and C_9–C_1–C_{11}–O_{12} (0.30°) is oriented with +ap conformation.[33]

4.2. Vibrational Spectral assignments

To establish the best possible fit between the computed and observed vibrational wave numbers, the Scaled Quantum Mechanical Force Field (SQMFF) was utilized. Because the DPSM molecule is made up of 38 atoms, it has 108 typical modes of vibration. Assignments of DPSM with potential energy distribution have been given in Table S3 to determine the greatest likelihood of vibrations, and the observed FT-IR spectrum, as well as the simulated spectra of DPSM, DP and SA are displayed in Figure 3 and Figure S2 for visual comparison.

4.2.1. Phenyl ring vibration

The scaled wavenumbers comprising of asymmetric di-substituted benzene rings are in excellent accordance with the various normal vibrations of the di substituted benzene rings assigned according to Wilson's numbering scheme.[34] In the vibrational spectrum of benzene derivatives, carbon stretching is normally prominent, and it enables five C–C stretching normal modes: 8a, 8b, 19a, 19b, and 14. Vibration pair 8 for o-di-substituted benzene ring ranges from 1565–1609 cm^{-1} to 1586–1625 cm^{-1} is observed in FT-IR at 1555 cm^{-1}. The diverse environmental impacts of the substituents account for the shift in the theoretical wavenumber. Vibration modes 19a and 19 b were detected in FT-IR at 1478 cm^{-1} and 1516 cm^{-1} respectively which agree with scaled values. The acceptor nature of the substitute diminishes both the frequency and intensity. Vibration mode 14 is recognized by a strong band at 1257 cm^{-1} in FT-IR that correlates to a scaled value at 1269 cm^{-1}.

Di-substituted benzene's C–H stretching frequencies are predicted to be in the range of 3000–3100 cm^{-1}.[35] For C–H stretching vibrations, the selection rules for di-substituted benzene

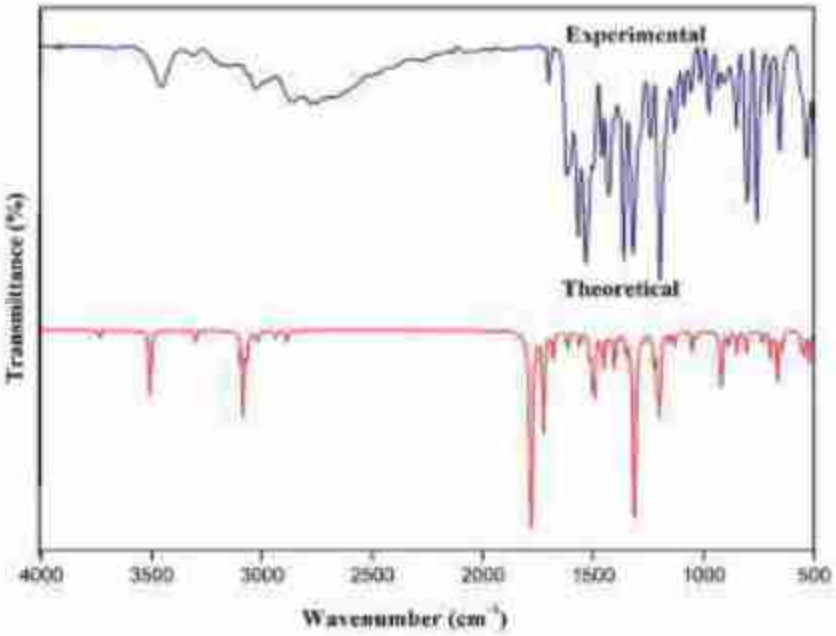

Figure 3. Experimental and simulated FT-IR spectra.

are 2, 7b, 20a, and 20b. Modes 20a and 2 have been attributed to the strong bands observed in FT-IR at 3080 cm^{-1}. Vibration 20b has a scaled value of 3035 cm^{-1}, while typical vibration 7b has a scaled value of 3054 cm^{-1}. The normal modes 3, 9a, 15, 18a, and 18b describe the C–H in plane bending vibrations, which fall between 1300 cm^{-1} and 1100 cm^{-1}. Mode 18 b has been assigned the strong band at 1068 cm^{-1} in IR, whereas mode 3 has been assigned the band at 1257 cm^{-1} in IR. Normal vibration 15 is observed at 1197 cm^{-1}, while vibration 9 b is detected at 1134 cm^{-1} and 1115 cm^{-1}. Ortho- di-substituted phenyl ring exhibits out of plane bending vibrations in the range of 1000–675 cm^{-1} and the permitted selection rules are 10a, 10b, 11 and 5. The strong bands seen in FT-IR at 945 cm^{-1} and 768 cm^{-1} have been attributed to modes 10a and 11 respectively, whereas the scaled band observed at 832 cm^{-1} has been given to mode 10b.

4.2.2. Pyridine ring vibration

C–C and C–N stretching of pyridine ring are typically perceived in the frequency ranges 1600–1450 cm^{-1} and 1450–950 cm^{-1}.[36] The experimental wavenumber of 1257 cm^{-1} observed in the FT-IR spectra corresponds to the C–N stretching mode scaled at 1271 cm^{-1} in the DPSM. In FT-IR spectra, scaled pyridine ring breathing vibrational modes at 1611 cm^{-1}, 1487 cm^{-1}, 1426 cm^{-1}, 1415 cm^{-1} harmonize with a strong peak at 1590 cm^{-1} and 1478 cm^{-1} respectively. Aromatic C–H stretching vibrations of nitrogen heterocyclic aromatic compounds give rise to a band at 3100–3010 cm^{-1},[37] which is perceived in FT-IR at 3114 cm^{-1}, and agrees well with scaled values in the 3104 cm^{-1} and 3092 cm^{-1} regions. The blue shift in the C–H stretching vibration is triggered by hyperconjugative interactions, which enables the C–H bond to retrench, as evidenced by optimized geometry and NBO analysis. Due to C–H in-plane deformation vibrations, bands of varying intensity are seen in the regions 1300–1180 cm^{-1} and 1100–1000 cm^{-1}, which is observed in DPSM as a strong band at 1209 cm^{-1}, 1102 cm^{-1} in FT-IR spectra coincide with scaled value. C–H out of plane deformation vibrations, which are typical of the site of substitution, is detected as prominent bands in the 850–690 cm^{-1} range. The scaled ring out of plane deformation of DPSM at 816 cm^{-1} corresponds to the observed wavenumber 810 cm^{-1} in FT-IR.

4.2.3. Methyl group vibrations

According to the DPSM orientation, methyl groups are expected to oscillate more elastically than pyridine rings. Asymmetric and symmetric CH_3 stretching vibrations are often observed at 2962 cm^{-1} and 2872 cm^{-1}.[37,38] The symmetric CH_3 stretching modes are attributed to the band obtained in FT-IR at 2823 cm^{-1} and the asymmetric stretching observed in FT-IR at 2905 cm^{-1} accord with the scaled value. The discrepancies in the CH_3 stretching mode were triggered by the stimulus of electronic impact persuaded by the hyper conjugation of the methyl group with the nitrogen atom and the aromatic ring system, which fallouts in an alteration in polarizability and dipole moment owing to electron delocalization.[39] Thus, the hyper conjugation of methyl group which results in a shift in IR, demonstrates that methyl hydrogen is directly implicated in the donation of electronic charge.

Asymmetric methyl deformation modes are often detected at $1460 \pm 10\,cm^{-1}$ in FT-IR as a prominent band at 1446 cm^{-1}, which corresponds to an asymmetric deformation. The presence of hyper conjugation is supported by the high value of the asymmetric bending mode, which is caused by a significant positive charge centered on hydrogen. Umbrella modes typically emerge at $1375 \pm 10\,cm^{-1}$, suggesting the presence of DPSM's methyl group, which is seen as a prominent band at 1379 cm^{-1} in FT-IR. The umbrella mode's location is less susceptible to changes in molecular structure than C–H stretching. CH_3 rocking mode vibration is anticipated to occur in the area of 1070–900 cm^{-1},[28] and it has been detected in FT-IR spectra at 1028 cm^{-1}, which agrees with the scaled value.

4.2.4. Carboxylate group vibrations

Carboxylate group asymmetric vibration, which is expected to occur between 1650 and 1540 cm^{-1},[37] is observed in FT-IR at 1690 cm^{-1} with a scaled value of 1696 cm^{-1}. In the DPSM, the symmetrical stretch of carboxylate expected to occur between 1360 cm^{-1} and 1450 cm^{-1} is scaled to 1350 cm^{-1}. In SA, the carboxylic group is present and the C–O and C = O stretching vibrations are expected to occur in the range 1320–1210 $cm^{-1}$and 1710–1680 cm^{-1} respectively. The very strong band observed at 1274 cm^{-1} is assigned to C–O stretching and the strong band at 1637 cm^{-1} is assigned to C = O stretching vibrations. Dropping of carbonyl stretching mode is attributed to the fact that the carbonyl group chelate with other nucleophilic groups, thereby forming both intra and intermolecular hydrogen bonding.[28]

4.2.5. Hydroxyl group vibrations

O–H stretching vibration is typically found in $3350 \pm 50\,cm^{-1}$. The observed O–H stretching vibrations as medium bands in the FT-IR spectrum at 3360 cm^{-1} agree with the scaled value at 3304 cm^{-1} with 99% PED contributions. The O–H group may bend in and out of the plane specified by the acid moiety, and in general, in plane O–H bending bands found in the range 1440–1350 cm^{-1} are typically broader than C–H bending bands, making them easily distinguishable. The O–H bending vibrations are attributed to the prominent peak at 1337 cm^{-1} in FT-IR spectra coincides with the scaled value. The red shift in theoretical wavenumber demonstrates spectral evidence for the occurrence of O–H … O hydrogen bonding interactions, which validates the compound's bioactivity. This is corroborated by optimized geometry findings, which reflect changes in bond length of O_{14}–H_{15} (0.99 Å) compared to the typical O–H bond length (0.96 Å) attributed to hydrogen bonding interactions. The second order perturbation energy that emerges between $n(O_{13}) \rightarrow \sigma^*(O_{14}\text{–}H_{15})$ with the stabilization energy of 29.02 kcal/mol and the occupancy of the interacting NBOs has also been used to substantiate the down shift in stretching frequency. Rehybridization also induces an elongation of the O–H bond and a red shift in the OH stretching frequency.

4.2.6. Water group vibration

Stretching vibrations of water molecules are expected to occur in the region 3300–3700 cm^{-1}[140] is been observed in DPSM as a broad band at 3512 cm^{-1} in FT-IR, agrees with the scaled value. The scissoring of two OH bands observed at 1641 cm^{-1} is a distinctive characteristic of water that distinguishes it from alcohol.[37] This band, combined with OH stretching vibrations, confirms the existence of liquid in a sample.

4.3. Donor-acceptor interactions

Second order Fock matrix was consummated to enumerate the donor-acceptor interactions in the NBO analysis is portrayed in Table 2 and composition of H-bonded NBO in terms of natural atomic hybrids is portrayed in Table S5.

Primary hyperconjugative interactions owing to the omnifarious types of orbital overlaps such as $n \rightarrow \sigma^*$ and secondary hyperconjugative interactions assignable to the orbital overlap between $\sigma \rightarrow \sigma^*$ are revealed in Table 2. Primary hyperconjugative interactions in lone pair $n(O_{13}) \rightarrow \sigma^*(C_{23}\text{-}H_{24})$, $n(O_{12}) \rightarrow \sigma^*(O_{36}\text{-}H_{37})$, $n(O_{13}) \rightarrow \sigma^*(N_{33}\text{-}H_{35})$, $n(O_{36}) \rightarrow \sigma^*(N_{33}\text{-}H_{35})$ are censurable for weak hydrogen bonding interactions with stabilization energy 0.86 kcal/mol, 0.41 kcal/mol, 0.06 kcal/mol, 0.06 kcal/mol respectively.[41] An additional primary hyperconjugative interaction which is liable for shrinking of C–N bond length of $C_{16}\text{–}N_{33}$ (1.345 Å) and $C_{23}\text{–}N_{33}$ (1.343 Å) from normal C–N (1.43 Å) bond length in optimized molecular geometry is validated from lone pair n $(O_{12}) \rightarrow \sigma^*(C_{16}\text{–}N_{33})$ and n $(O_{12}) \rightarrow \sigma^*(C_{23}\text{–}N_{33})$ with stabilization energy 0.12 kcal/mol, 0.16 kcal/mol respectively. Most stable interaction within the DPSM molecule is signified by the $n \rightarrow \pi^*$ transition occurring between n (C_1) to π^* $(C_{11}\text{–}O_{13})$ with the maximum stabilization energy 86.92 kcal/mol.

When compared to $C_2\text{–}O_{14}$ (1.9934 e) and $C_{11}\text{–}O_{12}$ (1.9937 e) bonds, the electron density of $C_{11}=O_{13}$ (1.9943 e) which exhibits double bond characteristics is grander. According to NBO analysis, $C_3\text{–}C_5$ (1.9774 e, 1.71327 e), $C_{11}\text{–}O_{13}$ (1.9943 e, 1.98499 e), $C_{16}\text{–}C_{18}$ (1.97988 e, 1.71986 e), $C_{20}\text{–}N_{34}$ (1.9853 e, 1.93706 e), and $C_{21}\text{–}C_{23}$ (1.97976 e, 1.71484 e) have two occupancy values, with higher occupancy bonds having both s and p hybridization and lower occupancy bonds having solely p hybridization. As the electronegativity of sp^2 hybridized atom is grander than that of sp^3 hybridized atom, C–C bonds with σ and π bonds are having lesser occupancy around 1.7 e than that of C–C bonds with only σ bonds having occupancy around 1.9 e.[42]

Despite the negative inductive effect of the nitrogen atom, electron density is not equally dispersed across the pyridine ring, and as a result, pyridine ring atoms have lower stabilization energy than phenyl ring atoms, as shown in Table 2. According to the pyridine resonance structure, only $C_{23}\text{–}C_{21}$ and $C_{16}\text{–}C_{18}$ display double band characteristics due to the presence of a dimethyl amino group in the fourth position.[43] Intermolecular charge transfer makes the molecule more polarizable is perceived between n $(O_{12}) \rightarrow \sigma^*(N_{33}\text{–}H_{35})$ with stabilization energy 75.65 kcal/mol, enhances the bioactivity of molecule. Occupancy of $O_{36}\text{–}H_{37}$ (1.9966 e) and $O_{36}\text{–}H_{38}$ (1.9986 e) is loftier than other bonds in molecule ascribed to intermolecular hydrogen bonding interaction.

Polarization coefficient of two atoms in anti-bond is opposite to the bonding orbital with opposing polarizations and phases. Table S4 shows that the polarization coefficients of C–C bonds are almost identical, whereas the polarization coefficient of C–O, N–H, C–H, and O–H bonds differs. The hydrogen atoms in the molecule have a 100% s hybridization and a nearly 0% p hybridization whereas π bond of $C_3\text{–}C_5$, $C_{11}\text{–}O_{13}$, $C_{16}\text{–}C_{18}$, $C_{21}\text{–}C_{23}$ exhibit nearly 100% p hybridization and 0% s hybridization.[42]

In comparison to DS and DP, NBO analysis of DPSM clearly reveals evidence for the formation of strong H-bonded interactions between lone electron pair n $(O_{12}) \rightarrow \sigma^*$ $(N_{33}\text{–}H_{35})$ and n $(O_{13}) \rightarrow \sigma^*$ $(O_{14}\text{–}H_{15})$ orbitals. When the occupancy of $O_{14}\text{–}H_{15}$ is raised by 0.022 e, the

Table 2. Second order perturbation theory analysis of Fock matrix in NBO basis.

Donor (i)	ED (e)	Acceptor (j)	ED (e)	E(2) kcal/mol	E(j)–E(i) (a.u)	F(i, j) (a.u)
$\sigma(C_1–C_2)$	1.97470	$\sigma^*(C_1–C_9)$	0.02185	4.45	1.26	0.067
$\sigma(C_1–C_2)$	1.97470	$\sigma^*(C_2–C_3)$	0.02603	3.94	1.25	0.063
$\sigma(C_2–C_3)$	1.97632	$\sigma^*(C_3–C_5)$	0.01451	3.11	1.29	0.057
$\sigma(C_3–C_5)$	1.97747	$\sigma^*(C_5–C_7)$	0.01753	3.06	1.27	0.056
$\sigma(C_2–C_3)$	1.97632	$\sigma^*(C_1–C_{11})$	0.06699	3.00	1.12	0.052
$\sigma(C_5–C_7)$	1.97854	$\sigma^*(C_7–C_9)$	0.01630	3.20	1.29	0.057
$\sigma(C_{16}–H_{17})$	1.97722	$\sigma^*(C_{16}–C_{18})$	0.01518	1.29	1.11	0.034
$\sigma(C_{18}–C_{20})$	1.97074	$\sigma^*(C_{16}–C_{18})$	0.01518	2.96	1.29	0.055
$\sigma(C_{20}–C_{21})$	1.97065	$\sigma^*(C_{20}–N_{34})$	0.03339	2.50	1.18	0.049
$\sigma(C_{20}–N_{34})$	1.98534	$\sigma^*(C_{16}–C_{18})$	0.01518	1.05	1.43	0.034
$\sigma(C_{20}–N_{34})$	1.98534	$\sigma^*(C_{18}–C_{20})$	0.02435	2.15	1.36	0.048
$n(O_{12})$	1.94770	$\sigma^*(C_{16}–N_{33})$	0.02132	0.12	0.84	0.009
$n(O_{12})$	1.94770	$\sigma^*(C_{23}–N_{33})$	0.02100	0.16	0.85	0.011
$n(O_{13})$	1.96300	$\sigma^*(O_{14}–H_{15})$	0.06886	4.57	1.08	0.063
$n(O_{13})$	1.96300	$\sigma^*(C_{23}–H_{24})$	0.01928	0.86	1.09	0.027
$n(O_{12})$	1.94770	$\sigma^*(O_{36}–H_{37})$	0.01950	7.26	1.05	0.078
$n(O_{36})$	1.99487	$\sigma^*(C_{16}–H_{17})$	0.02175	2.91	0.78	0.042
$n(O_{36})$	1.99487	$\sigma^*(N_{33}–H_{35})$	0.16526	0.06	0.68	0.006
n (C_1)	1.11258	π^* $(C_{11}–O_{13})$	0.37700	86.92	0.11	0.103
$n(O_{12})$	1.94770	$\sigma^*(N_{33}–H_{35})$	0.16526	75.65	0.70	0.207
$n(O_{12})$	1.94770	π^* $(C_{11}–O_{13})$	0.37700	79.87	0.28	0.136
$\sigma(O_{36}–H_{37})$	1.99662	$\sigma^*(N_{33}–H_{35})$	0.16526	0.10	1.06	0.010
$\sigma(C_{11}–O_{13})$	1.99433	$\sigma^*(O_{36}–H_{37})$	0.01950	0.07	1.44	0.009
$\sigma(C_1–C_{11})$	1.97554	$\sigma^*(O_{36}–H_{37})$	0.01950	0.05	1.09	0.007
n (O_{13})	1.96300	$\sigma^*(N_{33}–H_{35})$	0.16526	0.06	0.61	0.006
$n(O_{12})$	1.94770	$\sigma^*(O_{36}–H_{37})$	0.01950	0.41	0.72	0.017

E(2) means energy of hyper conjugative interactions. E(j)–E(i) Energy difference between donor and acceptor i and j NBO orbitals. F(i, j) is the Fock matrix element between i and j NBO orbitals.

bond strength wilts and the bond length elongates. This bond length elongation is also evident in optimized geometry, where the bond length of $O_{14}–H_{15}$ in DPSM is extended by 0.0208 Å from SA. The formation of hydrogen bonded intermolecular interactions between the oxygen n (O_{13}) → $\sigma^*(C_{23}–H_{24})$ with a stabilization energy of 0.860 kcal/mol is revealed by bonding orbital analysis of DPSM and DP. The existence of inappropriate hydrogen bonding is indicated by the fact that the C–H stabilization energy is less than 3 kcal/mol. When DPSM is compared to DP, the amount of charge transferred from lone pair oxygen atoms to hydrogen linked $C_{23}–H_{24}$ atoms is reduced by 0.0058 e, prompting bond length contraction and a blue shift in the C–H stretching frequency. Occupancy of $C_{11}–O_{12}$ and $C_{11}–O_{13}$ of the carboxylate group in DPSM, involved in hydrogen bonding interactions was decreased by 0.0017 e and 0.0005 e respectively compared to the SA molecule. Due to this deviation in occupancy of DPSM the bond length of $C_{11}–O_{13}$ and $C_{11}–O_{12}$ gets dilated and also resulting in red shift in C–O stretching frequency.

The elevation in the s-character of the $O_{14}–H_{15}$ hybrid orbital from $sp^{1.57}$ to $sp^{1.62}$ diminishes the $O_{14}–H_{15}$ bond strength, and its dilatation implies that there is a negative influence in these bonds attributed to the effect of rehybridization. The impact of rehybridization has been countered by the hyperconjugative effect, which results in O–H bond dilatation and a corresponding red shift in O–H stretching frequency. Similarly, as the s-character of the $C_{16}–H_{17}$, $C_{23}–H_{24}$ hybrid orbitals increases from $sp^{1.1}$ to $sp^{1.27}$ and $sp^{1.09}$ to $sp^{1.27}$, the corresponding bonds strengthen and shrink. This contraction is clearly replicated in optimized geometry, where the bond lengths of $C_{16}–H_{17}$ and $C_{23}–H_{24}$ in DPSM are dropped by 0.004 Å and 0.005 Å, respectively, compared to DP. The impact of rehybridization and hyper conjugation induces C–H retrenchment and dilatation. However, rehybridization dominates and excels the hyperconjugative interaction, resulting in C–H bond retrenchment and a blue shift in stretching frequency.[44]

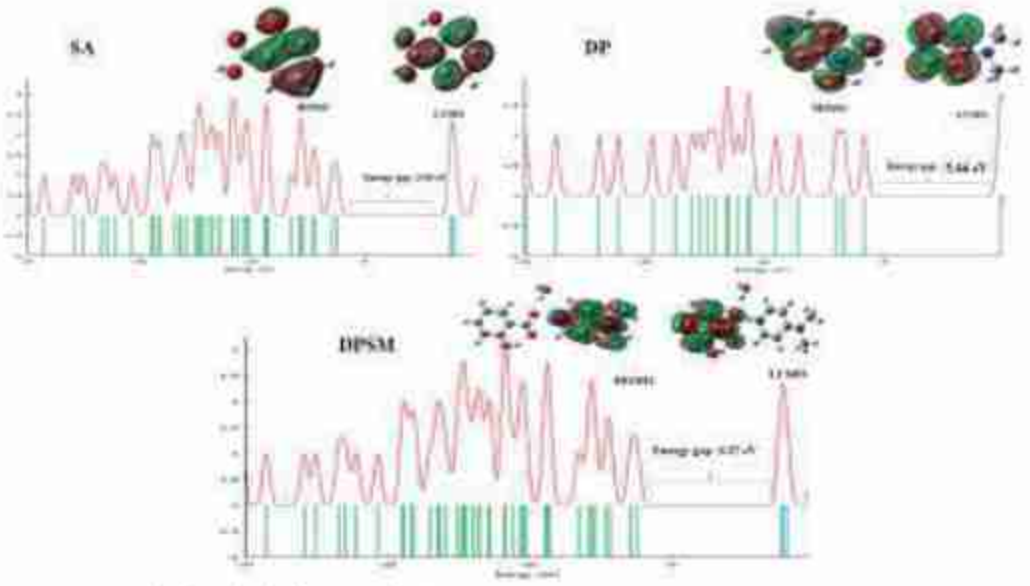

Figure 4. Frontier molecular orbitals of DP, SA and DPSM.

4.4. Frontier molecular orbital analysis

Figure 4 renders the FMOs of DP, SA & DPSM, where the red color bespeak the positive phase and the green color bespeaks the negative phase which demonstrates the charge transfer within the molecule.

The nucleophile HOMO is detected over the dimethyl amino pyridine, whereas the electrophile LUMO is detected over the salicylate. The HOMO orbital, which has an energy of −8.1838 eV, endows electron on the LUMO orbital, which has an energy of −4.9138 eV. The LUMO value is low attributable to the electron receiving propensity of oxygen atoms, but the HOMO value is elevated due to electron donating nitrogen atoms. Due to the obvious delocalization of the electron cloud in Carboxylate ions, electropositive hydrogen atoms are dragged to negatively charged oxygen atoms. The frontier orbital energy gap, which reflects a molecule's chemical activity, is projected to be 3.27 eV. The modest magnitude of the frontier orbital energy gap facilitates charge transfer interactions, which govern biological activity.[35] By dint of its small molecular orbital energy gap, DPSM is a soft molecule with high polarizability and chemical reactivity. For the SA compound, HOMO and LUMO are localized around the ring atoms and hydroxyl group whereas LUMO is mainly localized around the ring atoms and Carboxylic acid group. In DP, HOMO is localized around the dimethylamino group and pyridine ring atoms but LUMO is localized around pyridine ring atoms. The energy gap of SA and DP were found to be 3.69 eV and 5.64 eV respectively. The energy gap of the DPSM is small when compared to the precursor molecules. The salicylic acid with hydroxyl group is mainly responsible for the lowering of the frontier orbital energy gap of DPSM.

Indeed, many novel chemical reactivity descriptors were offered to better understand different aspects of medicinal chemistry, such as drug design and therapeutic compounds' potential ecotoxicological capabilities.[45] Table S6 depicts chemical reactivity characteristics such as chemical hardness, softness, electronegativity, chemical potential, and electrophilicity index of DP, SA and DPSM computed using HOMO and LUMO values. Chemical hardness, calculated to be 1.635 eV, preserves compound stability, whereas electronegativity, which describes the dexterity to entice shared electrons, is found to be 6.548 eV. The electrophilicity index of a molecule can be used to validate a compound's ability to adhere to biomolecules. Molecules indicating a stronger

electrophilicity index can function as an electrophile, whereas molecules with a lower electrophilicity index can operate as a nucleophile. A higher Electrophilicity index (13.40 eV) for DPSM implies that it has a substantial binding capacity with biomolecules and can function as an electrophilic species.[46] The chemical softness value of 0.611 eV evinces the compound's harmless nature and demonstrates its scope in medical and industrial applications.[47] From Table S6 it is seen that the electrophilicity index of SA is comparatively high electrophilic and the presence of SA in DPSM makes it an electrophilic species.

4.5. Density of states analysis

Density of states (DOS) plot of DP, SA and DPSM is also displayed in Figure 5. Furthermore, research on the nature of chemical bonding was conducted using Overlap Population of Density of States (OPDOS) diagrams. An important consideration was that the sign of the OPDOS value governed the bonding character, with a positive value signifying a bonding interaction, a zero-value revealing a non-bonding interaction, and a negative value implying an anti-bonding interaction, respectively.[48,49] It is hypothesized from the HOMO molecular orbital of Partial Density of States (PDOS) spectra that the orbital contribution of salicylate ring fragments is more than that of other fragments, however in the case of LUMO molecular orbital contribution of pyridine ring was substantially higher than that of the other three fragments. OPDOS of a HOMO molecule has both bonding and antibonding orbitals, whereas LUMO has antibonding interactions. It was grasped from Figure 5 that OPDOS of the HOMO orbital of DP has both the bonding and antibonding interactions but the LUMO has only antibonding interactions. In the case of SA, OPDOS of the HOMO orbital both the bonding and antibonding interactions but the LUMO has only antibonding interactions. From Figure 5 it is evident that the PDOS of Phenyl ring in SA is comparatively high for both the HOMO and LUMO.

4.6. Charge transfer excitation

Charge transfer owing to excitation deliberates the frontier orbital energy gap that causes charge transfer inside the molecule. Figure 6 and S2 depicts the distribution of electron holes (green-blue) across the compound DP, SA and DPSM for four excited states, and Table 3 and S8 depicts the values of overlap of electron-hole distribution (S), charge transfer length (D), Δr, and excitation energy (E) for distinct excitation modes of DPSM and SA respectively.

In the first excited state, electrons are spread over carbon and electronegative nitrogen atoms, implying the electron rich character of the pyridine ring, whereas holes are scattered over carbon and oxygen atoms in salicylate, implying the electron deficient nature of salicylate. For SA electrons are confined around the ring hydrogen atoms and carboxylic group whereas holes are confined around the ring carbon atoms and hydroxyl group. Regarding DP, holes are limited around the dimethyl amino group and nitrogen atoms in the first excited state, whereas electrons are bound around the nitrogen atoms in the ring in the second and third excited states. Electrons in the pyridine ring are constrained over the carbon and hydrogen atoms in all three excited states. The overlap integral of the hole-electron distribution (S) is a measure of the spatial separation of the hole and electron; the greater the overlap, the greater the charge transfer.[50] The distance between the centroid of the hole and electron is a measure of charge transfer length (D) and charge transfer excitation, which results in charge density migration from one location to another, occurs when the spatial separation between the hole and the electron is enormous.[51] The Δr index is a quantitative indication of electron excitation mode; the higher the value of Δr, the greater the charge transfers inside the molecule for that specific state. It can be seen from the table that the charge transfer length of the first excitation mode is significantly longer, and Δr is also greater for the same mode, implying that the first excitation mode corresponds to a strong

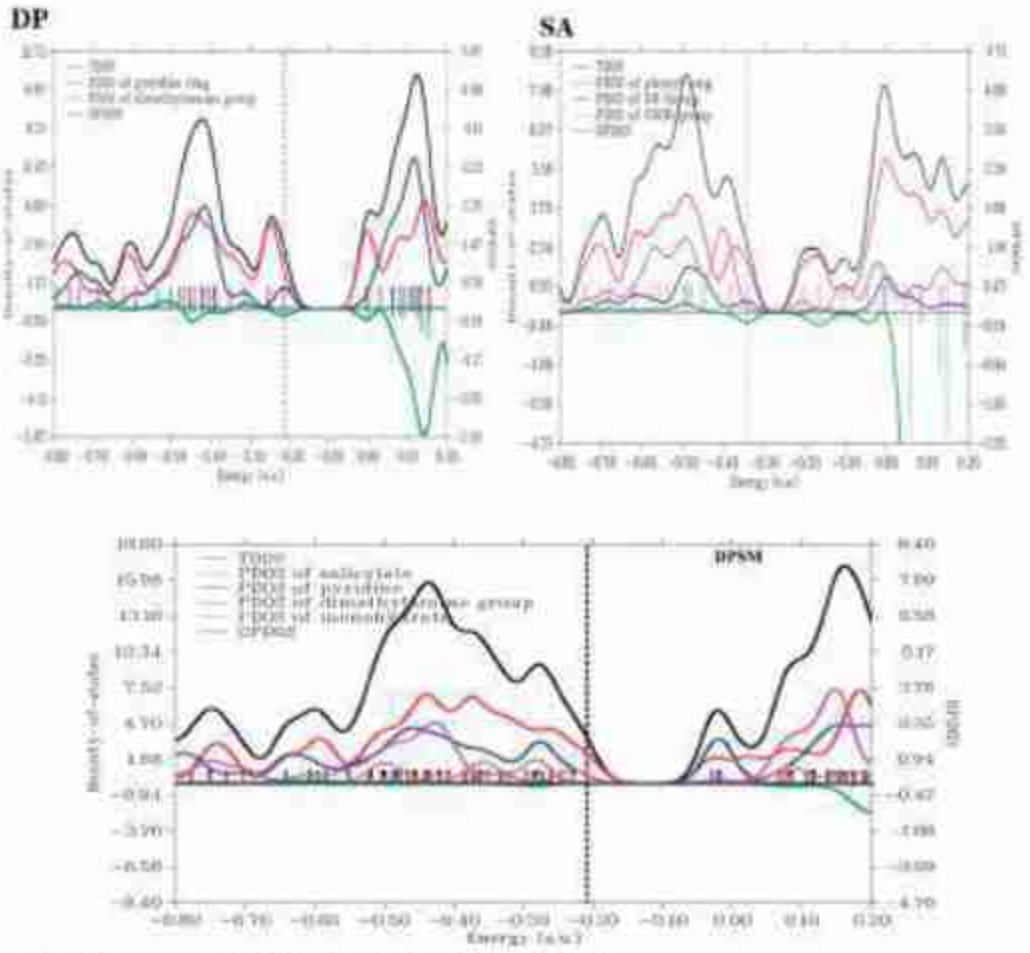

Figure 5. Density of states (TDOS, PDOS, OPDOS) plot of DP, SA and DPSM.

charge transfer excitation.[52] For SA, charge transfer excitation is high for the second excited when compared to other states.

4.7. UV-Visible spectral analysis

The time dependent density functional theory (TD-DFT). was used to assess the nature of the transitions in the observed UV–Visible spectrum of the title compound. The observed and simulated results were compared, and the resulting spectrum is displayed in Figure 7. Table S7 summarizes the estimated max value λ_{max}, excitation energies, band gap energy, oscillator strength (f), and relevant assignments. The UV-Vis spectrum of DP and SA is also displayed in Figure S1. A detailed explanation related to the UV-vis spectra of DP is reported in our previous work.[53] As per molecular orbital geometry calculations, the observed absorbance maxima of this molecule directly correlate to electron transitions among frontier orbitals, such as translation from HOMO to LUMO.

The UV spectrum is influenced by the role of substituents and the solvent and the solvent effects may cause these values to be somewhat shifted. According to the UV-vis spectra, the absorption maximum λ_{max} is observed to be 207 nm $\pi \rightarrow \pi^*$ and the second peak is observed at

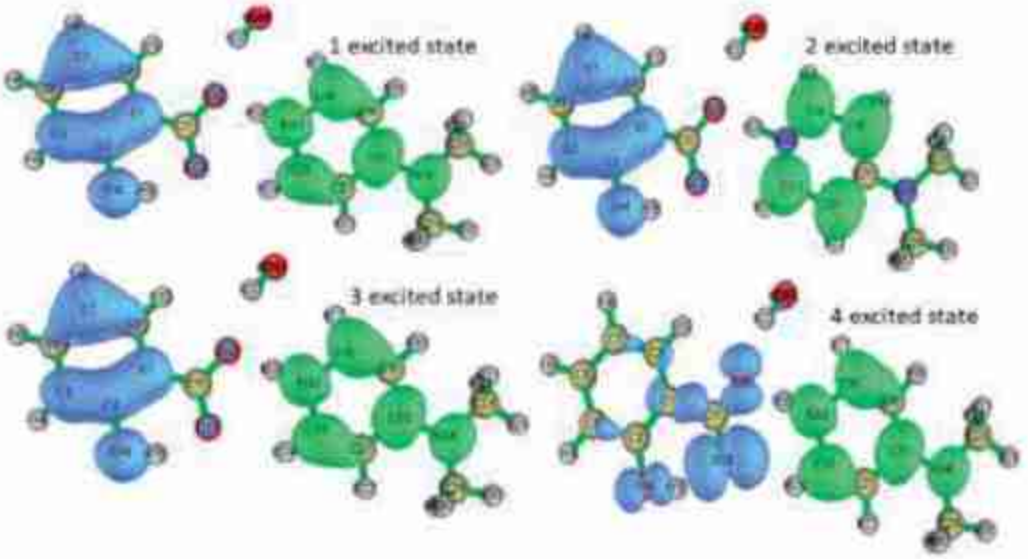

Figure 6. Electron hole distribution diagram.

Table 3. Overlap integral, charge transfer length, Ar and excitation energy for different excited states.

Excited states	Overlap integral of electron hole (S)	Charge transfer length (D) Å	Ar Å	Excitation energy (eV)
1	0.0375	7.431	7.455	3.473
2	0.0286	7.115	7.131	3.692
3	0.7580	0.883	0.866	4.434
4	0.1248	4.707	4.890	4.444

282 nm. The absorption maximum obtained at 282 nm is assigned to the n→ π^* transitions and this peak arises due to the transitions from a lone pair oxygen atom to the anti-bonding p orbital of the pyridine ring.[54] For the maximum absorption peak obtained at 263 nm the electronic transitions take place between HOMO-1→LUMO + 2 with 90% contributions. For DP and SA, the maximum absorption peak is observed at 225 nm and 215 nm respectively is assigned to the $\pi \rightarrow \pi^*$.

4.8. Hirshfeld surface analysis

The d_{norm}, d_i, d_e, shape index, and curvedness of DPSM, DP and SA and 2 D fingerprint plots of all the interactions within the atoms for the compounds were shown in Figure 8.

The complete absence of red color in the DP d_{norm} plot implies that there is no short contact between the atoms, however in SA red spots surrounding the carboxylic group and hydroxyl group validate the O–H ….O and C–H … O connections, and red spots in DPSM similarly validate the O–H ….O and C–H … O interactions. The van der Waals separation is depicted by white patches encircling the hydrogen atoms, whereas longer connections are depicted by blue. The distinguishing mark of π…π stacking interactions is the adjacent red and blue color patches on the surface of the shape index. Curvedness is a flat disk-like area on the surface that coincides to the surface area of a molecule's shape which helps to divide surfaces into spots that allow interaction between neighboring molecules. And the blue framework that divides flat patches indicates mounding interactions. 2 D fingerprint plots of DP depicts that the existence of a CH_3 group enhances the number of H…H interactions (60.5%), which tend to connect with neighboring aromatic or methyl hydrogens of yet another moiety and the second dominant interactions seen in DP is the C….H interactions. In SA, H…H interactions contributes 32.9% is the interaction

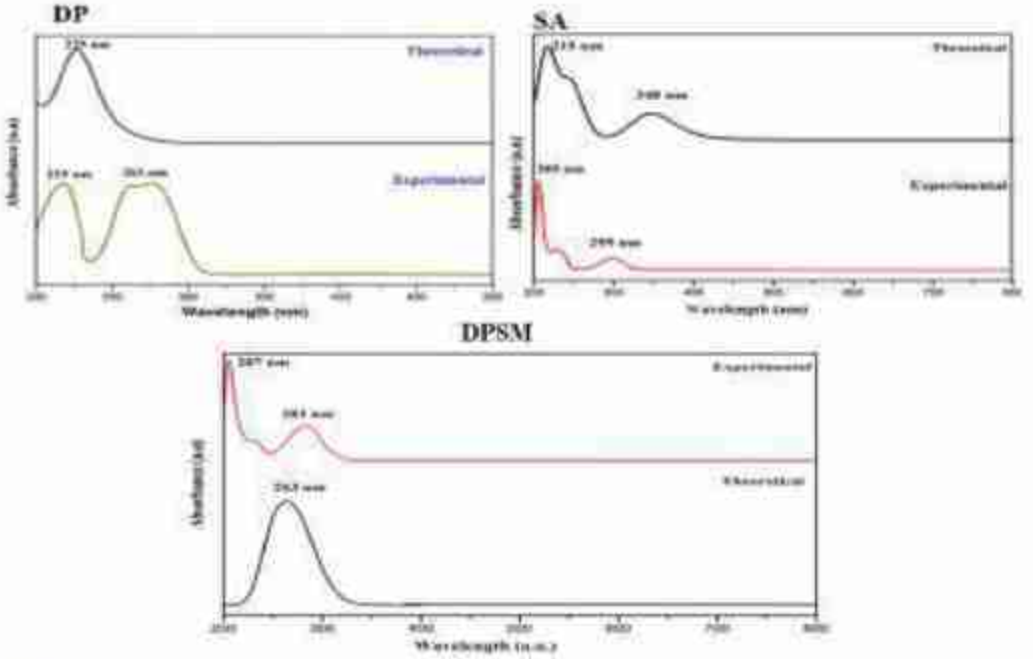

Figure 7. Experimental and Theoretical UV-Visible spectra of DP, SA and DPSM.

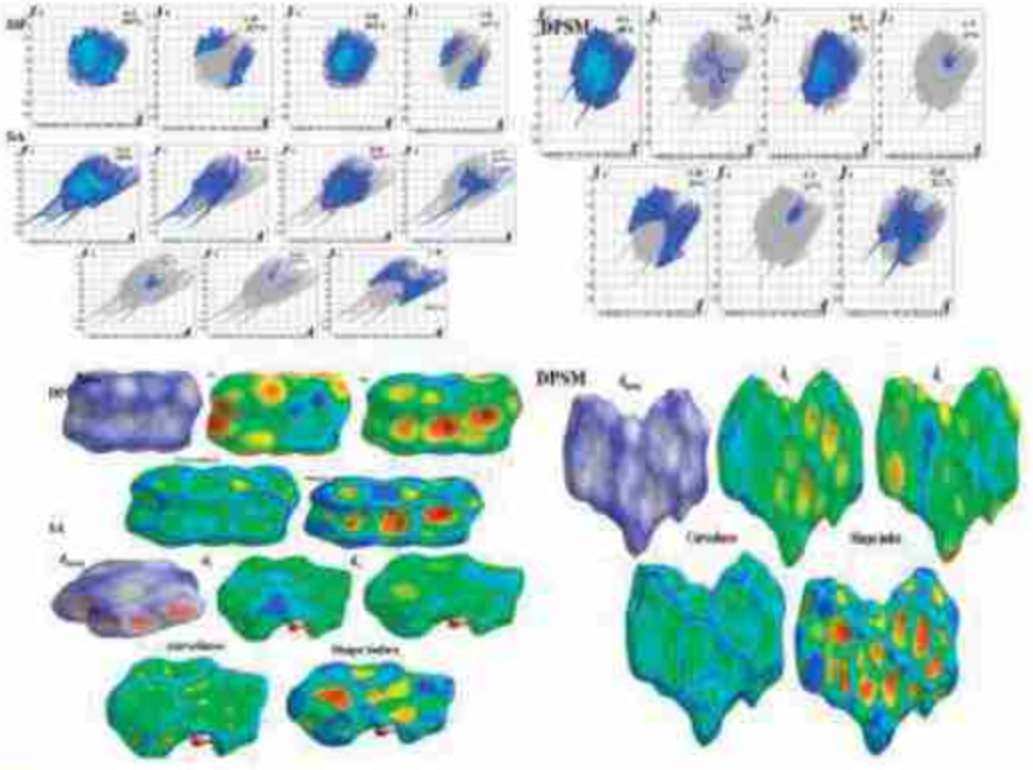

Figure 8. d_{norm}, d_i, d_e, shape index, and curvedness of DPSM, DP and SA and 2D fingerprint plots.

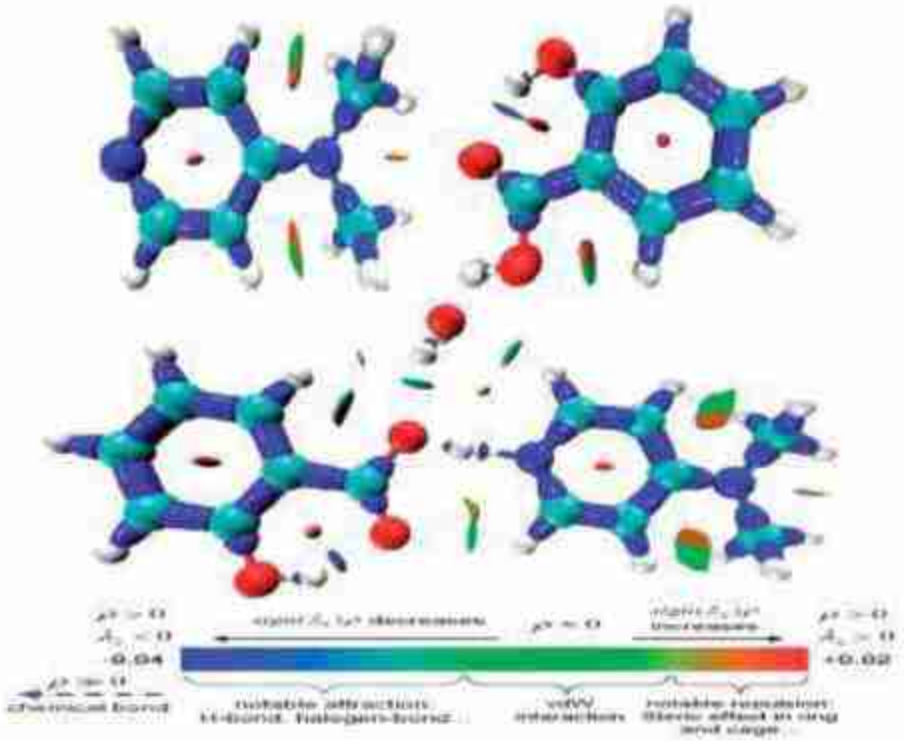

Figure 9. Isosurface density plots illustrating the bonded and non-bonded interactions.

between the hydrogen atoms of the ring and the Hydrogen atoms of the carboxylic and hydroxyl group. The next dominant interaction in SA is the O … H interaction which occurs between the hydroxyl and carboxylic acid group. The proportions of the O … H interactions in DPSM found to be 21.1% validates the intermolecular interactions between the salicylate and 4-dimethylamino-pyridinium moiety. The H … H interaction has the highest contribution in DP, SA and DPSM.

4.9. Interaction region indicator analysis

Reduced Density Gradient (RDG) analysis has been extensively utilized to help graphically demonstrate weak interaction zones; however, it also has the propensity to reveal chemical bonding sites. Unfortunately, RDG is incapable of portraying both types of interactions simultaneously time. Interaction region indicator (IRI), a subtle modification on RDG, can efficiently uncover chemical bonding and weak interaction zones, making it incredibly valuable in the research of many chemical systems and chemical processes. Figure 9 depicts isosurface density maps illustrating bound and non-bonded interactions DP, SA and DPSM.

Red patches in the center of the pyridine rings and phenyl ring indicate the presence of steric interaction, whereas green flaky patches indicate the presence of weak non-covalent H … H hydrogen bonding interaction. The blue color patch denotes a more favorable interaction, which is associated with strong hydrogen bonds (O–H … O, N–H … O). It is seen from the IRI plot of DP that there is no strong hydrogen bonding interaction. The blue color encircling the bonds signifies covalent bonds where bonds merge with the carbon's atomic region (C–C) is significantly greater than that of oxygen and nitrogen atoms (C–O, C–N, O–H) owing to a broader spatial extension of core electrons density ascribed to a smaller nuclear charge.

Table 4. Antibacterial activity of DPSM.

	Zone of inhibition (mm)		
Bacterial pathogens	0.1 µL	0.2 µL	0.3 µL
Bacillus subtilis	7	10	12
Streptococcus pneumoniae	7	11	14
Klebsiella pneumoniae	10	14	17

4.10. Biological evaluation

4.10.1. Antibacterial evaluation

DPSM was tested for antibacterial activity against Bacterial strains such as *Klebsiella pneumoniae*, *Streptococcus pneumoniae* and *Bacillus subtilis*. *Streptococcus pneumoniae* is an anaerobic gram-positive bacterium that causes pneumococcal infections. Streptococcus pneumoniae germs induce pneumococcal infection. This bacterium infects the lungs (pneumonia), the ears (otitis), the sinuses (sinusitis), the brain and spinal cord tissue (meningitis), and the blood (bacteremia). When people with pneumococcal illness cough or sneeze, they can transfer the bacterium toward others. *Klebsiella pneumoniae* is a gram-negative bacterium that can induce pneumonia, bloodstream infections, and meningitis. Klebsiella must enter the respiratory (breathing) tract to induce pneumoniae, or the bloodstream to generate a bloodstream infection. Klebsiella bacteria may be disseminated by person-to-person contact and not through the air. Patients in hospital settings may also be exposed to Klebsiella if they are on ventilators (breathing machines), have intravenous (vein) catheters, or have wounds (caused by injury or surgery). Bacillus subtilis, often referred as hay bacillus or grass bacillus, is a Gram-positive, catalase-positive bacteria found in soil, ruminant gastrointestinal tracts, humans, and marine sponges. The diameter of the inhibitory zone surrounding each disk was evaluated after 24 h of incubation at 37 °C, and the results are shown in Table 4. DPSM activity against bacterial pathogens is photographed and depicted in Figure 10.

From Table 4, it is evident that DPSM has high activity against *Klebsiella pneumoniae* when compared to other bacteria. These findings clearly show that the compound has antibacterial action against all the bacterial pathogens that were tested.

Among all the three DPSM inhibits the *K. pneumoniae* more and the second pathogen that was inhibited more was the *Streptococcus pneumoniae*. Both these bacteria's are the main source for the pneumococcal infections and as DPSM inhibits these bacteria it is clear that DPSM can be used to treat the infections caused by these bacteria. Moreover, DPSM can be used as an oral drug to treat the antibacterial infections which are reported in our previous work. Substitution of methyl group in pyridine ring is responsible for the antibacterial activity of DPSM.

4.10.2. Molecular docking

Molecular docking is a meticulously used computational tool for assessing binding patterns in protein. Intending to endorse the biological activity of DPSM was chosen to dock into the active site of antibacterial proteins, Escherichia coli enonyl acyl carrier protein (1QG6), Staphylococcus aureus enonyl acyl carrier protein reductase (3GR6), staphylococcus aureus, an antibacterial protein (4QLO) Escherichia coli (5I5H), 5XUN a Klebsiella pneumoniae protein and 6LNW, Streptococcus pneumoniae protein. These proteins were selected as the antibacterial evaluation of DPSM compound was performed with those bacterial strains and PDB structures of target proteins were downloaded from RCSB protein data bank. Table 5 depicts docking characteristics such as predicted inhibition constant, binding energy, and bond distance, which all play a role in determining the nature of a molecule. The binding energy value of the target protein is associated to its docking score, and the more negative the binding energy value, the better the docking score. DPSM bind with the amino acid residues LYS'163 of protein 1QG6 with the binding

Figure 10. DPSM activity against bacterial pathogens.

Table 5. Docking parameters of DPSM.

Protein	Bonded residue	Bonded distance Å	Binding energy kcal/mol	Inhibition constant milli Molar (mM)
1QG6	LYS'163	1.8	−4.73	0.341
3GR6	SER'44	2.2	−5.19	0.156
5I5H	LEU'547	2.3	−4.34	0.655
	ARG'554	2.2		
	ARG'554	2.4		
	ASN'432	2.4		
	ILE'427	1.8		
	GLY'269	2.5		
4QLO	ALA'77	1.7	−4.04	1.09
	SER'154	2.7		
5XUN	LEU'132	2.8	−5.84	0.102
6LNW	LYS'252	2.2	−3.85	0.160
	ILE'279	2.6		
	VAL'242	1.2		

energy of −4.73 kcal/mol and in the 3GR6 protein, DPSM forms hydrogen bonds with the amino acid SER'44 with binding energy of −5.19 kcal/mol, DPSM binds with the amino acids LEU'547, ARG'554, ARG'554, ASN'432, ILE'427 and GLY'269 of the protein 5I5H with binding energy of −4.34 kcal/mol and with 4QLO it binds with the amino acid ALA'77, SER'154, with binding energy −4.04 kcal/mol. Amino acid LEU'132 of 5XUN forms hydrogen bonds with DPSM with a binding energy of −5.84 kcal/mol and also amino acids LYS'252, ILE'279, VAL'242 of 6LNW with binding energy of −3.85 kcal/mol . Among these proteins, 5XUN has the lowest binding energy and the smallest inhibition constant, implying that it has a great affinity toward DPSM.

Figure 11 exhibits the interactions of the DPSM molecule as the ligand with all four target proteins. Hydrogen bonds are a major component in drug binding affinity with receptors. A sturdy hydrogen bonding interaction exemplifies a lofty binding capacity between ligand and protein.[55,56] In general, hydrogen bonds emerge when hydrogen is linked to an electronegative atom (oxygen, nitrogen) and another atom with a single electron pair. Figure 11 shows that hydrogen bonds are formed between the hydrogen atoms and the oxygen/nitrogen atoms of the ligand and the protein. Docking conformation of the ligand with the proteins reveals that hydrogen bonds are exclusively formed at the atoms O15, O13. The hydrogen atoms in the hydroxyl group act as hydrogen bond donors, whereas the oxygen atoms in the carbonyl group operate as hydrogen bond acceptors, according to the MEP plot and Fukui functions. From FMO analysis, a high electrophilicity index of 13.40 eV, implies that DPSM has a high affinity for protein binding. The interaction of DPSM with antibacterial proteins supports the compound's antibacterial efficacy and the results of the molecular docking investigations are additionally bolstered by topological analyses of DPSM. From the molecular docking and antibacterial evaluation, it is validated that

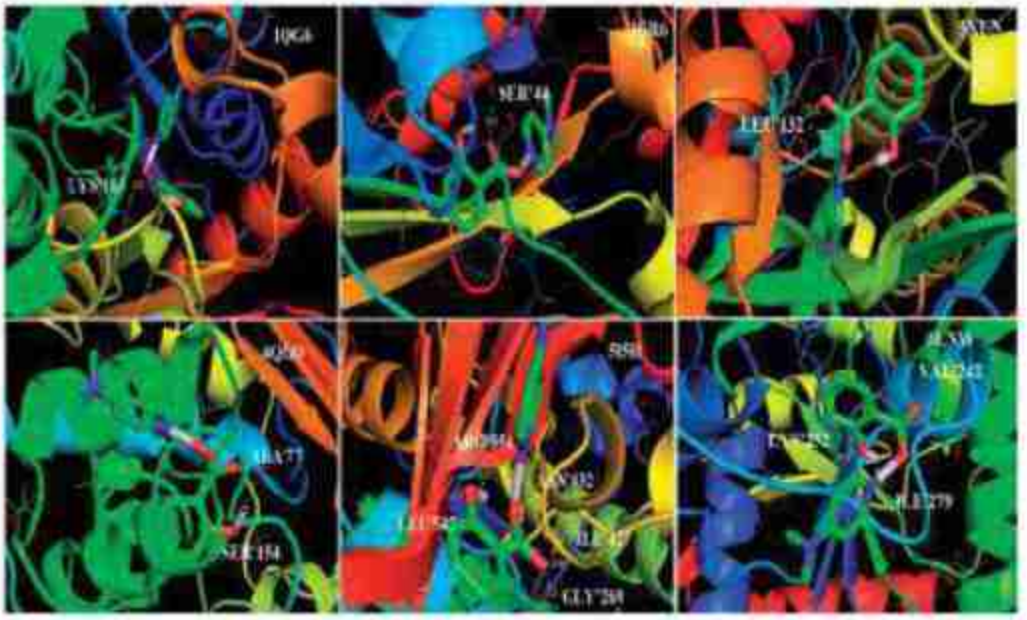

Figure 11. Molecular docking of target proteins with DPSM.

the DPSM compound inhibits the bacteria Klebsiella pneumoniae more when compared with others. Deephlin et al. reported the pharmaceutical properties of DPSM and was proposed to be used as an orally active drug. As the antibacterial evaluation and molecular docking evaluation validates that DPSM inhibits Klebsiella pneumoniae DPSM can be used as a drug to treat Pneumococcal infections.

5. Conclusion

In the present work, a study on the impact of hydrogen bonding interactions on structural, vibrational, electronic and biological properties of DPSM was effectuated using quantum chemical computation method. The optimized geometrical parameters for DPSM correlate well with experimental data. The deviations of carboxylic group bond length in DPSM and SA provide clear evidence for the deprotonation. The presence of intermolecular hydrogen bonding N–H…O interaction is revealed by NBO analysis, which is caused by a hyperconjugative interaction between the carbonyl oxygen atom donor and the pyridine ring N–H acceptor. From vibrational analysis, it is endorsed that stretching wave number of hydrogen bond donor O–H and hydrogen bond acceptor C–O is red shifted due to elongation in respective bond lengths. FMO analysis reveals the presence of intermolecular charge transfer from electron rich pyridine to electron deficient salicylate which is further confirmed by charge transfer due to excitation. Band gap of DPSM established to be 3.27 eV endorses the high chemical reactivity of molecule upholds the biological activity and electrophilicity index reckoned to be 13.40 eV bespeak that DPSM has high binding capacity with bio molecules owing to its electrophilic nature. The energy gap of the DPSM is small when compared to the precursor molecules. The salicylic acid with hydroxyl group is mainly responsible for the lowering of the frontier orbital energy gap of DPSM. From the molecular docking and antibacterial evaluation, it is validated that the DPSM compound inhibits the bacteria Klebsiella pneumoniae more when compared with others. Deephlin et al. reported the pharmaceutical properties of DPSM and was proposed to be used as an orally active

drug. As the antibacterial evaluation and molecular docking evaluation validates that DPSM inhibits Klebsiella pneumoniae DPSM can be used as a drug to treat Pneumococcal infections.

Acknowledgements

The authors thank Dr. I. Hubert Joe, Associate Professor of Department of Physics, Kerala University for granting us permission to do computational works in their Research Lab.

Disclosure statement

No potential conflict of interest was reported by the author(s).

References

1. Y. Hamada, "Role of Pyridines in Medicinal Chemistry and Design of BACE1 Inhibitors Possessing a Pyridine Scaffold," in *Pyridine* (Rijeka: Intechopen, 2018).
2. C. Neelakanda Pillai, and J. Chellapan, "Effect of Protonation and Hydrogen Bonding on 2, 4, 6-Substituted Pyrimidine and Its Salt Complex-Experimental and Theoretical Evidence," *Journal of Molecular Modeling* 20, no. 3 (2014): 2139.
3. A. Arunkumar, and P. Ramasamy, "Synthesis, Crystal Structure, Spectral and Thermal Properties of 4-Dimethylaminopyridinium Salicylate Monohydrate," *Applied Physics A* 111, no. 4 (2013): 1165–73. https://doi.org/10.1007/s00339-012-7336-1
4. X.D. Divya Dexlin, J.D. Deephlin Tarika, S. Madhan. Kumar, A. Mariappan, and T. Joselin. Beaula, "Synthesis and DFT Computations on Structural, Electronic and Vibrational Spectra, RDG Analysis and Molecular Docking of Novel anti COVID-19 Molecule 3, 5-Dimethyl Pyrazolium 3, 5-Dichloro Salicylate," *Journal of Molecular Structure* 1246 (2021): 131165.
5. Stevan. Armakovic, Sanja J. Armakovic', Jovan P. Šetrajcic, and Igor J. Šetrajcic, "Optical and Bowl-to-Bowl Inversion Properties of Sumanene Substituted on Its Benzylic Positions; a DFT/TD-DFT Study," *Chemical Physics Letters* 578 (2013): 156–61.
6. Vidya V. Menon, Edakot. Faral, YSheena. Mary, CYohannan. Panicker, Stevan. Armakovic, Sanja J. Armakovic, f Subhan Nagarajan, and C. Van Alsenoy, "FT-IR, FT-Raman and NMR Characterization of 2-Isopropyl-5-Methylcyclohexyl Quinoline-2-Carboxylate and Investigation of Its Reactive and Optoelectronic Properties by Molecular Dynamics Simulations and DFT Calculations," *Journal of Molecular Structure* 1127 (2017): 124–37.
7. Milan Vranes, Stevan Armaković, Aleksandar Tot, Snežana Papović, Nebojša Zec, Sanja Armaković, Nemanja Banić, Biljana Abramović, and Slobodan Gadžurić, "Structuring of Water in the New Generation Ionic Liquid – Comparative Experimental and Theoretical Study," *The Journal of Chemical Thermodynamics* 93 (2016): 164–71.
8. Y.M. Issa, S.A. Abdel-Latif, A.L. El-Ansary, and H.B. Hassib, "The Synthesis, Spectroscopic Characterization, DFT/TD-DFT/PCM Calculations of the Molecular Structure and NBO of the Novel Charge-Transfer Complexes of Pyrazine Schiff Base Derivatives with Aromatic Nitro Compounds," *New Journal of Chemistry* 45, no. 3 (2021): 1482–99.
9. S.A. Abdel-Latif, and H. Moustafa, "Synthesis, Characterization, Electronic Structure, and Non-Linear Optical Properties (NLO) of Mn(II), Co(II), Ni(II), Cu(II) and Zn(II) Complexes with 5-Phenylazo-8-Hydroxyquinoline Using DFT Approach," *Applied Organometallic Chemistry* 31, no. 12 (2017): e3876.
10. S.A. Abdel-Latif, and A.A. Mohamed, "Synthesis, Structure, Spectroscopic Properties and DFT Studies on Some 7-Hydroxy-4-Methyl-8-(Arylazo)-2H-1-Benzopyran-2-One and Their Complexes with Some Divalent Transition Metal Ions," *Journal of Molecular Structure* 1134 (2017): 307–18.
11. A.F. Darweesh, N.A. Abd El-Fatah, S.A. Abdel-Latif, I.A. Abdelhamid, A.H.M. Elwahy, and M.E. Salem, "Synthesis and DFT Studies of Novel Aminoimidazodipyridines Using 2-(3H-Imidazo [4, 5-b] Pyrid-2-yl) Acetonitrile as an Efficient Key Precursor," *Arkivoc* 2021, no. 8 (2021): 23–37.
12. A.D. Becke, "Density-Functional Thermochemistry. III. The Role of Exact Exchange," *The Journal of Chemical Physics* 98, no. 7 (1993): 5648–52. https://doi.org/10.1063/1.464913
13. R. Ditchfield, W.J. Hehre, and J.A. Pople, "Self-Consistent Molecular Orbital Methods. 9. Extended Gaussian-Type Basis for Molecular-Orbital Studies of Organic Molecules," *The Journal of Chemical Physics* 54, no. 2 (1971): 724–8.

14. M.J. Frisch, G.W. Trucks, H.B. Schlegel, G.E. Scuseria, M.A. Robb, J.R. Cheeseman, G. Scalmani, V. Barone, B. Mennucci, G.A. Petersson, et al., *Gaussian 09, Revision C.02* (Wallingford CT: Gaussian Inc., 2010).
15. E.D. Glendening, A.E. Reed, J.E. Carpenter, and F. Weinhold, *NBO Version 3.1* (Wisconsin, MI: TCI, University of Wisconsin, 1998).
16. J.E. Carpenter, and F. Weinhold, "Analysis of the Geometry of the Hydroxymethyl Radical by the Different Hybrids for Different Spins Natural Bond Orbital Procedure," *Journal of Molecular Structure: Theochem* 169 (1988): 41–62.
17. F. Weinhold, and J.E. Carpenter, *The Structure of Small Molecules and Ions*, ed. R. Naaman and Z. Vager (New York: Plenum, 1988), 227–36.
18. A.E. Reed, L.A. Curtiss, and F. Weinhold, "Intermolecular Interactions from a Natural Bond Orbital, Donor-Acceptor Viewpoint," *Chemical Reviews* 88, no. 6 (1988): 899–926.
19. T. Sundius, "Scaling of ab Initio Force Fields by MOLVIB," *Vibrational Spectroscopy* 29, no. 1–2 (2002): 89–95. https://doi.org/10.1016/S0924-2031(01)00189-8.
20. T. Sundius, "MOLVIB - A Flexible Program for Force Field Calculations," *Journal of Molecular Structure* 218 (1990): 321–6. https://doi.org/10.1016/0022-2860(90)80287-T.
21. P. Pulay, G. Fogarasi, G. Pongor, J.E. Boggs, and A. Vargha, "Combination of Theoretical ab Initio and Experimental Information to Obtain Reliable Harmonic Force Constants," *Journal of the American Chemical Society* 105, no. 24 (1983): 7037–47. https://doi.org/10.1021/ja00362a005.
22. Tian. Lu, and Feiwu. Chen, "Multiwfn: A Multifunctional Wave Function Analyser," *Journal of Computational Chemistry* 33, no. 5 (2012): 580–92. https://doi.org/10.1002/jcc.22885.
23. W. Humphrey, A. Dalke, and K. Schulten, "VMD: Visual Molecular Dynamics," *Journal of Molecular Graphics* 14, no. 1 (1996): 33–8. https://doi.org/10.1016/0263-7855(96)00018-5.
24. G.M. Morris, R. Huey, W. Lindstrom, M.F. Sanner, R.K. Belew, D.S. Goodsell, and A.J. Olson, "Autodock4 and AutoDockTools4: Automated Docking with Selective Receptor Flexibility," *Journal of Computational Chemistry* 30, no. 16 (2009): 2785–91.
25. R. Arivazhagan, C. Sridevi, and A. Prakasam, "Exploring Molecular Structure, Spectral Features, Electronic Properties and Molecular Docking of a Novel Biologically Active Heterocyclic Compound 4-Phenylthiosemicarbazide," *Journal of Molecular Structure* 1232 (2021): 129956. https://doi.org/10.1016/j.molstruc.2021.129956
26. T. Joselin Beaula, and C. James, "FT-IR, FT-Raman Spectra and Chemical Computations of Herbicide 2-Phenoxy Propionic acid-A DFT Approach," *Spectrochimica Acta. Part A, Molecular and Biomolecular Spectroscopy* 122 (2014): 661–9. https://doi.org/10.1016/j.saa.2013.10.126
27. C. Jesintha John, M. Amalanathan, A.R. Twinkle, P. Srinivasan, and I. Hubert Joe, "Vibrational Spectra and First Order Hyper Polarizability Studies of Dimethyl Amino Pyridinium 4-Nitrophenolate 4-Nitrophenol," *Spectrochimica Acta. Part A, Molecular and Biomolecular Spectroscopy* 81, no. 1 (2011): 151–61. https://doi.org/10.1016/j.saa.2011.05.086
28. T.Joselin. Beaula, P. Muthuraja, M. Dhandapani, and V. Bena Jothy, "Effect of Charge Transfer with Spectral Analysis on the Antibacterial Compound 4-(Dimethyl Amino) Pyridine: 3,5-Dinitrobenzoic Acid: Experimental and Theoretical Perspective," *Journal of Molecular Structure* 1171 (2018): 511–26. https://doi.org/10.1016/j.molstruc.2018.06.026.
29. T.Joselin Beaula, D. Manimaran, I. Hubert Joe, V.K. Rastogi, and V. Bena Jothy, "Vibrational Spectroscopic Studies and DFT Computation of the Nonlinear Optical Molecule L-Valinium Formate," *Spectrochimica Acta. Part A, Molecular and Biomolecular Spectroscopy* 126 (2014): 170–7. https://doi.org/10.1016/j.saa.2014.01.088.
30. R.A. Engh, and R. Huber, "Accurate Bond and Angle Parameters for X-Ray Protein-Structure Refinement," *Acta Crystallographica Section A Foundations of Crystallography* 47, no. 4 (1991): 392–400. https://doi.org/10.1107/S0108767391001071
31. H. Arslan, U. Florke, N. Kulcu, and G. Binzet, "The Molecular Structure and Vibrational Spectra of 2-Chloro-N-(Diethylcarbamothioyl)Benzamide by Hartree-Fock and Density Functional Methods," *Spectrochimica Acta. Part A, Molecular and Biomolecular Spectroscopy* 68, no. 5 (2007): 1347–55. https://doi.org/10.1016/j.saa.2007.02.015.
32. R.J. Gillespie, "The VSEPR Model Revisited," *Chemical Society Reviews* 21, no. 1 (1992): 59–69. https://doi.org/10.1039/CS9922100059.
33. G. Velraj, S. Soundharam, and C. Sridevi, "Investigation of Structure, Vibrational, Electronic, NBO and NMR Analyses of 2-Chloro-4-Nitropyridine (CNP), 2-Chloro-4-Methyl-5-Nitropyridine (CMNP) and 3-Amino-2-Chloro-4-Methylpyridine (ACMP) by Experimental and Theoretical Approach," *Spectrochimica Acta. Part A, Molecular and Biomolecular Spectroscopy* 137 (2015): 790–803. https://doi.org/10.1016/j.saa.2014.08.075.
34. G. Varsanyi, *Assignments for Vibrational Spectra of Seven Hundred Benzene Derivaties*, Vol. 1 (London: Adam Hilger, 1974).

35. G. Socretes, *Infrared and Raman Characteristic Group Frequencies: Tables and Charts*, 3rd ed. (Chichester: Wiley, 2001).
36. K.R. Santhy, M. Daniel Sweetlin, S. Muthu D, Christina Susan Abraham, and M. Raja, "Molecular Structure, Spectroscopic (FT-IR, FT-Raman) Studies, HOMO–LUMO and Fukui Function Calculations of 2-Acetyl Amino-5-Bromo-4 Methyl Pyridine by Density Functional Theory," *Chemical Data Collections* 24 (2019): 100291. https://doi.org/10.1016/j.cdc.2019.100291.
37. Brian C. Smith, *Infrared Spectral Interpretation: A Systematic Approach* (Boca Raton, FL: CRC Press, 1998).
38. N.B. Colthup, L.H. Daly, and S.E. Wiberly, *Introduction to Infrared and Raman Spectroscopy* (New York: Academic Press, 1990).
39. V. Hernandez, C. Castiglioni, and G. Zerbi, "Hyperconjugation from Infrared Intensities:The Case of Methyl Acetate and of Its Selectively Deuterated Derivatives," *Journal of Molecular Structure* 324, no. 1–2 (1994): 189–98. https://doi.org/10.1016/0022-2860(94)08239-1.
40. Chenefa AitYoucef Hakima, and Riadh. Bourzami, "Synthesis, Single Crystal X-Ray Structure and Vibrational Spectroscopic Characterization Study of a New Hybrid Material Crystal: Bis(2,4,6-Trihydroxy-1,3,5-Triazin-1-Ium) Bischloride Monohydrate," *Journal of Molecular Structure* 1191 (2019): 218–24. https://doi.org/10.1016/j.molstruc.2019.03.039.
41. R.N. Singh, Amit Kumar, R.K. Tiwari, Poonam Rawat, and V.P. Gupta, "A Combined Experimental and Quantum Chemical (DFT and AIM) Study on Molecular Structure, Spectroscopic Properties, NBO and Multiple Interaction Analysis in a Novel Ethyl 4-[2-(Carbamoyl)Hydrazinylidene]-3,5-Dimethyl-1Hpyrrole-2-Carboxylate and Its Dimer," *Journal of Molecular Structure* 1035 (2013): 427–40. https://doi.org/10.1016/j.molstruc.2012.11.059.
42. V. Balachandran, S. Rajeswari, and S. Lalitha, "DFT Computations, Vibrational Spectra, Monomer, Dimer, NBO and NMR Analyses of Antifungal Agent: 3, 5-Dibromosalicylic Acid," *Journal of Molecular Structure* 1007 (2012): 63–73. https://doi.org/10.1016/j.molstruc.2011.10.014.
43. J.D. Deephlin Tarika, X.D. Divya Dexlin, S. Madhan Kumar, D.Deva. Jayanthi, and T.Joselin. Beaula, "Tuning the Computational Evaluation of Spectroscopic, ELF, LOL, NCI Analysis and Molecular Docking of Novel anti COVID-19 Molecule 4-Dimethylamino Pyridinium 3, 5-Dichlorosalicylate," *Spectrochimica Acta. Part A, Molecular and Biomolecular Spectroscopy* 259 (2021): 119907. https://doi.org/10.1016/j.saa.2021.119907
44. S.J. Jenepha Mary, Mohd Usman Mohd. Siddique, Sayantan. Pradhan, Venkatesan. Jayaprakash, and C. James, "Quantum Chemical Insight into Molecular Structure, NBO Analysis of the Hydrogen-Bonded Interactions, Spectroscopic (FT–IR, FT–Raman), Drug Likeness and Molecular Docking of the Novel anti COVID-19 Molecule 2-[(4,6-Diaminopyrimidin-2-yl)Sulfanyl]-N-(4-Fluorophenyl)Acetamide Dimer," *Spectrochimica Acta Part A: Molecular and Biomolecular Spectroscopy* 244 (2021): 118825. https://doi.org/10.1016/j.saa.2020.118825.
45. Mariana Rocha, Alejandro Di Santo, Juan Marcelo Arias, Diego M. Gil, and Aída Ben Altabe, "Ab-Initio and DFT Calculations on Molecular Structure, NBO, HOMO–LUMO Study and a New Vibrational Analysis of 4-(Dimethylamino) Benzaldehyde," *Spectrochimica Acta Part A: Molecular and Biomolecular Spectroscopy* 136, no. 136 (2015): 635–43. https://doi.org/10.1016/j.saa.2014.09.077.
46. Mohammad Abdul Mumit, Tarun Kumar Pal A, Md Ashraful Alam, Md Al-Amin-Al-Azadul Islam, Subrata Paul, and Chanmiya Sheikh, "DFT Studies on Vibrational and Electronic Spectra, HOMO-LUMO, MEP, HOMA, NBO and Molecular Docking Analysis of Benzyl-3-N-(2,4,5-Trimethoxyphenylmethylene) Hydrazine Carbodithioate," *Journal of Molecular Structure* 1220 (2020): 128715. https://doi.org/10.1016/j.molstruc.2020.128715.
47. P. Manjusha, Johanan Christian Prasana, S. Muthu, and B. Fathima Rizwana, "Spectroscopic Elucidation (FT- IR, FT- Raman and UV- Visible) with NBO, NLO, ELF, LOL, Drug Likeness and Molecular Docking Analysis on 1-(2-Ethylsulfonylethyl)-2-Methyl-5-Nitro-Imidazole: An Antiprotozoal Agent," *Computational Biology and Chemistry* 88 (2020): 107330. https://doi.org/10.1016/j.compbiolchem.2020.107330
48. R. Mohamed Asath, R. Premkumar, T. Mathavan, and A. Milton Franklin Benial, "Spectroscopic and Molecular Docking Studies on N, N-di-Tert-Butoxycarbonyl (Boc)-2-Amino Pyridine: A Potential Bioactive Agent for Lung Cancer Treatment," *Journal of Molecular Structure* 1143 (2017): 415–23. https://doi.org/10.1016/j.molstruc.2017.04.117
49. Hadjer Bougherara, Rayene Kadri, Mekki Kadri, Mohamed Yekhlef, and Abdecharif Boumaza, "Complex of 4-(2-Aminophenyl) 1, 2, 3-Thiadiazole with 2, 3-Dichloro-5, 6- Dicyano-1, 4-Benzoquinone: Experimental Study and Investigation at Different Exchange-Correlation Functionals. DOS, NBO, QTAIM and RDG Analyses," *Journal of Molecular Structure* 1223 (2021): 128855–6860. https://doi.org/10.1016/j.molstruc.2020.128855.
50. Fathima Rizwana B, Johanan Christian Prasana, S. Muthu, and Christina Susan Abraham, "Molecular Docking Studies, Charge Transfer Excitation and Wave Function Analyses (ESP, ELF, LOL) on Valacyclovir:

A Potential Antiviral Drug," *Computational Biology and Chemistry* 78 (2019): 9–17. https://doi.org/10.1016/j.compbiolchem.2018.11.014.

51. A. Guido, P. Cortona, B. Mennucci, and C. Adamo, "On the Metric of Charge Transfer Molecular Excitations: A Simple Chemical Descriptor," *Journal of Chemical Theory and Computation* 9, no. 7 (2013): 3118–26.
52. B. Fathima Rizwana, Johanan Christian Prasana, Christina Susan Abraham, and S. Muthu, "Spectroscopic Investigation, Hirshfeld Surface Analysis and Molecular Docking Studies on anti-Viral Drug Entecavir," *Journal of Molecular Structure* 1164 (2018): 447–58. https://doi.org/10.1016/j.molstruc.2018.03.090.
53. J.D. Deephlin Tarika, C.L. Shiny, X.D. Divya Dexlin, D.Deva. Jayanthi, S. Antony, and TJoselin. Beaula, "Probing into the Outcome of Charge Transfer Interactions and Hyperconjugative Effect on the Antibacterial Molecule 4-Dimethylaminopyridine Using Spectroscopic Elucidations and DFT Calculations," *Journal of Molecular Structure* 1251 (2022): 132059. https://doi.org/10.1016/j.molstruc.2021.132059
54. M. Chen, U.V. Waghmare, C.M. Friend, and E. Kaxiras, "A Density Functional Study of Clean and Hydrogen-Covered α-MoO3(010): Electronic Structure and Surface Relaxation," *Journal of Chemical Physics* 109 (1998): 6854. https://doi.org/10.1063/1.477252
55. J. Lanie, W. Leung-Ng, K. Kazmierczak, T. Andrzejewski, T. Davidsen, K. Wayne, H. Tettelin, J. Glass, M. Winkler, and M. "Genome Sequence of Avery's Virulent Serotype 2 Strain D39 of Streptococcus pneumoniae and Comparison with That of Unencapsulated Laboratory Strain R6," *Journal of Bacteriology* 189, no. 1 (2007): 38–51.
56. T. Pantsar, and A. Poso, "Binding Affinity via Docking: fact and Fiction," *Molecules* 23, no. 8 (2018): 1899.
57. K. Arulaabaranam, G. Mani, and S. Muthu, "Computational Assessment on Wave Function (ELF, LOL) Analysis, Molecular Confirmation and Molecular Docking Explores on 2-(5-Amino-2-Methylanilino)-4-(3-Pyridyl) Pyrimidine," *Chemical Data Collections* 29 (2020): 100525. https://doi.org/10.1016/j.cdc.2020.100525

Wireless Personal Communications: An International Journal

H.264 Video Compression Using Novel Refined Huffman Codes for Omnipresent Applications

Authors: T. Kavitha, K. Jaya Sankar Authors Info & Claims

Wireless Personal Communications: An International Journal, Volume 131, Issue
• Aug 2023 • pp 2949–2967 • https://doi.org/10.1007/s11277-023-10590-2

Published: 20 July 2023 Publication History

Abstract

Abstract

data. To efficiently store and transmit huge volumes of data is a challenge. The data compression addresses the problem of efficient storing and transmitting of

Peak-Signal-to-Noise-Ratio (PSNR) is always in demand. In this research work, compression of video is considered to achieve higher Compression Ratio and reduce the effective overheads involved in coding. The research work is compared to the state-of-the-art existing H.264 video Compression technique. The H.264 video standard uses standard Huffman tables to encode the DCT transform coefficients. The proposed methodology adopts quantization followed by entropy coding with Refined Huffman (RH) codes which replaces the existing standard Huffman tables used for entropy coding. The performance parameters like Peak-Signal to Noise-Ratio (PSNR), Compression Ratio (CR) and Structural Similarity Index (SSIM) are evaluated to test the performance of the proposed RH codes. The proposed RH method attains improved PSNR of 8.4%, 1.3% improvement in SSIM and CR improvement of 2.76% compared to the existing MPEG compression. The experimental results using Refined Huffman codes performed well compared to the existing Standard Huffman tables.

References

1. Liu, S. (1996). Performance comparison of MPEG1 and MPEG2 video compression standards. COMPCON 96. Technologies for the Information Superhighway Digest of

Quest Journals
Journal of Electronics and Communication Engineering Research
Volume 9 ~ Issue 5 (2023) pp: 10-15
ISSN(Online) : 2321-5941
www.questjournals.org

Research Paper

Some Studies on Shielding Effectiveness for Oblique EM Waves Incidence on Dual Shields

Dr Srivalli Gundala
G Narayanamma Institute of Technology and Science, Hyderabad, INDIA

Dr VSSN Srinivasa Baba
Methodist college of Engineering and Technology, Hyderabad, INDIA

Srigada Sathwika
G Narayanamma Institute of Technology and Science, Hyderabad, INDIA

Nenavath Pooja
G Narayanamma Institute of Technology and Science, Hyderabad, INDIA

Kancharla Preethi lilly
G Narayanamma Institute of Technology and Science, Hyderabad, INDIA

Abstract *-Shielding effectiveness of various shields against angle of attack with conductors and conducting polymers using plane wave theory is carried out in this paper. The shielding efficiency of these new material combinations against EM waves is evaluated according to the angle of incidence of the dual shield. With recent advances in the synthesis of stable high-conductivity polymers, these lightweight, mechanically strong materials appear to be viable alternatives to metals for EMI shielding. A specific frequency analysis is performed ondual shield materials.*

Keywords– *shielding effectiveness, Electromagnetic Interfsrence; Dual shields; angle of incidence.*

Received *01 May, 2023;* ***Revised*** *08 May, 2023;* ***Accepted*** *10 May, 2023* © *The author(s) 2023.*
Published *with open access at* ***www.questjournals.org***

I. INTRODUCTION

Electromagnetic Interference (EMI) refers to the interference or disruption of the operation of an electronic device caused by either electromagnetic conduction or radiation from an external source. This source could be either natural or artificial and is characterized by rapidly changing electrical currents. The resulting disturbance can interrupt, obstruct, degrade or limit the effective performance of the

device.To prevent the undesired coupling of radiated electromagnetic energy into equipment, shielding is used. The design and development of electromagnetic shields aim to minimize electromagnetic interference and improve circuit compatibility. Different types of electromagnetic shields have been proposed, including single, double and multi-layered conductors, as well as conductive polymers sandwiched between conductive layers. The focus of the design is on optimizing the performance of the shielding effectiveness.

Most of the difficult shielding problems occur in communication systems where many transmitters, receivers and other sensitive equipment must be located closely together, and weight is minimized. It is difficult to predict the shielding effectiveness of any enclosure, such as an equipment package or room filtration. Therefore, it is only necessary to treat problems of this kind theoretically. Several light-weight polymers, which are essentially non-conductive but are conductive upon doping, have been studied in recent years [1-5]. These materials have several potential applications, such as electromagnetic interference (EMI) shielding, microwave attenuators, gas sensors, display units, junction devices, etc. [3,5]. Properties such as conductivity variation over a wide temperature range, light weight and high mechanical strength of the polymers make them attractive in

A Broadband MIMO Array with Gap Coupling For 5G Applications

Publisher: IEEE

Srivalli Gundala ; VSSN Srinivasa Baba ; Adepu Vijaya All Authors

Abstract:A Multiple Input Multiple Output (MIMO) array was designed using a Broadband thre which has both electric and magnetic elements to couple. A step desig... **View more**

Metadata

Abstract:

A Multiple Input Multiple Output (MIMO) array was designed using a Broadband three-patch g both electric and magnetic elements to couple. A step design is implemented between the ele Electromagnetic coupling. A MIMO Antenna of four element with a gap is designed at 3.75 GH of wideband and multiband capabilities, lower in weight, less volume with thinner dimensions. 5G Applications is the state of art Technology in which the proposed antenna is most suitable. input multiple output four element array is designed at a frequency of 3.75 GHz. The designec impedance matching and high isolation between channels. A Comparison with different substr

Compact and Hexaband Rectangular Microstrip Patch Antenna for Wireless Applications

Published: 19 September 2022

Volume 128, pages 345–363, (2023) Cite this article

Revanasiddappa Kinagi, Ravi M. Yadahalli & Siddarama Patil

Abstract

A Compact Corner Split Ring with Split C Slot Rectangular Microstrip Patch Antenna fed by a 50 Ω microstripline is discussed. A Corner split ring with C shaped slot has been etched in rectangular microstrip antenna. The slot increases the length of the surface current for the dominant mode TM_{10} leading to the decrease in resonance frequency. Size reduction and hexaband is obtained for the proposed antenna. The proposed antenna provides both size reduction and hexaband and is best suited for wireless communication. The proposed work is simulated using 3DEM of Mentorgraphics and validated. The results show that Hexaband with compactness is achieved.

Bimonthly Since 1986
ISSN 1004-9037

Publication Details

Edited by: Editorial Board of Journal of Data Acquisition and Processing
P.O. Box 2704, Beijing 100190, P.R. China
Sponsored by: Institute of Computing Technology, CAS & China Computer Federation
Undertaken by: Institute of Computing Technology, CAS
Published by: SCIENCE PRESS, BEIJING, CHINA
Distributed by:
China: All Local Post Offices

05 July 2023, Volume 38 Issue 3
Article

GENERALIZED ENERGY DETECTOR- DUAL THRESHOLDING (GED-DT) FOR COOPERATIVE SPECTRUM SENSING IN CRNS

Bosupally Nandakumar*1, Dr. K. Jaya Sankar2

Journal of Data Acquisition and Processing, 2023, **38** (3): 5096-5110 .

Abstract
Spectrum sensing is a major task in Cognitive Radio Networks which determines the presence or absence of Primary User (PU) such that the Secondary User (SU) or opportunistic user can use the unoccupied spectrum. Energy based Primary user Detection is the mostly employed strategy for spectrum sensing while it suffers from ambiguous results due to single threshold based decision making strategy. Hence, this paper proposes a new thresholding mechanism called as Dual Thresholding and applied on the Generalized Energy Detection (GED) to identify whether the Primary user is present or not. In addition, we also introduce a new fusion concept in cooperative spectrum sensing where the decision of Secondary User not only depends on his/her own decision but also on the decisions of other secondary users. Simulation experiments reveal the efficiency of proposed approach in terms of bit error rate, probability of false alarm, probability of detection.

Keyword
Cognitive Radio Networks, cooperative spectrum sensing, Single Thresholding, Dual thresholding, Fusion, Probability of false alarm, Probability of detection.

RESEACH ARTICLE

Spectrum Sensing Based Trust Aware Routing For Cognitive Radio Ad Hoc Networks (CRAHNs)

by Bosupally Nanda Kumar, K. Jaya Sankar

International Journal of Computer Applications

Foundation of Computer Science (FCS), NY, USA

Volume 185 - Number 43

Year of Publication: 2023

Authors: Bosupally Nanda Kumar, K. Jaya Sankar

10.5120/ijca2023923242

ACMRef BibTeX EndNote

Bosupally Nanda Kumar, K. Jaya Sankar , Spectrum Sensing based Trust Aware Routing for Cognitive Radio Ad hoc Networks (CRAHNs), International Journal of Computer Applications 185, 43 (Nov 2023), 36-42. DOI=10.5120/ijca2023923242

Abstract

Routing in Cognitive Radio Ad hoc Networks (CRAHNs) is a regarded as a challenging task due to the dynamic nature of frequency bands in Cognitive Radio technology. Due to varying frequency bands, the traditional networking routing protocols cannot be applied over CRAHNs. Further, the unavailability of channel information also impacts the network performance. Along with these issues, the presence of adversary nodes and their malicious actions deteriorates the network performance drastically. Hence, this paper introduces a new routing mechanism called as Spectrum Sensing based Trust Aware Routing (SSTAR) for CRAHNs. According to SSTAR, each node subjects to the computation of a trust value, cost associated with channel linked and the probability of the presence of Primary users. SSTAR forms a composite metric is formulated and establishes a secure path for source and destination node pair in the network. Simulation experiments on the proposed SSTAR prove the efficiency in terms of packet delivery ratio, delay and malicious detection rate.

References

1. Li, J., Feng, Z., Wei, Z., Feng,Z., Zhang,P., "Security management based on trust determination in cognitive radio networks", EURASIP Journal on Advances in Signal Processing, Vol. 2014, No. 1, pp. 48, 2014.
2. Vivekanand, C. V., Bagan, K.B., "Secure Distance Based Improved Leach Routing to Prevent PUEA in Cognitive Radio Network", Wireless Personal Communications, Vol. 113, pp. 1823-1837, 2020.
3. Elangovan, K., Subashini, S., "Particle bee optimized convolution neural network for managing security using cross-layer design in cognitive radio network", Journal of Ambient Intelligence and Humanized Computing, pp. 1-9, 2018.
4. Patnaik, M., Kamakoti, V., Matyáš, V., chák, V., "PROLEMus: A proactive learning-based MAC protocol against PUEA and SSDF attacks in energy constrained cognitive radio networks", IEEE Transactions on Cognitive Communications and Networking, Vol. 5, No. 2, pp. 400-412, 2019.
5. Guo, J., Zhou, X., "Secure distributed routing algorithm with optimizing energy consumption for cognitive radio networks", Wireless Personal Communications, Vol. 72, No. 4, pp. 2533-2550, 2013.
6. Nguyen-Thanh, N., Ciblat, P., Pham, A. T., Nguyen, V. T., "Surveillance strategies against primary user emulation attack in cognitive radio networks", IEEE Transactions on Wireless Communications, Vol. 14, No. 9, pp. 4981-4993, 2015.
7. Jararweh, Y., Salameh, H.A.B., Alturani, A., Tawalbeh, L., and H. Song, "Anomaly-based framework for detecting dynamic spectrum access attacks in cognitive radio networks", Telecommunication Systems, Vol. 67, No. 2, pp. 217-229, 2018.
8. Xin, C., Song, M., "Detection of PUE attacks in cognitive radio networks based on signal activity pattern", IEEE Transactions on Mobile Computing, Vol. 13, No. 5, pp. 1022-1034, 2014.
9. Karimi, A., Taherpour, A., Cabric, D., "Smart traffic-aware primary user emulation attack and its impact on secondary user throughput under rayleigh flat fading channel", IEEE Tr

International Journal on Recent and Innovation Trends in Computing and Communication
ISSN: 2321-8169 Volume: 11 Issue: 3s
DOI: https://doi.org/10.17762/ijritcc.v11i3s.6159
Article Received: 05 December 2022 Revised: 12 January 2023 Accepted: 20 January 2023

A Novel Hybrid Based Method in Covid 19 Health System for Data Extraction with Blockchain Technology

[1]Dr. C. R. Rene Robin, [2]Dr Diana Moses, [3]Dr. D. Vijendra Babu, [4]Dr. Balambigai Subramanian, [5]Dr. Siva Shankar S
[1]Professor & Dean(Innovation), Sri Sairam Engineering College, Chennai 44,
[2]Associate Professor, Department of Computer Science and Engineering, Methodist College of Engineering and Technology, King Koti, Hyderabad -500001
[3]School of Electronics Engineering, Vellore Institute of Technology, Vellore 632014.Tamil Nadu.
[4]ASSOCIATE PROFESSOR, Department of ECE, Kongu Engineering College , Perundurai , Pin code 638060.
[5]Associate Professor,Department of Computer Science and Engineering, KG REDDY COLLEGE OF ENGINEERING &TECHNOLOGY, Moinabad, Hyderabad, Telangana-501504.
[1]renerobin@sairam.edu.in, [2]itsdianamoses@gmail.com, [3]drdvijendrababu@gmail.com, [4]sbalambigai@gmail.com, [5]drsivashankars@gmail.com

Abstract: Millions of people have been afflicted by the COVID-19 epidemic, which has resulted in hundreds of thousands of fatalities throughout the world. Extracting correct data on patients and facilities with and without COVID-19 with high confidence for medical specialists or the government is extremely difficult. As a result, utilizing blockchain technology, a reliable data extraction methodology for the COVID-19 database is constructed. In this accurate data extraction model development and validation study in blockchain technology for COVID analysis, here a novel Hybrid Deep Belief Lionized Optimization (HDBLO) approach is proposed. The weights of the deep model are optimized by the fitness of lion optimization. The implementation of this work is executed using MATLAB software. The simulation outcomes shows the effective performance of proposed model in blockchain technology in COVID paradigm in terms of Mean Absolute Error (MAE), Root Mean Square Error (RMSE), accuracy, F-measure, Processing time, precision and error. Consequently, the proposed approach is compared with the conventional strategies for significant validation.

Keywords: Data Extraction, blockchain technology, COVID-19, optimization, Deep learning and performance metrics.

I. INTRODUCTION

In general, the healthcare approach has worked inside a closed loop system of submerged organizations, with physicians, radiologists, physicians, and academics serving as the key stakeholders of health data [1]. Information has only flowed in one direction, from healthcare professional to patient. Data is expanding and moving along a closed health system quicker than anything else in the era of computerized patient health information [2].Since the epidemic in Wuhan, China in December 2019, the new corona virus illness (COVID-19) has spread to practically every country. Together within month of the virus's widespread dissemination, the severity of the pandemic had grown significantly [3]. As a result, the World Health Organization (WHO) declared a Public Health Emergency of International Concern. To contain the spread of COVID-19, numerous countries had to block their borders, implement lockdowns, and employ social distance [4]. Many parts of the economy, including manufacturing, banking, agriculture, distribution networks, transportation, and tourism, experienced enormous disruptions as a result of these events [5].

In such instances, the majority of corona virus data gathered from the general population, hospitals, and diagnostic centers may be inaccurate [6]. Because of the immensity of computerized patient health information, data is not acquired according to specified criteria and is not managed or preserved effectively [7]. Existing healthcare equipment necessitates reliable data, which is critical for disseminating accurate information about the new corona virus [8]. Moreover, due of the inaccuracy and manually interpretation of huge amounts of data, viral testing utilizing medical equipment for identifying corona virus infections might take several days [9]. Lastly, following or monitoring sick individuals or their connections presents a number of privacy concerns. COVID-19's inadequacies have pushed healthcare companies to change their current digital healthcare infrastructure in order to prevent pandemic circumstances [10]. Moreover, leveraging digital platforms to battle COVID-19 and potential pandemics, it is critical to

International Journal of Soft Computing and Engineering (IJSCE)
ISSN: 2231-2307 (Online), Volume-13 Issue-1, March 2023

Secure and Light Weight Aodv (Slw-Aodv) Routing Protocol for Resilience Against Blackhole Attack in Manets

M V D S Krishna Murty, Lakshmi Rajamani

Abstract: This paper aimed at the detection of blackhole attacks and proposed a new method called as Secure and Light Weight Adhoc On demand Distance Vector Routing (SLW-AODV). SLW-AODV is an extended version of the traditional AODV routing protocol. The proposed SLW-AODV ensures resilience for both blackhole and cooperative blackhole attacks. It employs a simple Challenge, Response and Confirm (CRC) strategy with chaotic maps for the identification of both blackhole and cooperative blackhole attacks. SLW-AODV identifies the attacked nodes at both route discovery and data forwarding process. For experimental validation, we have conducted extensive simulations and the performance is validated through Packet Delivery Ratio, Throughput and Average end-to-end delay. The obtained performance metrics shows an outstanding performance than the state-of-the art methods.

Keywords: Average End-To-End Delay, Chaotic Maps, Cooperative Blackhole, MANETs

I. INTRODUCTION

Mobile Adhoc networks (MANETs) are one of the wireless networks formed with the mobile devices as nodes. Due to the nature of decentralized communication, MANETs gained huge interest in different applications including emergency rescue operations, military operations, collaborative distributed computing, disaster management and some personal area network applications [1]. In MANETs, there exists mobile nodes which don't have any fixed infrastructure and can communicate with each other through multiple hops. Since MANET is characterized as a decentralized network, communication between any two nodes requires multi-hop relays to act as routers. Every node in MANET is permitted to move arbitrarily in the network. In a MANET, all nodes are treated equivalently and so every node has the ability to transfer data between any source and destination pairs. However, the major issues in MANETs are their varying mobility nature which consequences to serious link failures, network security and quality of services challenges for researchers [2-4]. Due to the dynamic nature of MANETs and their lack of fixed infrastructure, they are generally vulnerable to several types of attacks. These attacks include sinkhole, DoS (Denial of Service), DDoS (Distributed DoS), and blackhole attacks. For example, Kalita *et al.* [5] surveyed different types of attacks associated with ad hoc networks and provided countermeasures for these attacks. Nguyen and Nguyen [6] introduced the impact of different types of attacks associated with MANETs based on a simulation study. Among the several attacks, blackhole attack is a major attack which causes serious damage to the network. Panos *et al.* [7] presented a comprehensive analysis of the blackhole attack (BHA) related to MANETs. In addition, they introduced the blackhole intensity as a new attack factor and evaluated its impact on the network performance. Khanna and Sachdeva [8] presented different aspects of blackhole attack together with the weaknesses of current literature. In addition, they introduced comprehensive classifications of the mitigation and detection schemes along with reviewing and also comprising several published work associated with those classifications. Even though several methods are proposed for blackhole attack identification in MANETs, no method was concentrated on the determination of cooperative blackhole attacks as well as on the nodes attacked by blackhole attack during data forwarding process. Hence, this paper proposes a simple and effective mechanism called as Secure and Light Weight AODV (SLW-AODV) for both blackhole and cooperative blackhole attacks detection. SLW-AODV is an extended version of the traditional AODV routing protocol. SLW-AODV follows a three-phase mechanism called as Challenge-Response-Confirm (CRC) to discover a route with no blackhole attacked nodes. The SLW-AODV can detect malicious nodes that behave abnormally during the route discovery process along with the malicious node that behaves normally during the routing process but behaves maliciously during the forwarding process. The remaining paper is organized as follows; section II explores the literature survey on blackhole detection methods. Section III explores the details of proposed SLW-AODV. Section IV explores the details of simulation experiments and the final section concludes the paper.

II. LITERATURE SURVEY

In this survey, we have explored different earlier methods those were mainly aimed for the detection of blackhole attacks in MANETs. S.

Manuscript received on 08 February 2023 | Revised Manuscript received on 13 February 2023 | Manuscript Accepted on 15 March 2023 | Manuscript published on 30 March 2023.

*Correspondence Author(s)
M V D S Krishna Murty*, Research Scholar, Department of Computer Science and Engineering, Jawaharlal Nehru Technological University Hyderabad (Telangana), India. E-mail: mkris@mvsrec.edu.in, ORCID ID: https://orcid.org/0000-0002-4705-3818
Dr. Lakshmi Rajamani, Professor and Head (Retd), Department of Computer Science and Engineering, Osmania University, Hyderabad (Telangana), India. E-mail: @lakshmanan@gmail.com

Retrieval Number: 100.1/ijsce.A35920313123
DOI: 10.35940/ijsce.A3592.0313123

Published By:
Blue Eyes Intelligence Engineering and Sciences Publication (BEIESP)

International Journal of Emerging Science and Engineering (IJESE)
ISSN: 2319-6378 (Online), Volume-11 Issue-4, March 2023

Neighbour Node Ratio AODV (NNR-AODV) Routing Protocol for Wormhole Attack Detection in Manets

M V D S Krishna Murty, Lakshmi Rajamani

Abstract: This paper aimed at the detection of wormhole attack and proposed a new method called as Neighbour Node Ratio Adhoc On demand Distance Vector Routing (NNR-AODV). NNR-AODV is an extended version of the traditional AODV routing protocol. The proposed NNR-AODV calculates the neighbour node count for every node and based on that it will decide whether the wormhole is present or not. Furthermore, NNR-AODV is able to detect both external and internal wormhole attacked nodes. Also, NNR-AODV derived a Neighbor node Threshold value which is based on the cumulative distances between nodes present in the wormhole attack. For experimental validation, we have accomplished an extensive simulation and the performance is measured through Number of bogus links, Detection rate, False positive Rate, Packet delivery ratio and Packet loss ratio. The obtained results have shown superior performance in the detection of wormhole attacks than the existing methods.

Keywords: Wormhole, Neighbor Node Threshold, Bogus Links and Node Degree.

I. INTRODUCTION

From the past few years, rapid progress in the development of Mobile Ad Hoc Networks (MANETs) has encouraged different wireless applications that can be employed in different areas viz. Entrainment, Education, Military, Emergency services and Collaborative computing [1]. Due to the special characteristics of MANETs viz. independent infrastructure and self-organizing nodes, MANETs have become an ideal choice to use in information sharing and communications. Thus, the mobile nodes of MANET can execute both for routing and hosting. In the case of routing, they work as relay nodes and forward the data of a node to its destination through standard protocols. However, the major issue in MANETs is their mobility which introduces several serious constraints on network lifetime, quality of service and security [2-4]. Due to the nature of decentralization and openness of MANETs, the mobile nodes are not reliable to constrain the membership. The mobile nodes are susceptible to different attacks [5] when those who try to compromise the node and force it to misbehave. Based on the nature of attack, they ranges from passive eavesdropping to serious battery draining. Some more attacks are there which aim at data tampering and traffic analysis through eavesdropping. In general, the attackers mainly concentrate on the resources of mobile nodes like bandwidth exhaustion, battery draining and data manipulations etc. Based on the mode of attack, they are categorized as external mode attacks and internal mode attacks [6]. The former attacks concentrate on the manipulation of routing information that propagates between mobile nodes in the network. They inject erroneous data and try to disturb the original behavior of network. An example for such kind of attack is worm-hole attack (WHA) in which a routing loop is established by the creation of a worm-hole node. Next, the internal attacks mainly target at compromising internal nodes. They distribute false data and try to disrupt the data flow. Sybil attack, grayhole attack and blackhole attack are the best examples to such kind of attacks.

Wormhole attacks are the most severe and sophisticated security threats to the MANET routing protocols where malicious nodes are placed strategically to distort the network topology and tunnel packets selectively using the false established routes [7], [8]. Wormhole detection and prevention are very challenging issues [9], [10]. The wormhole attacks can be executed by external nodes (who only forward packets and do not process the cryptographic data) or by internal nodes (the compromised nodes inside the network who process packets like other normal nodes) [11]. The internal attackers are more dangerous and difficult to detect. However, Chen *et al.* [12] hold the view that the wormhole attack is a typical external attack. Moreover, majority works of literature pay excessive attention to the external wormholes but ignore internal wormholes which are also common in MANETs.

This paper proposed a new method called as Neighbour Node Ratio AODV(NNR-AODV) routing protocol to prevent the MANETs from wormhole attacks. The proposed NNR-AODV detects both the external and internal wormhole attacks effectively. NNR-AODV derived a metric called as neighbour node threshold, which avoids the attack by performing wormhole (WH) detections for all nodes in MANETs, thus contributes in improving the accuracy of wormhole detection and saves energy.

Manuscript received on 01 March 2023 | Revised Manuscript received on 14 March 2023 | Manuscript Accepted on 15 March 2023 | Manuscript published on 30 March 2023.

*Correspondence Author(s)
M V D S Krishna Murty*, Research Scholar, Department of CSE, Jawaharlal Nehru Technological University Hyderabad (Telangana), India. E-mail: mkrishnamurty@gmail.com, ORCID ID: https://orcid.org/0000-0002-4705-3818
Dr. Lakshmi Rajamani, Professor and Head (Retd), Department of CSE, Osmania University, Hyderabad (Telangana), India. E-mail: drlrajamani@gmail.com

Retrieval Number: 100.1/ijese.D25470311423
DOI: 10.35940/ijese.D2547.0311423

Published By:
Blue Eyes Intelligence Engineering and Sciences Publication (BEIESP)

International Journal of Inventive Engineering and Sciences (IJIES)
ISSN: 2319-9598 (Online), Volume-10 Issue-2, February 2023

A Simple and Effective Intrusion Detection System for Manets

M V D S Krishna Murty, Lakshmi Rajamani

Abstract. This work proposes a simple and effective Intrusion Detection System (IDS) to classify different attacks in MANETs. IDS extracts four features for every traffic pattern and applies Support Vector Machine algorithm over them for the classification. Before applying the feature extraction, the input traffic pattern is subjected to pre-processing as it is composed of non-uniform features. IDS classifies the input traffic pattern into three classes; they are normal, blackhole and wormhole. Finally, this work analyses the feasibility of machine learning algorithms for the detection of security attacks in MANETs. For experimental validation, we have referred a self-created dataset which was acquired from the observations of blackhole and wormhole attacked node's traffic patterns. Moreover, we have also validated the proposed method through NSL-KDD dataset.

Keywords: Intrusion Detection System, Preprocessing, Feature Extraction, Support Vector Machine, Self-Created Dataset.

I. INTRODUCTION

Mobile Ad hoc networks (MANETs) are one of the wireless networks formed with the mobile devices as nodes. Due to the nature of decentralized communication, MANETs have gained huge interest in different applications including emergency rescue operations, military operations, collaborative distributed computing, disaster management and some personal network applications [1] etc. Due to the unique characteristics of mobile nodes, there are several challenges in MANETs which need to be solved. Among the several challenges, the mobility is the major challenge and it consequences to several sub-challenges. Almost all the problems in MANETs are linked with mobility of nodes. Among several sub-challenges, secure data exchange between mobile nodes is the major challenge. Due to the open network topology, distributed nature, and the absence of centralized administration in MANETs, the mobile nodes are susceptible for various attacks [2].

The impact of these attacks ranges from naive passive eavesdropping to serious battery draining attacks [3]. Majorly the attackers focus on the resources of mobile nodes like battery power, bandwidth, and data. Among the several security attacks in MANETs, blackhole attack [4] and wormhole attack [5] are the two major attacks which cause serious damages to the network. These two attacks are dynamic in nature and varies based on several network parameters. Hence, the identification of mobile nodes those were attacked with blackhole and wormhole attacks is much difficult. Recently, the involvement of artificial intelligence has been increased in different applications. Compared to the static algorithms which cannot provide any prior information about the attacks to mobile nodes, the machine learning algorithms which train the nodes can help in proper and accurate detection of attacks. A mobile node trained with the attack's characteristics can easily identify the attacked or compromised neighbour node. Hence our research has got motivated with these issues and focused over the development of effective Intrusion Detection System to solve these problems up to certain extent. This paper explains a simple and effective Intrusion Detection System for the classification of mobile nodes into three classes; they are normal, blackhole and wormhole. The overall system composed of three phases; they are pre-processing, features extraction and classification. At the initial phase, the input data is normalized and transformed into a unique format because the raw data collected from MANETs is non-uniform in nature. For feature extraction, we have employed four statistical features namely mean, variance, maximum and minimum. After feature extraction, we have applied principal component analysis for dimensionality reduction and finally Support Vector Machine (SVM) algorithm is used for classification.

The remaining paper is organized as follows; Section II explores the literature survey on IDS methods. Section III explores the details of proposed approach. Section IV explores the details of experimental analysis and the final Section concludes the paper.

II. LITERATURE SURVEY

IDS mainly works based on the principle of machine learning and information processing. In IDS, the mobile node initially learns about the characteristics of different attacks through machine learning algorithms and it becomes ready to identify the attack if occurs. IDS works on the features of network traffic (data packet and control packets).

Manuscript received on 31 January 2023 | Revised Manuscript received on 06 February 2023 | Manuscript Accepted on 15 February 2023 | Manuscript published on 28 February 2023.

*Correspondence Author
M V D S Krishna Murty*, Research Scholar, Department of Computer Science and Engineering, Jawaharlal Nehru Technological University, Hyderabad (Telangana), India. E-mail: mkrishnamurty@gmail.com, ORCID ID: https://orcid.org/0000-0002-4705-3818
Dr. Lakshmi Rajamani, Professor and Head (Retd), Department of Computer Science and Engineering, Osmania University, Hyderabad (Telangana), India. E-mail: rajlakshmi@gmail.com

Retrieval Number: 100.1/ijies.B10770210223
DOI: 10.35940/ijies.B1077.0210223

Published By:
Blue Eyes Intelligence Engineering
and Sciences Publication (BEIESP)

International Journal For Recent Developments in Science & Technology
Crossref
4575

Development and Analysis of improvised TORA Routing Protocol based on Machine Learning Model for optimal Network Performance in MANETs

M V D S Krishna Murty[1], Dr.Lakshmi Rajamani[2]

[1]M V D S Krishna Murty,Asst.Prof.,Dept of CSE,MCET,Hyderabad,Research scholar -JNTUH,mskrishnamurty@gmail.com
[2]Dr. Lakshmi Rajamani, Prof.& Head(Retd.),Dept of CSE, Osmania University, Hyderabad, drlakshmiraja@gmail.com

Abstract – *A MANET is a self configurable wireless ad-hoc network in which node mobility exists. Due to this flexibility many security threats can occur in the routing. So, in order to address this, the performance of IDS should be improvised. In this paper, a methodology is proposed based on Machine Learning(ML) algorithm in terms of accuracy and detection rate for IDS improvisation for TORA routing protocol.*

Key Words: MANET, Support Vector Machine, Intrusion Detection System, TORA (Temporally Ordered Routing Algorithm).

1.INTRODUCTION

IDS is to detect the attack before the malicious node(s) causes security threat to the network.It looks into monitoring, detecting and notifying aspects. The Blackhole attack is the most affected type on MANETs. Usage of an anomaly IDS protects the network from Black hole attack with the help of Machine Learning algorithm ,SVM

1.1 Malicious Node(s) causing Black hole attack in TORA Routing Protocol.

Black hole attack is one of the major attacks in MANETs. Malicious Node(s) causing this attack on MANET security has the data viz.Source node, Destination node and Neighbouring node. The source node sends a QRY (Query Packet) to its neighbouring nodes to search for the route destination. However, black hole node sends a fake route reply to the source node resulting packet loss which will degrade the performance of the network. In order to prevent this, the performance of the IDS should be improvised with machine learning algorithm by detecting the malicious node(s).

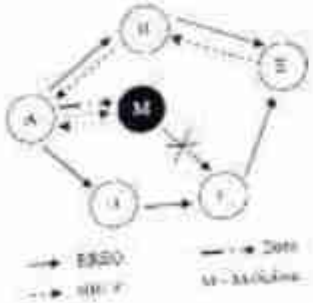

Fig(1) : Malicious Node Causing Black hole Attack

2. RELATED WORK

Kwan Hui Lim et.al Proposed two modifications to improve TORA using a network localization approach and selective node participation approach. The network localization approach initializes and maintains a localized portion of the entire network while the selective node participation approach selects a subset of nodes to participate as part of the network

Pooja Rani et.al In this paper, the protection against dual attacks has been presented for BHA and GHA by using the concept of Artificial Neural Network (ANN) as a deep learning algorithm along with the swarm-based Artificial Bee Colony (ABC) optimization technique. The performance of the system has been increased by the selection of appropriate and best nodes for data packets transmission

Shweta Pandey et.al The proposed approach uses the Artificial neural network (ANN) and the Support Vector Machine (SVM) for the discovery of the black hole attacks in the network. The results are carried out between the black hole AODV and the security mechanism that was provided as the Secure AODV (SAODV) ,shows an improvement viz. energy consumption of 54.72%, throughput of 88.68kbps, packet delivery ratio of 92.91% , E to E delay of about 37.27ms

Indira N et.al Proposed Anomaly based intrusion detection technique using the SOM classification method provides higher detection rate than other anomaly detection method. As anomaly-based intrusion detection techniques are based on statistical data they can result in false positive identification of normal pattern as an attack. This false identification of benign behavior as abnormal can result in isolation of non-malicious node as malicious, thus may result in partitioning of the network

Sankaranarayanan.S et. al proposed RSA algorithm in intrusion detection system in MANET. It successfully identifies the malicious node(s) and results show that secure IDS method improvises packet deliver ratio in presence of malicious node(s).

Sujithra L et. al In this paper ,the approach improves the conservation of energy in heterogenous network and also reduces the active time of IDS running in the nodes. In order to achieve this, proabilistic approach is implemented, here optimal proabilistic of node is to be set, thus decreases active time of IDS in each node and conserves the energy of the node , hence increases the network lifetime significantly.

International Journal of Emerging Science and Engineering (IJESE)
ISSN: 2319-6378 (Online), Volume-11 Issue-4, March 2023

Neighbour Node Ratio AODV (NNR-AODV) Routing Protocol for Wormhole Attack Detection in Manets

M V D S Krishna Murty, Lakshmi Rajamani

Abstract: This paper aimed at the detection of wormhole attack and proposed a new method called as Neighbour Node Ratio Adhoc On demand Distance Vector Routing (NNR-AODV). NNR-AODV is an extended version of the traditional AODV routing protocol. The proposed NNR-AODV calculates the neighbour node count for every node and based on that it will decide whether the wormhole is present or not. Furthermore, NNR-AODV is able to detect both external and internal wormhole attacked nodes. Also, NNR-AODV derived a Neighbor node Threshold value which is based on the cumulative distances between nodes present in the wormhole attack. For experimental validation, we have accomplished an extensive simulation and the performance is measured through Number of bogus links, Detection rate, False positive Rate, Packet delivery ratio and Packet loss ratio. The obtained results have shown superior performance in the detection of wormhole attacks than the existing methods.

Keywords: Wormhole, Neighbor Node Threshold, Bogus Links and Node Degree.

I. INTRODUCTION

From the past few years, rapid progress in the development of Mobile Ad Hoc Networks (MANETs) has encouraged different wireless applications that can be employed in different areas viz. Entrainment, Education, Military, Emergency services and Collaborative computing [1]. Due to the special characteristics of MANETs viz. independent infrastructure and self-organizing nodes, MANETs have become an ideal choice to use in information sharing and communications. Thus, the mobile nodes of MANET can execute both for routing and hosting. In the case of routing, they work as relay nodes and forward the data of a node to its destination through standard protocols. However, the major issue in MANETs is their mobility which introduces several serious constraints on network lifetime, quality of service and security [2-4]. Due to the nature of decentralization and openness of MANETs, the mobile nodes are not reliable to constrain the membership. The mobile nodes are susceptible to different attacks [5] when those who try to compromise the node and force it to misbehave. Based on the nature of attack, they ranges from passive eavesdropping to serious battery draining. Some more attacks are there which aim at data tampering and traffic analysis through eavesdropping. In general, the attackers mainly concentrate on the resources of mobile nodes like bandwidth exhaustion, battery draining and data manipulations etc. Based on the mode of attack, they are categorized as external mode attacks and internal mode attacks [6]. The former attacks concentrate on the manipulation of routing information that propagates between mobile nodes in the network. They inject erroneous data and try to disturb the original behavior of network. An example for such kind of attack is worm-hole attack (WHA) in which a routing loop is established by the creation of a worm-hole node. Next, the internal attacks mainly target at compromising internal nodes. They distribute false data and try to disrupt the data flow. Sybil attack, grayhole attack and blackhole attack are the best examples to such kind of attacks.

Wormhole attacks are the most severe and sophisticated security threats to the MANET routing protocols where malicious nodes are placed strategically to distort the network topology and tunnel packets selectively using the false established routes [7], [8]. Wormhole detection and prevention are very challenging issues [9], [10]. The wormhole attacks can be executed by external nodes (who only forward packets and do not process the cryptographic data) or by internal nodes (the compromised nodes inside the network who process packets like other normal nodes) [11]. The internal attackers are more dangerous and difficult to detect. However, Chen *et al.* [12] hold the view that the wormhole attack is a typical external attack. Moreover, majority works of literature pay excessive attention to the external wormholes but ignore internal wormholes which are also common in MANETs.

This paper proposed a new method called as Neighbour Node Ratio AODV(NNR-AODV) routing protocol to prevent the MANETs from wormhole attacks. The proposed NNR-AODV detects both the external and internal wormhole attacks effectively. NNR-AODV derived a metric called as neighbour node threshold, which avoids the attack by performing wormhole (WH) detections for all nodes in MANETs, thus contributes in improving the accuracy of wormhole detection and saves energy.

Manuscript received on 01 March 2023 | Revised Manuscript received on 14 March 2023 | Manuscript Accepted on 15 March 2023 | Manuscript published on 30 March 2023.

*Correspondence Author(s)
M V D S Krishna Murty*, Research Scholar, Department of CSE, Jawaharlal Nehru Technological University Hyderabad (Telangana), India. E-mail: [redacted] ORCID ID: [redacted]
Dr. Lakshmi Rajamani, Professor and Head (Retd), Department of CSE, Osmania University, Hyderabad (Telangana), India. E-mail: [redacted]

Retrieval Number: 100.1/ijese.D5234031423
DOI: 10.35940/ijese.D5234.03114
Journal Website: www.ijese.org

International Journal of Inventive Engineering and Sciences (IJIES)
ISSN: 2319-9598 (Online), Volume-10 Issue-2, February 2023

A Simple and Effective Intrusion Detection System for Manets

M V D S Krishna Murty, Lakshmi Rajamani

Abstract: *This work proposes a simple and effective Intrusion Detection System (IDS) to classify different attacks in MANETs. IDS extracts four features for every traffic pattern and applies Support Vector Machine algorithm over them for the classification. Before applying the feature extraction, the input traffic pattern is subjected to pre-processing as it is composed of non-uniform features. IDS classifies the input traffic pattern into three classes; they are normal, blackhole and wormhole. Finally, this work analyses the feasibility of machine learning algorithms for the detection of security attacks in MANETs. For experimental validation, we have referred a self-created dataset which was acquired from the observations of blackhole and wormhole attacked node's traffic patterns. Moreover, we have also validated the proposed method through NSL-KDD dataset.*

Keywords: *Intrusion Detection System, Preprocessing, Feature Extraction, Support Vector Machine, Self-Created Dataset.*

I. INTRODUCTION

Mobile Ad hoc networks (MANETs) are one of the wireless networks formed with the mobile devices as nodes. Due to the nature of decentralized communication, MANETs have gained huge interest in different applications including emergency rescue operations, military operations, collaborative distributed computing, disaster management and some personal network applications [1] etc. Due to the unique characteristics of mobile nodes, there are several challenges in MANETs which need to be solved. Among the several challenges, the mobility is the major challenge and it consequences to several sub-challenges. Almost all the problems in MANETs are linked with mobility of nodes. Among several sub-challenges, secure data exchange between mobile nodes is the major challenge. Due to the open network topology, distributed nature, and the absence of centralized administration in MANETs, the mobile nodes are susceptible for various attacks [2].

The impact of these attacks ranges from naive passive eavesdropping to serious battery draining attacks [3]. Majorly the attackers focus on the resources of mobile nodes like battery power, bandwidth, and data. Among the several security attacks in MANETs, blackhole attack [4] and wormhole attack [5] are the two major attacks which cause serious damages to the network. These two attacks are dynamic in nature and varies based on several network parameters. Hence, the identification of mobile nodes those were attacked with blackhole and wormhole attacks is much difficult. Recently, the involvement of artificial intelligence has been increased in different applications. Compared to the static algorithms which cannot provide any prior information about the attacks to mobile nodes, the machine learning algorithms which train the nodes can help in proper and accurate detection of attacks. A mobile node trained with the attack's characteristics can easily identify the attacked or compromised neighbour node. Hence our research has got motivated with these issues and focused over the development of effective Intrusion Detection System to solve these problems up to certain extent. This paper explains a simple and effective Intrusion Detection System for the classification of mobile nodes into three classes; they are normal, blackhole and wormhole. The overall system composed of three phases; they are pre-processing, features extraction and classification. At the initial phase, the input data is normalized and transformed into a unique format because the raw data collected from MANETs is non-uniform in nature. For feature extraction, we have employed four statistical features namely mean, variance, maximum and minimum. After feature extraction, we have applied principal component analysis for dimensionality reduction and finally Support Vector Machine (SVM) algorithm is used for classification.

The remaining paper is organized as follows. Section II explores the literature survey on IDS methods. Section III explores the details of proposed approach. Section IV explores the details of experimental analysis and the final Section concludes the paper.

II. LITERATURE SURVEY

IDS mainly works based on the principle of machine learning and information processing. In IDS, the mobile node initially learns about the characteristics of different attacks through machine learning algorithms and it becomes ready to identify the attack if occurs. IDS works on the features of network traffic (data packet and control packets).

Manuscript received on 31 January 2023 | Revised Manuscript received on 06 February 2023 | Manuscript Accepted on 15 February 2023 | Manuscript published on 28 February 2023.
*Correspondence Author
M V D S Krishna Murty*, Research Scholar, Department of Computer Science and Engineering, Jawaharlal Nehru Technological University, Hyderabad (Telangana), India. E-mail: mvdskrishnamurty@gmail.com, ORCID ID: https://orcid.org/0000-0002-0205-3515
Dr. Lakshmi Rajamani, Professor and Head (Retd), Department of Computer Science and Engineering, Osmania University, Hyderabad (Telangana), India. E-mail: drlrajamani@gmail.com

Retrieval Number: 100.1/ijies.B10770210223
DOI: 10.35940/ijies.B1077.02102023
Journal Website: www.ijies.org

International Journal For Recent Developments in Science & Technology
2581-4575

Development and Analysis of improvised TORA Routing Protocol based on Machine Learning Model for optimal Network Performance in MANETs

M V D S Krishna Murty[1], Dr.Lakshmi Rajamani[2]

[1]M V D S Krishna Murty,Asst.Prof.,Dept of CSE,MCET,Hyderabad,Research scholar-JNTUH,mvdskrishnamurty@gmail.com
[2]Dr. Lakshmi Rajamani, Prof.& Head(Retd.),Dept of CSE, Osmania University, Hyderabad, drlakshmiraja@gmail.com

Abstract – *A MANET is a self configurable wireless ad-hoc network in whichnode mobility exists. Due to this flexibility many security threats can occur in the routing. So, in order to address this, the performance of IDS should be improvised. In this paper, a methodology is proposed based on Machine Learning(ML) algorithm in terms of accuracy and detection rate for IDS improvisation for TORA routing protocol.*

Key Words: MANET, Support Vector Machine, Intrusion Detection System, TORA (Temporally Ordered Routing Algorithm).

1.INTRODUCTION

IDS is to detect the attack before the malicious node[s] causes security threat to the network.It looks into monitoring, detecting and notifying aspects. The Blackhole attack is the most affected type on MANETs. Usage of an anomaly IDS protects the network from Black hole attack with the help of Machine Learning algorithm ,SVM

1.1 Malicious Node(s) causing Black hole attack in TORA Routing Protocol.

Black hole attack is one of the major attacks in MANETs. Malicious Node(s) causing this attack on MANET security has the data viz.Source node, Destination node and Neighbouring node. The source node sends a QRY (Query Packet) to its neighbouring nodes to search for the route destination. However, black hole node sends a fake route reply to the source node resulting packet loss which will degrade the performance of the network. In order to prevent this, the performance of the IDS should be improvised with machine learning algorithm by detecting the malicious node(s) .

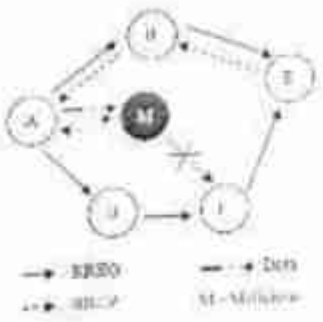

Fig(1) : Malicious Node Causing Black hole Attack

2. RELATED WORK

Kwan Hui Lim et.al Proposed two modifications to improve TORA using a network localization approach and selective node participation approach. The network localization approach initializes and maintains a localized portion of the entire network while the selective node participation approach selects a subset of nodes to participate as part of the network

Pooja Rani et.al In this paper, the protection against dual attacks has been presented for BHA and GHA by using the concept of Artificial Neural Network (ANN) as a deep learning algorithm along with the swarm-based Artificial Bee Colony (ABC) optimization technique. The performance of the system has been increased by the selection of appropriate and best nodes for data packets transmission

Shweta Pandey et.al The proposed approach uses the Artificial neural network (ANN) and the Support Vector Machine (SVM) for the discovery of the black hole attacks in the network. The results are carried out between the black hole AODV and the security mechanism that was provided as the Secure AODV (SAODV) ,shows an improvement viz. energy consumption of 54.72%, throughput of 88.68kbps, packet delivery ratio of 92.91% , E to E delay of about 37.27ms

Indira N et.al Proposed Anomaly based intrusion detection technique using the SOM classification method provides higher detection rate than other anomaly detection method. As anomaly-based intrusion detection techniques are based on statistical data they can result in false positive identification of normal pattern as an attack. This false identification of benign behavior as abnormal can result in isolation of non-malicious node as malicious, thus may result in partitioning of the network

Sankaranarayanan.S et. al proposed RSA algorithm in intrusion detection system in MANET. It successfully identifies the malicious node(s) and results show that secure IDS method improvises packet deliver ratio in presence of malicious node(s).

Sujithra L et. al In this paper ,the approach improves the conservation of energy in heterogenous network and also reduces the active time of IDS running in the nodes. In order to achieve this, probabilistic approach is implemented, here optimal probabilistic of node is to be set, thus decreases active time of IDS in each node and conserves the energy of the node , hence increases the network lifetime significantly.

SEGMENTATION OF MICROARRAY IMAGES USING MULTIPLE FEATURE CLUSTERING ALGORITHMS

***Ulli Moulali, **Dr. Syed Umar**
**Research Scholar, **Supervisor,*
Department of Computer Science, Faculty of Computing & Information Technology (Computer Science), Himalayan University, Itanagar

ABSTRACT:

In a single experiment, utilizing Microarray Technology, one may examine the function of thousands of genes simultaneously. Medical diagnostics, drug development, and biomedical research all rely on microarrays. Numerous copies of a single DNA sequence may be found in every single one of the microarray's many thousands of locations. There are three steps to the microarray image analysis process: gridding, segmentation, and extraction of information (or data). Data from microarray image analysis may be used to classify and identify differentially expressed genes by creating spot metrics from spot intensities. Each spot's intensity shows the gene's expression level. Multi-feature clustering techniques for microarray image segmentation are presented in this study, which expands the single-feature (pixel intensity) k-means clustering approach to multiple features. Multi-feature clustering methods are more efficient than single-feature k-means clustering algorithms in sizing the spot area, thereby generating more accurate expression-ratio results.

Keywords: Image processing, Microarray Image Analysis, Multi-feature Clustering methods

1. INTRODUCTION:

Microarray image processing relies heavily on picture segmentation in order to concurrently capture the emotions of individual spots. Disturbances may affect the performance of modern clustering-based segmentation algorithms. In order to deal with this issue and enhance the precision of segmentation, several modifications are made to the rapid and basic clustering algorithms in this study. Microarray image segmentation relies only on pixel intensity information when performing clustering procedures. Nevertheless, in the microarray image segmentation process, depending on where a pixel is located and how close it is to its neighbor's median values, the clustering and segmentation results will differ. Numerous feature-clustering algorithms were developed as a result of this finding. For microarray image segmentation, k-means clustering with a single feature (pixel intensity) may be improved using the multiple feature clustering algorithms discussed in this paper. Clustering algorithms are the primary focus of this investigation. They don't need a starting condition of pixels and don't require any post-processing since these algorithms aren't restricted to a certain size and form of spot. These algorithms were created only using information about the pixel intensities (one feature). Microarray image segmentation, however, takes into account not just the brightness of individual pixels, but also their distance from the median intensity of the pixels around them, all of which have an effect on the final result. It's critical to use feature selection when dealing with huge datasets that include a significant number of features and metrics. A fraction of the components could include the high point of characteristics, and they might corrupt the execution and impair the many-sided computational quality of the networks. So the efficiency may be increased by the selection of

Webology (ISSN: 1735-188X)
Volume 19, Number 2, 2022

Adaptive Data Clustering Algorithms For Microarray Image Analysis

[1]ULLI MOULALI* , [2]Dr. SYED UMAR

[1*]Research Scholar, Department of Computer Science, Faculty of Computing & Information Technology, Himalayan University, Itanagar.

[2]Supervisor, Department of Computer Science, Faculty of Computing & Information Technology (Computer Science), Himalayan University, Itanagar.

Abstract:
By adopting Microarray Technology, in a single study one may analyse the function of thousands of genes in parallel. Microarrays are utilised in different applications including illness diagnostics, medication development and bio-medical research. A Microarray picture has thousands of spots and each of the spot contains multiple copies of one DNA sequence. The analysis of microarray picture is done in three stages: gridding, segmentation and information extraction. The microarray image analysis takes the spot intensity data as input and provides the spot metrics as output which are utilised in categorization and identification of differentially expressed genes. The intensity of each area shows the expression level of the given gene. Generally, clustering methods are employed for the segmentation of microarray pictures. These algorithms have the benefits that they are not bound to a certain spot size and form, does not need an initial state of pixels and have no requirement for post-processing. These methods have been built based on the knowledge about the intensities of the pixels solely. Clustering algorithm such as K-means, Fuzzy c-means etc., has been utilised in the literature. The basic prerequisite for every clustering technique is the number of clusters K. Estimating the value of K is challenging assignment with given data. This work introduces adaptive data clustering algorithms which delivers appropriate segmentation results with easy operation and eliminates the interactive input K (number of clusters) value for segmentation of microarray picture. The qualitative and quantitative findings reveal that adaptive data clustering algorithms are more effective than standard data clustering algorithms in segmenting the spot region, thereby providing more accurate expression-ratio.

Keywords: Image processing, Microarray Image Analysis, Clustering methods

1. INTRODUCTION:

Several interpolation functions are employed in the decomposition of the picture in this paper to show a noise reduction approach using two-dimensional Empirical Mode Decomposition

Design Engineering

ISSN: 0011-9342 | Year 2021
Issue: 7 | Pages: 631-646

EPFSESD: An Enhanced Pipeline Feature Selection Algorithm for Erythemato-Squamous Disease Detection

Rajashekar Deva[1], Dr. G .Narsimha[2]

[1]Asst.Prof, Department of CSE, Methodist College of Engineering & Technology, Hyderabad, Telangana, India.

[2]Professor, Department of CSE, JNTUH, Hyderabad, Telangana, India.

[1]rajshekardeva@gmail.com

[2]narsimha06@gmail.com

Abstract:

Erythemato-Squamous Disease (ESD) is one of the common skin diseases. In machine learning, the current trends are focusing on automation of health care, agriculture, and manufacturing domains. The proposed system automates the Erythemato-Squamous Disease (ESD) to help the skin doctors for identification of skin diseases easily. In this paper, the system utilizes the dataset that is freely available at the UCI repository, which contains 34 features, which takes high computation time for determining the disease. To overcome this problem, the proposed system performs dimensionality reduction by identifying the important features and the selection of important attributes plays a vital role in the detection of class labels of the disease. The dataset contains 6 classes, multi-class problem. In Multi-class problems, the best features are identified using an enhanced pipeline algorithm in combination with recursive elimination feature, an embedded method to design a robust system. The pipeline algorithm has sequenced 5 different types of classifiers Logistic Regression, Multi-Layer Perceptron, CART, Random Forest, and Gradient Boost Algorithm.

Keywords: *Enhanced Pipelined Feature Selection, Random Forest, Recursive Elimination Feature*

I. INTRODUCTION

The proposed system is mainly concerned with dimensionality reduction which is sometimes referred to as "Feature Selection". In the existing studies, there are various ways to perform these operations. According to machine learning mechanisms, the feature selection is divided into 3 categories as shown in figure1.

Design Engineering

ISSN: 0011-9342 | Year 2021
Issue: 7 | Pages: 631-646

EPFSESD: An Enhanced Pipeline Feature Selection Algorithm for Erythemato-Squamous Disease Detection

Rajashekar Deva[1] , Dr. G .Narsimha[2]

[1]Asst.Prof, Department of CSE, Methodist College of Engineering & Technology, Hyderabad, Telangana, India.

[2]Professor, Department of CSE, JNTUH, Hyderabad, Telangana, India.

[1]rajshekardeva@gmail.com

[2]narsimha06@gmail.com

Abstract:

Erythemato-Squamous Disease (ESD) is one of the common skin diseases. In machine learning, the current trends are focusing on automation of health care, agriculture, and manufacturing domains. The proposed system automates the Erythemato-Squamous Disease (ESD) to help the skin doctors for identification of skin diseases easily. In this paper, the system utilizes the dataset that is freely available at the UCI repository, which contains 34 features, which takes high computation time for determining the disease. To overcome this problem, the proposed system performs dimensionality reduction by identifying the important features and the selection of important attributes plays a vital role in the detection of class labels of the disease. The dataset contains 6 classes, multi-class problem. In Multi-class problems, the best features are identified using an enhanced pipeline algorithm in combination with recursive elimination feature, an embedded method to design a robust system. The pipeline algorithm has sequenced 5 different types of classifiers Logistic Regression, Multi-Layer Perceptron, CART, Random Forest, and Gradient Boost Algorithm.

Keywords: *Enhanced Pipelined Feature Selection, Random Forest, Recursive Elimination Feature*

I. INTRODUCTION

The proposed system is mainly concerned with dimensionality reduction which is sometimes referred to as "Feature Selection". In the existing studies, there are various ways to perform these operations. According to machine learning mechanisms, the feature selection is divided into 3 categories as shown in figure1.

Erythemato-Squamous Disease Detection using Best Optimized Estimators of ANN

Rajashekar Deva[1], Dr G .Narsimha[2]
Asst.Prof. Department of C.S.E., Methodist College of Engineering &Technology, Abids, Hyderabad, Telangana, 500001, India[1]
Principal and Professor, JNTUH, Sulthanpur, Sangareddy, Telangana, India[2]

***Abstract*—Medical area focused on automating skin cancer detection after the pandemic era of "Monkey Pox". Previous works proposed ANN mechanisms to classify the type of skin cancer. However, all those models implement layers of ANN with standard estimator components like hidden layers implemented using the ReLu activation function, several neurons are generally a power of two and others, but these values are not always perfect. Few researchers implemented optimization techniques for tuning the estimators of A.I. algorithms, but all those mechanisms require more resources and don't guarantee the best values for each estimator. The proposed method analyzes all the essential estimators of every possible neural network layer. Then it applies a modified version of Bayesian optimization because it avoids the disadvantages of Grid and Random optimization techniques. It picks the best estimator by using the conditional probability of naive Bayesian for every combination.**

***Keywords*—Conditional probability; naive Bayesian; bayesian optimization; grid search; optimization techniques; estimators**

I. Introduction

Most researchers utilize machine learning to identify skin cancers but suffer from overfitting and more resource consumption. The problem can be solved using artificial neural networks, but traditional networks become complicated for smaller datasets. So, the proposed research aims to customize the parameters of the network by performing "Hyper Parameterization".

Hyperparameter tuning is required for behavioural control of the machine-learning model [11]. Hyperparameters can be configured differently for each machine-learning model. Our expected model parameters will yield less-than-ideal outcomes if the hyperparameters are not appropriately tweaked to optimize the loss function [12]. This implies that our model has further problems. When building a model from a particular dataset, hyper-tuning identifies the potential optimal sets of hyperparameters. A single training task executes several trials for hyperparameter tweaking. The task of hyperparameter tweaking involves meta-optimization [27]. The hyperparameter tuner produces the hyperparameter setting, those results in the best-performing model after assessing various hyperparameter settings. By employing the algorithm and the defined limits of hyperparameters, hyperparameter tuning runs multiple training sessions on your dataset to determine which model version is the best.

A. Hyper Parameter Tuning

The accuracy of models for machine learning can be significantly increased by using hyperparameter adjustment. Hyperparameter tuning is identifying a collection of appropriate hyperparameter variables for a prediction model and applying this adjusted algorithm to any piece of data. The model's efficiency is maximized by employing that collection of hyperparameters, which minimizes a preset loss function and produces better results with fewer errors. To use an Exhaustive Grid Search in Scikit Learn is a well-known and conventional method for hyperparameter tweaking [13]. Every permutation of each collection of hyperparameters is tested using this procedure. This approach allows us to locate the ideal set of values within the variable search space. Since this approach must test every permutation in the grid size, it typically consumes more computer resources and requires a long time to run. Multiplication of all the variables will determine the size of the parameter grid. Each time a random collection of hyperparameters is tested, the model's performance is recorded. After multiple repetitions, it returns to the mixture with the most significant outcome.

B. Types of Hyper Tuning

Irrespective of the type of machine and deep learning models, these tuning algorithms help achieve the minimum error rate with minimum learning rate.

1) Grid search: Grid search optimization takes much time to compute every possible combination of estimators. Suppose we have two parameters for designing the ANN in which parameter-1 can be estimated in X ways, and parameter-2 can be estimated in Y ways. The system needs X into Y ways to apply grid search for this type of neural network. So this can be claimed as an exhaustive search.

2) Random search: Random search only checks some possible estimated values [14]. It randomly selects a few values from each parameter, so this will reduce the number of ways than grid search since random search doesn't cover all possible combinations. So this tuning process only guarantees the best values.

3) Successive halving: The S.H.A. (Successive Halving Algorithm) algorithm can optimize hyperparameters and solve multi-armed bandits challenges. The algorithm's primary goal is to correctly determine the best arm within a strict budget, a constrained time or resource [15]. The algorithm consistently evaluates each arrangement. The weakest performers are removed at the conclusion of each round. The procedure repeats itself until only one configuration is left, with the remaining configurations being examined twice as much as in

A Tuned Stacking Algorithm to Detect Skin Cancer Using Multi-classification Algorithms

Rajashekar Deva and G. Narsimha

1 Introduction

The power of ensemble mechanisms lies in their strengthening the unity among the poorly resulted algorithms. It strongly believes that combining weak models can generate more reliable results than traditional approaches. Any machine learning model is better explained by two extreme degrees of freedom parameters, namely "Bias" and "Variance". The model with both values as high or one of them as high is considered to be weak or base model. So, to reduce the degree of freedom, one of the better solutions is to replace the traditional with ensemble approaches. During the early days of ensemble, researchers used to combine homogenous algorithms, but the present technology is mainly focusing on the heterogeneous environment. Based on the concept of combining the algorithms, the classification of ensemble models is represented in Fig. 1.

Bagging is a process of combining homogenous algorithms, in which it learns the features from individual algorithms separately and in parallel. The major focus of the bagging algorithms is to reduce the variance of the model and it also tries to reduce the error rate by taking the mean value of the obtained results. Boosting is also a process of combining the homogenous algorithms but it considers the algorithms in sequence, tries to reduce the bias and, at the same time, also keeps the variance value as low as possible. Stacking provides a chance to integrate heterogeneous algorithms in which parts of the problem grab more attention than covering the entire problem

R. Deva (✉)
Department of CSE, Methodist College of Engineering & Technology, Hyderabad, Telangana, India
e-mail: rajshekardeva@gmail.com

G. Narsimha
JNTUH, Sulthanpur, Hyderabad, Telangana, India
e-mail: narsimha06@gmail.com

R. J. Kannan et al. (eds.), *International Virtual Conference on Industry 4.0*, Lecture Notes in Electrical Engineering 1003, https://doi.org/10.1007/978-981-19-9989-5_8

International Journal of Engineering Technology and Management Sciences
Website: ijetms.in Issue: 2 Volume No.7 March - April – 2023
DOI:10.46647/ijetms.2023.v07i02.005 ISSN: 2581-4621

A Deep Exposition of GAN and its applications

Dr. Syed Azahad[1], Dr. Shaik Hameeda[2]
[1]Associate Professor, Methodist College of Engineering and Technology,
Dept. of Computer Science and Engineering, Hyderabad, Telangana.
[2]Associate Professor, Avanthi Institute Of Engineering & Technology,
Dept. of Computer Science and Engineering, Hyderabad, Telangana
Dr. Syed Azahad : Orcid ID : 0000-0002-5736-0045
Dr. Shaik Hameeda : Orcid ID : 0000-0002-0686-8084

Abstract
Generative Adversarial Networks (GANs) have revolutionized the field of machine learning and artificial intelligence by providing a powerful framework for generating realistic and high-quality synthetic data. GANs consist of two networks, a generator that produces synthetic data and a discriminator that distinguishes between the synthetic data and real data. The two networks are trained together in a game-theoretic setting, where the generator tries to produce synthetic data that is similar to the real data, while the discriminator tries to distinguish between the two.
This paper provides a deep exposition of GAN and its applications, starting with the basics of GANs, their architecture, and how they work. We then discuss the training process of GAN, the challenges associated with it, and the techniques used to address these issues. We also describe the different variants of GANs, including conditional GAN, progressive GAN, and style-based GAN, and their applications.
Next, we provide a comprehensive overview of the various domains where GANs have been successfully applied, such as image and video synthesis, text generation, and music composition. We discuss the potential future directions of GANs and their applications, including research areas that need further investigation.
Finally, we highlight the challenges and limitations associated with GANs, such as mode collapse, vanishing gradients, and instability, and the ethical and legal issues associated with their applications. We conclude by summarizing the key points of the paper and highlighting the potential of GANs as a tool for generating realistic and high-quality synthetic data.
Keywords: Generative Adversarial Networks, Deep learning, Neural networks, Unsupervised learning, Data synthesis, Mode collapse, Training stability, Hyper parameter tuning, Evaluation metrics, Data quality and quantity, Generalization

1. Introduction :

Generative Adversarial Networks (GANs) are a type of neural network architecture that has gained significant attention in the field of artificial intelligence and machine learning over the past few years. GANs have shown remarkable success in generating high-quality synthetic data that can be used for a variety of applications, including image and video synthesis, text generation, and music composition, among others.
GANs consist of two networks, a generator and a discriminator, which are trained together in a game-theoretic setting. The generator is responsible for producing synthetic data that is similar to the real data, while the discriminator is trained to distinguish between the synthetic data and the real data. The two networks are trained in an adversarial manner, where the generator tries to fool the discriminator by producing synthetic data that is indistinguishable from the real data, while the discriminator tries to correctly classify the synthetic and real data.
The success of GANs can be attributed to their ability to generate high-quality synthetic data that can be used in a variety of applications. The synthetic data generated by GANs can be used to augment existing data sets, perform data imputation, and generate new data sets that can be used for training

International Journal of Engineering Technology and Management Sciences
Website: ijetms.in Issue: 2 Volume No:7 March - April – 2023
DOI:10.46647/ijetms.2023.v07i02.005 ISSN: 2581-4621

A Deep Exposition of GAN and its applications

Dr. Syed Azahad[1], Dr. Shaik Hameeda[2]
[1]Associate Professor, Methodist College of Engineering and Technology,
Dept. of Computer Science and Engineering, Hyderabad, Telangana.
[2]Associate Professor, Avanthi Institute Of Engineering & Technology,
Dept. of Computer Science and Engineering, Hyderabad, Telangana
Dr. Syed Azahad : Orcid ID : 0000-0002-5736-0045
Dr. Shaik Hameeda : Orcid ID : 0000-0002-0686-8084

Abstract
Generative Adversarial Networks (GANs) have revolutionized the field of machine learning and artificial intelligence by providing a powerful framework for generating realistic and high-quality synthetic data. GANs consist of two networks, a generator that produces synthetic data and a discriminator that distinguishes between the synthetic data and real data. The two networks are trained together in a game-theoretic setting, where the generator tries to produce synthetic data that is similar to the real data, while the discriminator tries to distinguish between the two.
This paper provides a deep exposition of GAN and its applications, starting with the basics of GANs, their architecture, and how they work. We then discuss the training process of GAN, the challenges associated with it, and the techniques used to address these issues. We also describe the different variants of GANs, including conditional GAN, progressive GAN, and style-based GAN, and their applications.
Next, we provide a comprehensive overview of the various domains where GANs have been successfully applied, such as image and video synthesis, text generation, and music composition. We discuss the potential future directions of GANs and their applications, including research areas that need further investigation.
Finally, we highlight the challenges and limitations associated with GANs, such as mode collapse, vanishing gradients, and instability, and the ethical and legal issues associated with their applications. We conclude by summarizing the key points of the paper and highlighting the potential of GANs as a tool for generating realistic and high-quality synthetic data.
Keywords: Generative Adversarial Networks, Deep learning, Neural networks, Unsupervised learning
Data synthesis, Mode collapse, Training stability, Hyper parameter tuning, Evaluation metrics, Data quality and quantity, Generalization

1. Introduction :

Generative Adversarial Networks (GANs) are a type of neural network architecture that has gained significant attention in the field of artificial intelligence and machine learning over the past few years. GANs have shown remarkable success in generating high-quality synthetic data that can be used for a variety of applications, including image and video synthesis, text generation, and music composition, among others.
GANs consist of two networks, a generator and a discriminator, which are trained together in a game-theoretic setting. The generator is responsible for producing synthetic data that is similar to the real data, while the discriminator is trained to distinguish between the synthetic data and the real data. The two networks are trained in an adversarial manner, where the generator tries to fool the discriminator by producing synthetic data that is indistinguishable from the real data, while the discriminator tries to correctly classify the synthetic and real data.
The success of GANs can be attributed to their ability to generate high-quality synthetic data that can be used in a variety of applications. The synthetic data generated by GANs can be used to augment

algorithms

MDPI

Review

Enhanced Maximum Power Point Techniques for Solar Photovoltaic System under Uniform Insolation and Partial Shading Conditions: A Review

Laxman Bhukya [1], Narender Reddy Kedika [2] and Surender Reddy Salkuti [3,*]

[1] Department of Electrical and Electronics Engineering, Methodist College of Engineering and Technology, Hyderabad 500001, India
[2] Department of Electrical and Electronics Engineering, Institute of Aeronautical Engineering, Hyderabad 500043, India
[3] Department of Railroad and Electrical Engineering, Woosong University, Daejeon 34606, Korea
* Correspondence: surender@wsu.ac.kr

Abstract: In the recent past, the solar photovoltaic (PV) system has emerged as the most promising source of alternative energy. This solar PV system suffers from an unavoidable phenomenon due to the fluctuating environmental conditions. It has nonlinearity in I-V curves, which reduces the output efficiency. Hence, the optimum maximum power point (MPP) extraction of the PV system is difficult to achieve. Therefore, for maximizing the power output of PV systems, a maximum power point tracking (MPPT) mechanism, which is a control algorithm that can constantly track the MPP during operation, is required. However, choosing a suitable MPPT technique might be confusing because each method has its own set of advantages and disadvantages. Hence, a proper review of these methods is essential. In this paper, a state-of-the-art review on various MPPT techniques based on their classifications, such as offline, online, and hybrid techniques under uniform and nonuniform irradiances, is presented. In comparison to offline and online MPPT methods, intelligent MPPT techniques have better tracking accuracy and tracking efficiency with less steady state oscillations. Unlike online and offline techniques, intelligent methods track the global MPP under partial shade conditions. This review paper will be a useful resource for researchers, as well as practicing engineers, to pave the way for additional research and development in the MPPT field.

Keywords: photovoltaic system; maximum power point; nonlinearity; hybrid techniques

Citation: Bhukya, L.; Kedika, N.R.; Salkuti, S.R. Enhanced Maximum Power Point Techniques for Solar Photovoltaic System under Uniform Insolation and Partial Shading Conditions: A Review. *Algorithms* 2022, *15*, 365. https://doi.org/10.3390/a15100365

Academic Editor: Abdulsalam Yassine

Received: 23 July 2022
Accepted: 26 September 2022
Published: 29 September 2022

1. Introduction

1.1. Motivation and Incitement

Solar energy has become the most popular renewable energy source, since it can be used in any location and is available every day. Because of its simple structure, low pollution, low or no carbon greenhouse emissions, and low maintenance costs, it has become a dominant renewable source [1]. Solar power is currently the world's preferred alternative energy source [2]. Nonetheless, the solar PV system suffers from the unavoidable problem of current and voltage nonlinearity, which occurs primarily in partially shaded conditions (PSC). In general, PV systems have a unique operating point where the power is at its maximum. Hence, the PV system needs to operate at this point to harvest the maximum efficiency [3]. For maximizing output power under all abnormal conditions, the PV system takes account of the MPPT mechanism.

ISSN No:-2456-2165

An Innovative Solar Based Robotic Floor Cleaner

Namburi Nireekshana
Assistant Professor, EEED
Methodist College of engineering & technology

Tanvi H Nerlekar
160719734005
BE, EEE
Methodist College of Engineering & Technology

Palle Nitish Kumar
160719734307
BE, EEE
Methodist college of Engineering & Technology

Mohammed Mohsin Bajaber
160719734024
BE, EEE
Methodist college of Engineering & Technology

Abstract:- Conventional floor cleaning equipment is most commonly found in airports, train platforms, hospitals, bus stops, shopping malls, and a variety of other commercial settings. These devices require electrical energy to operate and are not user-friendly. Around India, particularly during the summer, there is a power outage, and most floor cleaning machines are ineffective as a result, particularly around bus stops. As a result, there is a need to design low-cost, user-friendly floor cleaning machines. In this project, we will create solar-powered mobile floor cleaning equipment that may be used as an alternative to traditional floor cleaning machines. Because of the high cost of manpower, time, effort, and affordability, automated floor cleaning devices have been widely employed in developing countries for many years. This abstract is based on our creative concept to design, develop, and manufacture a semi-automatic solar-powered mobile floor cleaning machine that will run on solar energy, mobile communication, battery power, or electricity. A semi-automatic floor cleaning machine will be created with basic considerations for less energy consumption, machine and operating cost reduction, reduction of human effort, environmental friendliness, and ease of use in mind. The project's foundation is the utilisation of renewable energy, which is abundant in most nations, has a low environmental impact, and is simple to build on a commercial scale in the future.

Keywords:- Sensors, controllers, solar energy, and a floor cleaning mechanism.

I. INTRODUCTION

Conventional floor cleaning equipment is most commonly found in airports, train platforms, hospitals, bus stops, shopping malls, and a variety of other commercial settings. These devices require electrical energy to operate and are not user-friendly[1]. Around India, particularly during the summer, there is a power outage, and most floor cleaning machines are ineffective as a result, particularly around bus stops. As a result, there is a need to design low-cost, user-friendly floor cleaning machines. In this project, we will create solar-powered mobile floor cleaning equipment that may be used as an alternative to traditional floor cleaning machines. Because of the high cost of manpower, time, effort, and affordability, automated floor cleaning devices have been widely employed in developing countries for many years.

Cleaning may appear to be a simple task, but having a clean, clutter-free living area has been linked to numerous favourable outcomes, such as being free of disease and allergies. Cleaning is a necessary task in almost every location. This is sometimes easy and sometimes challenging because certain sites have big floor surfaces that require more than one person to clean, so we needed some way to compensate for this problem.[2] Robotic cleaners have received significant attention in robotics research in recent years because of their usefulness in assisting humans in floor cleaning applications at homes, hotels, restaurants, workplaces, hospitals, workshops, warehouses, and universities, among other places. Essentially, robotic cleaners are defined by their cleaning abilities, such as floor mopping, dry vacuum cleaning, and so on. Some devices rely on simple obstacle avoidance using infrared sensors, whereas others rely on laser mapping. Each cleaning and operation mechanism in robotic floor cleaners has its own set of benefits and drawbacks.[3] Fully automatic and semi-automatic machines are both expensive and heavyweights on the market. As a result of focusing on both weight and cost, they are out of reach for many people, including the organising committees of hotels, hospitals, and hostels. As a result, there is a need to design and build a floor cleaning machine that is both simple to use and cost-effective. This machine is simple to use, and not only does it save time and money when cleaning. The cost of maintenance is likewise relatively low.[3]

II. LITERATURE SURVEY

A solar-powered floor cleaning machine, "AKASH NAGTODE (2017). He has created a solar-powered cleaning system. He employed a photovoltaic panel to transform energy particles (photons) into electricity. He powers his cleaning machine with this clean energy."[4] According to M. Ranjit Kumar (2016), "regular floor cleaning machines are most commonly used as a part of aeroplane terminal stages, railway stages, healing centres, transportation stands, and shopping centres, as well as in numerous other business places." These devices require an electrical current to function and are difficult to use. In India, particularly during the summer, there is a control emergency, and the vast majority of floor cleaning machines are not used effectively as a result, particularly in transit stands. The floor cleaning machine was demonstrated and investigated in this study using proper, financially accessible programming. We can see from the restricted component analysis that the emotion of worry in the physically performed floor cleaning

ISSN No:-2456-2165

Solar Powered Multipurpose Agriculture Robot

[1]Namburi Nireekshma
Assistant Professor,
EEED,
Methodist College of Engineering &Technology

[2]M. Anil Goud
160719734315
BE, EEE
Methodist College of engineering & Technology

[3]R. Bhavani Shankar
160719734301
BE, EEE
Methodist College of Engineering & Technology

[4]G. Nitin Sai chandra
160719734004
BE, EEE
Methodist College of Engineering & Technology

Abstract:- In India, more than 60 percent of the people works in agriculture as their main job. Due to a growing lack of workers, there is now more interest in developing robots and other self-driving cars for use in agriculture. A robot called a "agriculture robot" has been made to reduce the amount of work farmers have to do and to speed up and improve the quality of their work. The goal of the proposed system is to make a multipurpose autonomous agricultural robotic vehicle that can be controlled through Bluetooth. This vehicle could be used for sowing seeds, cutting grass, ploughing, detecting soil moisture, spraying pesticides, and detecting leaf diseases with a Raspberry Pi and suggesting what kind of pesticides should be used for that disease. Autonomous cars are used so that people don't have to do as much work. This leads to a higher yield and better use of resources.

Keywords: Raspberry Pi, Arduino Uno Mini, Controllers, Solar Energy.

I. INTRODUCTION

Agriculture is the backbone of India. India is now the world's second-largest agricultural product producer. The agricultural special vehicle field is gradually expanding its manufacturing. Growing input prices, a paucity of qualified workers, a scarcity of water resources, and crop monitoring are all critical challenges in India's agricultural economy. Automation technologies have been used in agriculture to address these concerns. The agricultural census provides critical information about the distribution of land ownership in our country.

According to the census, the majority of farmers hold less than one hectare of land. This is one of the most serious drawbacks of agricultural mechanisation in India. Vehicles are being built for a variety of operations, including ploughing, seed planting, levelling, water spraying, and grass cutting. These tasks have yet to be achieved with a single vehicle. The robots in this project are meant to focus effectively and do tasks independently. The proposed design employs a vehicle to do duties such sloughing, sowing, grass cutting, pesticide spraying, and detecting and recommending pesticides for leaf disease. These responsibilities are consolidated and carried out in a single vehicle. Farmers may reduce environmental impact, improve accuracy and efficiency, and manage individual plants in novel ways by monitoring farms 24 hours a day, seven days a week. Because the capacity to replace human operators provides cost-effective solutions with a high return on investment, instrumental robotics applications are expanding every day to encompass new disciplines. This is especially important when the jobs that must be done pose a risk to the employees' safety or health, or when robots allow for more conservative concerns. As autonomous solutions are deployed, heavy chemical or pharmaceutical distributors, manure or fertilizer spreaders, and other activities are getting more concerned. However, the agricultural situation is deteriorating. This is because of a lack of automation. Furthermore, development requires coordination between electrical and agricultural professionals.

II. LITERATURE SURVEY

Vishnu Prakash Karunakare et al. discuss a project aimed at creating, implementing, and testing an autonomous multipurpose vehicle capable of operating in a safe, efficient, and cost-effective manner. This self-driving vehicle travels through crop lines on agricultural property, performing activities that are tiresome and/or dangerous to farmers. It was first outfitted for spraying, but alternative configurations, such as a seeding, plug platform to reach the highest portion of the plants to do various jobs (pruning, harvesting, etc.), and a trailer to transport the fruits, plants, and crop waste, have also been built.

Burra Hymavathi, J Hariharan, K Manideep, D V Srikanth, and others present an agricultural multipurpose robot project aimed at designing, implementing, and testing an autonomous multipurpose vehicle with efficiency and economic operations for tilling, sowing seeds, spraying fertilisers, and sprinkling water simultaneously. It runs on solar power, is entirely automated, and can be utilised by a single person in arid and semi-arid areas. This vehicle goes through the crop lines and completes tasks, decreasing the need for personal intervention.

Chetan Patil, Vishal Deshmukh, Shailesh Deshmukh, Govind Rai, Parag Bute, and others: create a robot capable of autonomous ploughing, seed distributing, and pesticide

FOREX Publication
Open Access | Rapid and quality publishing

International Journal of
Electrical and Electronics Research (IJEER)
Research Article | Volume 11, Issue 2 | Pages 465-472 | e-ISSN: 2347-470X

Design and Control of a Tricycle with a Hybrid Electric Motor Cooling System Powered By Solar Photovoltaics

Jarapala Ramesh Babu[1*], Manas Ranjan Nayak[2] and B.Mangu[3]

[1,2]Department of Electrical Engineering, Biju Patnaik University of Technology Rourkela, Odisha, 769015, India, babu.ramesh444@gmail.com[1], manasnk72@gmail.com[2]

[3]Department of Electrical Engineering, University college of Engineering, Osmania University, Hyderabad, 500007, India, bmanguou@gmail.com[3]

*Correspondence: Jarapala Ramesh Babu, Email: babu.ramesh444@gmail.com.

ABSTRACT- The power for a standard electric tricycle used for transportation comes from a battery, which can lose power after a certain amount of time. In this regard, the standard tricycle in the proposed concept will have a battery that will be charged by solar panels mounted on a stand on the rear of the tricycle. A solar-based renewable energy source is also used along with the traditional charging mechanism to make a hybrid system. The proposed tricycle is more stable in braking turns because it has a lower center of gravity compared to a bicycle. The proposed tricycle has movement in both directions, i.e., forward and reverse, for disabled persons. The proposed model was validated using the finite element analysis approach in solid work for different points of the frame and different types of loads. Also Electric motors have a great efficiency of operation, but they create a lot of heat depending on the torque and speed they need to run. As a result, an effective motor cooling system is required to keep the temperature within restrictions. Although the coolant pump and radiator fan in a conventional motor liquid cooling system do an efficient job, they are also energy hogs. The FEA approach was used to identify the maximum stress, displacement, and safety factors.

Keywords: Solar Power, Battery, Finite element analysis, solid work, tricycle, BLDC motor.

ARTICLE INFORMATION

Author(s): Jarapala Ramesh Babu, Manas Ranjan Nayak and B.Mangu;

Received: 06/09/2022; **Accepted:** 21/01/2023; **Published:** 30/06/2023;
E-ISSN: 2347-470X;
Paper Id: IJEER220611;
Citation: 10.37391/IJEER.110229
Webpage-link:
https://ijeer.forexjournal.co.in/archive/volume-11/ijeer-110229.html

1. INTRODUCTION

Automobiles, buses, trains, and motorcycles are all modes of transportation that have a number of negative consequences for their users and the environment. The expense, air pollution, and health hazards associated with these difficulties might all be different[1] [2]. According to the Washington Post, 13 billion people do not have access to electricity around the world. This is due to the high cost of electrical sources, which many countries are unable to afford to offer their citizens. Furthermore, car exhaust contributes to air pollution, which is harmful to the environment. Furthermore, long-term use of automobiles, motorcycles, and various forms of public transit will result in obesity due to the lack of activity that these modes of transportation provide. In fact, the World Health Organization estimates that about 650 million individuals are obese. Bicyclists utilise their tricycles to get from one point to another all over the world, and many of them use tricycles to travel. As a result, it's critical to devise a method for these bikers to relax during their long-distance journeys. As a result, developing a new clean, renewable, and healthier mode of transportation is one of the most pressing issues facing engineers today. As engineering students, we think that using solar energy and a dynamo to power a hybrid (electric and manual) tricycle can be a cheap and easy way for people to get around on a daily basis[3].

The Central Mechanical Engineering Research Institute in Kolkata designed it as an alternative to auto rickshaws powered by IC engines. A solar-powered charging system was also incorporated into the prototype[4]. One shock absorber and a flashlight were included in the suspension system to make night time riding more comfortable. This could also be beneficial in a foggy or rainy environment to improve visibility. Additionally, the back wheels could be driven manually or by a motor. The vehicle had a maximum weight capacity of 200 kg and a maximum speed of 15 km/h[5].

The major drawback of conventional wheelchairs is their characteristic feature of the necessity of manual operation with a handheld rotary pedal [6] [7]. Hence, the electric wheelchair was introduced to overcome the necessity of manual operation with a handheld rotary pedal. However, an electric wheelchair requires rechargeable batteries to be operated, and his major drawback of an electric wheelchair vehicle is its incapability to travel longer distances due to inadequate battery life. In addition, disabled people operating the electric wheelchair vehicle may not be able to plug in the charger to recharge the batteries. Hence, in this paper, a three-wheeler hybrid electric vehicle based on solar energy is proposed.

These approaches include air cooling, liquid cooling, heat pipes, and hybrid cooling are some examples of these methods. Air

FOREX Publication
Open Access | Rapid and quality publishing

International Journal of
Electrical and Electronics Research (IJEER)
Research Article | Volume 11, Issue 2 | Pages 457-464 | e-ISSN: 2347-470X

Development and Application of an Energy Management System for Electric Vehicles Integrated with Multi-input DC-DC Bidirectional Buck-Boost Converter

Jarapala Ramesh Babu[1*], Manas Ranjan Nayak[2] and B.Mangu[3]

[1,2]Department of Electrical Engineering, Biju Patnaik University of Technology Rourkela, Odisha, 769015, India, babu.ramesh444@gmail.com[1], manasnk72@gmail.com[2]
[3]Department of Electrical Engineering, University college of Engineering, Osmania University, Hyderabad, 500007, India, bmanguou@gmail.com[3]

*Correspondence: Jarapala Ramesh Babu, Email: babu.ramesh444@gmail.com

ABSTRACT- The rise in environmental pollution, demand for fossil fuels, and higher fuel economy vehicles has raised concerns about the creation of new and efficient transportation vehicles in recent days. These days, most developments in electric vehicles concentrate on making the vehicles more pleasant to ride in. Nonetheless, the emphasis now should be on energy and its most efficient use. To do this, you must give your attention to the origin of the automobile. The answer to this problem may be found in hybrid energy storage systems (HESS). This work is concerned with the design and implementation of an effective energy management system in electric vehicles (EVs) equipped with an active HESS consisting of a battery and a super capacitor via the incorporation of load sharing into this hybridization under a variety of load demand scenarios. To address the demands of high fuel efficiency vehicles, automotive firms are focusing on the development of diesel-engine operated vehicles, electric vehicles, fuel-cell vehicles, plug-in electric vehicles, and hybrid electric vehicles. A Multi-input Bidirectional Buck-Boost (MIB^3) DC-DC converter is proposed in this dissertation to provide a greater conversion ratio to the input DC voltage. The multi-input converter recommended has fewer components and a simpler control method, making it more trustworthy and cost-effective. This converter also has bidirectional power flow functionality, making it suitable for charging the battery during regenerative braking in an electric or hybrid vehicle. Three different energy sources are used in the suggested topology: a photovoltaic (PV) panel, a battery, and an ultra-capacitor.

Keywords: Multi-input dc-dc converter, Hybrid energy storage system (HESS), ultra-capacitor (UC), BLDC motor.

ARTICLE INFORMATION
Author(s): Jarapala Ramesh Babu, Manas Ranjan Nayak and B.Mangu;
Received: 18/2/2023; **Accepted:** 13/06/2023; **Published:** 30/06/2023;
E- ISSN: 2347-470X;
Paper Id: IJEER230207;
Citation: 10.37391/IJEER.110228
Webpage-link:
https://ijeer.forexjournal.co.in/archive/volume-11/ijeer-110228.html

Publisher's Note: FOREX Publication stays neutral with regard to jurisdictional claims in Published maps and institutional affiliations

1. INTRODUCTION

The main drawbacks of internal combustion engine-powered autos are rising fuel costs, pollution issues, and fossil fuel depletion. To address the aforementioned challenges, the automobile industry has begun to demonstrate an interest in vehicles that use alternative energy sources. As a result, electric vehicles (EVs) and plug-in hybrid EVs are becoming increasingly popular. Thus, energy storage equipment such as batteries and ultra-capacitors can be used to convert traditional vehicular systems into electric or hybrid electric vehicle.

Concerns about environmental degradation have raised demand for non-polluting and energy-efficient automobiles (Shiue & Lin 2011, Wyczulek 1995, Rajashekara & Martin 1995, Yang et al. 2002, Shiue & Lin 2011). Because of the growing demand for non-polluting vehicles, the automotive industry is concentrating on the development of electric vehicles (EV), fuel cell vehicles (FCV), plug-in hybrid electric vehicles (PHEV), PV interfaced electric vehicles, and hybrid electric vehicles (HEV) (Emadi et al. 2008, Daya et al. 2016, Kim 2011). Among these, electric vehicles (EVs) and hybrid electric vehicles (HEVs) offer a viable solution for reducing CO2 emissions and fossil fuel consumption (Gao et al. 2007, Chau et al. 2008, Miet al. 2005). During acceleration, the EV and HEV use electrical energy to complement the output of an internal combustion (IC) engine, and during braking, the energy supplied by the electric motor is restored[1] [2] [3] [4].

The following criteria define the EV and HEV's capability: 1) the ability to reduce the battery storage unit's power consumption during acceleration. 2) The system's ability to recover electrical energy lost during braking. 3) the ability to eliminate the IC Engine's perfect operation, and 4) the capacity to produce enough torque to fulfil demand. Researchers have come up with a lot of different ways to make HEVs and EVs more efficient and cheaper. Xiong et al. (2008), Chan 2007, and Rajashekara (2013) are some of them[5].
To govern the power flow from car to home and home to vehicle, the smart controller has been connected to the status of

ScienceDirect

International Journal of Lightweight Materials and Manufacture

Volume 6, Issue 2, June 2023, Pages 264-277

Original Article

Effect of retrogression and reaging (RRA) on pitting and stress corrosion cracking (SCC) resistance of stir zone of high strength AA7075-T651 alloy joined by friction stir welding

P. Prabhuraj [a], S. Rajakumar [b], Tushar Sonar [c], Mikhail Ivanov [c], I. Rajkumar [d], D. Elil Raja [e]

Show more

https://doi.org/10.1016/j.ijlmm.2022.12.002

Get rights and content

Abstract

The main purpose of this study is to investigate the influence of retrogression and re-aging post weld heat treatment (RRA-PWHT) on potentiodynamic corrosion (PC) and stress corrosion cracking resistance (SCC) of stir zone (SZ) of AA7075-T651 alloy butt joints developed using friction stir welding (FSW). FSW was employed to overcome the problems in fusion welding of AA7075-T651 alloy such as solidification cracking, heat affected zone (HAZ) softening, grain coarsening, dissolution of strengthening precipitates and inferior mechanical performance. The SZ of joints were subjected to potentiodynamic corrosion test in 3.56wt% NaCl solution. The circumferential notch tensile (CNT) specimens were subjected to SCC test at various conditions of axial stress level in 3.56wt% NaCl solution. The microstructural features of butt joints SZ were characterized using optical (OM), scanning electron (SEM) and transmission electron microscope (TEM). The results disclosed that RRA-PWHT joints exhibited greater PC and SCC resistance compared to as-welded joints. The threshold stress level for the failure of CNT specimens of parent metal, as-welded joints and RRA-PWHT joints was 242MPa, 175MPa and 198MPa, respectively. The threshold stress level of RRA-PWHT joints and as-welded joints is 81.81% and 72.31% of parent metal threshold stress level. It is correlated to increase in vol% and coarsening of grain boundary precipitates with enrichment of copper at the grain boundaries.

e-ISSN: 2582-5208
International Research Journal of Modernization in Engineering Technology and Science
(Peer-Reviewed, Open Access, Fully Refereed International Journal)
Volume:04/Issue:07/July-2022 Impact Factor- 6.752 www.irjmets.com

DESIGN AND FLOW ANALYSIS OF AIR-CONDITIONED SPACE

Dr. Md. Fakhruddin H.N.*1, Mohammed Adeel Ahmed*2, Salman Khan*3, Raheel Khan*4, Izhaan Mohiuddin*5

*1Associate Professor, Department Of Mechanical Engineering, Methodist College Of Engineering And Technology, Hyderabad, Telangana State, India.

*2,3,4,5Alumni Students, Department Of Mechanical Engineering, Muffakham Jah College Of Engineering And Technology, Hyderabad, Telangana State, India.

ABSTRACT

Today, the field of air conditioning design is more technologically challenging than ever before. While design innovations and product improvement promise sleeker, more versatile, more powerful and more energy-efficient air conditioners, the challenge today lies in identifying the most appropriate products, for their application at hand. Indeed, today the emphasis is no more on understanding air conditioning "products" but on crating "solutions" and not just solutions, but "customized solutions" that suit specific needs i.e., heating/cooling or ventilation. To quantify the air distribution required plays a vital role in HVAC. Quantity of air, which is evaluated from the heat gains/loss into the space need to be properly evaluated considering the orientation if the building, type of glass/structure, occupancy and nature of work in the conditioned area, so is the quantity of air need to be exhausted for the design of duct and to execute the flow analysis for the same.

Keywords: HVAC, Air Distribution, Duct Design, Analysis.

I. INTRODUCTION

Chilled water central air conditioning plant is more useful for large buildings comprising of a number of floors. It has the plant room where all the important units like the compressor, condenser, throttling valve and the evaporator are housed. The evaporator is a shell and tube. On the tube side the Freon fluid passes at extremely low temperature, while on the shell side the brine solution is passed. After passing through the evaporator, the brine solution gets chilled and is pumped to the various air handling units installed at different floors of the building. The air handling units comprise the cooling coil through which the chilled brine flows, and the blower. The blower sucks hot return air from the room via ducts and blows it over the cooling coil. The cool air is then supplied to the space to be cooled through the ducts. The brine solution which has absorbed the room heat comes back to the evaporator, gets chilled and is again pumped back to the air handling unit.

II. LITERATURE REVIEW

While moving heat via machinery to provide air conditioning is a relatively modern invention, the cooling of buildings is not. Wealthy ancient Romans circulated aqueduct water through walls to cool their luxurious houses.

The 2nd century Chinese inventor Ding Huan of the Han Dynasty invented a rotary fan for air conditioning, with seven wheels 3 m (10 ft) in diameter and manually powered. In 747, Emperor Xuanzong of the Tang Dynasty had the Cool Hall built in the imperial palace, which the Tang Yulin describes as having water-powered fan wheels for air conditioning as well as rising jet streams of water from fountains. During the subsequent Song Dynasty (960–1279), written sources mentioned the air conditioning rotary fan as even more widely used.

III. METHODOLOGY

Estimation of heating/cooling load may be done both E-20 method and using Carrier made hourly analysis program (HAP)- software. Hourly Analysis Program (HAP) is a computer tool which assists engineers in designing HVAC systems for providing estimation for AC load for a given building or occupancy. HAP is two tools in one. First it is a tool for estimating loads and designing systems. Second, it is a tool for simulating building energy use and calculating energy costs. In this capacity it is useful for LEED®, schematic design and detailed design energy cost evaluations. HAP uses the ASHRAE transfer function method for load calculations and detailed 8,760 hour-by-hour simulation techniques for the energy analysis.

(https://www.ijraset.com/)

Journal Statistics & Approval Details (https://www.ijraset.com/journal-impact-factor.php)
Recent Published Paper (https://www.ijraset.com/recent-papers.php)
Our Author's Feedback (https://www.ijraset.com/user-feedbacks.php)

- ISRA Impact Factor 7.894 (https://www.israjif.org/single.php?did=2321-9653)
- SJIF Impact Factor: 7.538 (http://sjifactor.com/passport.pl

ISSN: 2321-9653
Estd : 2013

Ijraset Journal For Research in Applied Science and Engineering Technology

On This Page

Computational Fluid Dynamics in Coronary and Intra-Cardiac Flow Simulation

Authors: Mohammed Abdul Mannan, Dr. Md Fakhruddin H. N.

DOI Link: https://doi.org/10.22214/ijraset.2022.45280 (https://doi.org/10.22214/ijraset.2022.45280)

Certificate: View Certificate (https://www.ijraset.com/print-certificate/computational-fluid-dynamics-in-coronary-and-intracardiac-flow-simulation)

Abstract

Computational fluid dynamics (CFD) is a field of mechanical engineering for the analysis of fluid flows, heat tran sfer, and related phenomena, using computer simulations. CFD is a widely adopted methodology for solving co mplex problems in many areas of modern engineering. The merits of CFD are the development of new and impr oved equipment and system designs, and optimizations are performed on existing equipment through simulatio n, leading to increased efficiency and reduced costs. However, in the biomedical sector, CFD are still emerging

Effect of pH value, chloride ion concentration and salt spraying time on salt fog corrosion resistance of friction stir welded AA7075-T651 alloy joints

Original Paper Published: 27 June 2023

(2023) Cite this article

International Journal on Interactive Design and Manufacturing (IJIDeM)

Aims and scope

Submit manuscript

P. Prabhuraj ✉, S. Rajakumar, V. Balasubramanian, Tushar Sonar, Mikhail Ivanov & D. Elil Raja

Hindawi

Advances in Materials Science and Engineering

Special Issue

Processing and Characterization of Advanced Lightweight Composites for Engineering Applications

View this Special Issue

Research Article | Open Access

Volume 2023 | Article ID 2131077 | https://doi.org/10.1155/2023/2131077

Show citation

Investigating the Microstructure, Tensile Strength, and Acidic Corrosion Behaviour of Liquid Metal Stir Casted Aluminium-Silicon Carbide Composite

S. Prathap Singh,[1] D. Ananthapadmanaban,[2] **D. Elil Raja**,[1] Tushar Sonar,[3] Mikhail Ivanov,[3] P. Prabhuraj,[4] and V. Sivamaran[5]

Show more

Academic Editor: P. M. Gopal

WIRE EDM INVESTIGATION ON AL 7475 ALLOY: PARAMETER, VARIATION, MRR, SR AND MICROSTRUCTURE COMPASSION

T. Rahul Shanker Goud
M.E student

Dr Md. Fukhruddin H.N
Associate Professor

Department of Mechanical Engineering
Methodist College of Engineering and Technology
Hyderabad, Telangana, India

Abstract: *The Wire electrical discharge machining (WEDM) is a specialized thermal machining process capable of accurately machining parts with varying hardness or complex shapes, which have sharp edges that are very difficult to be machined. This practical technology of the WEDM process is based on the conventional EDM sparking phenomenon utilizing the widely accepted non-contact technique of material removal. The objective of the present project is to analyze the effect of various wire cut EDM process parameters on surface quality, maximum material removal rates and obtain optimal sets of process on alloy ALUMINIUM 7475 by various parameters. The optimization is done by using Taguchi technique and Minitab software.*

Keywords: *Alloy, Aluminium 7475, Microstructure, Taguchi technique, Minitab software, Wire electrical discharge machining.*

1. INTRODUCTION

Electric Discharge Machining (EDM), a machining technique primarily applied to hard metals, proves effective where traditional methods fall short. Notably, EDM is applicable only to materials exhibiting electrical conductivity [1-2]. State-of-the-art EDM machinery enables precision cutting of intricate angles, detailed contours, and cavities in hardened steel, as well as challenging metals like Titanium, Hastelloy, Kovar, Inconel, and ceramics. Widely employed in the Tool and Die industry for mold-making, EDM has increasingly become integral to crafting prototype and production components, particularly in sectors such as aerospace and electronics, where production quantities remain limited[3]. The EDM process involves reducing the distance between two electrodes, causing an increase in the electrical field's intensity. When this surpasses the insulator's strength at certain points, a breakdown occurs, allowing current to flow between the electrodes and consequently removing material from both. After the cessation of this flow (or intentional interruption, depending on the generator type), a fresh liquid insulator is typically introduced into the inter-electrode volume [4-5]. This serves to remove solid particles (debris) and restore the insulating properties of the insulator. The process of introducing new liquid insulator into the inter-electrode volume is commonly referred to as flushing[6-7] Additionally, when the current flow is interrupted, a potential difference between the two electrodes is reset to its pre-breakdown level. This ensures that a new breakdown of the liquid insulator can occur when the conditions are met again[8-10].

Wire Electrical Discharge Machining (Wire EDM) is a pivotal manufacturing process employing a slender wire electrode to intricately shape conductive materials. Originating in the 1960s, this technique has become indispensable in diverse industries such as moldmaking, aerospace, and automotive. The inaugural commercially available wire EDM machine surfaced in the Soviet Union in 1967; however, these early models were limited in accuracy and applicable only to rudimentary shapes. The 1970s witnessed a

DE GRUYTER

Requires Authentication | Published by De Gruyter | November 29, 2022

Microstructure, tensile properties and fracture toughness of friction stir welded AA7075-T651 aluminium alloy joints

Prabhuraj Parasuraman, Tushar Sonar and Selvaraj Rajakumar

From the journal Materials Testing
https://doi.org/10.1515/mt-2022-0212

Abstract

The main objective of this investigation is to study the microstructure, tensile properties and fracture toughness of friction stir welded (FSW) butt joints of 10 mm thick AA7075-T651 plates. The microstructural features of stir zone (SZ), thermos-mechanically affected zone (TMAZ), heat affected zone (HAZ) were analyzed using optical microscopy technique. The tensile properties were evaluated using smooth and notch tensile specimens and compared to base metal properties. The microhardness survey was done across the weld cross section and

Modeling of Water Distribution Network Using WATERGEMS

Vijay Kaushik
Department of Civil Engineering, Delhi Technological University, Delhi, 110042

Munendra Kumar
Department of Civil Engineering, Delhi Technological University, Delhi, 110042

Bandita Naik
Department of Civil Engineering, Methodist College of Engineering, Hyderabad, 500001

Keywords: Water Distribution Network (WDN), Population growth, Delhi, Hydraulic simulation, WATERGEMS

Abstract

The primary issue with the current water distribution network is the available head and necessary quantity of water. Designing a new or upgrading an existing WDN is needed to tackle such problems using software. Because of water shortages and pressure variations in Delhi, a small town in the city has been chosen to assess the current WDN using WATERGEMS V8i. This research aims to use WATERGEMS V8i to assess the existing WDN and make recommendations for the current WDN to meet current and imminent demand. The obtained results confirmed that pressures, flow rate and velocities in the pipes and junctions are insufficient to give enough water. The established water delivery network was then proposed to be modified to fulfil current and future demands. In any circumstances, a sufficient amount of water must be delivered to the user endpoint with sufficient head and volume.

Estimation of Surface Runoff Using SWAT Model and ArcGIS Approach

Abhijeet Satapathy
Department of Civil Engineering, Methodist College of Engineering, Hyderabad, Telangana, 500001

Bandita Naik
Department of Civil Engineering, Methodist College of Engineering, Hyderabad, Telangana, 500001

Noopur Awasthi
Department of Civil Engineering, Delhi Technological University, Delhi, 110042

Vijay Kaushik
Department of Civil Engineering, Delhi Technological University, Delhi, 110042

Keywords: LU/LC change, SWAT model, Rainfall-Runoff, Nash Sutcliffe Efficiency, Coefficient of Determination

Abstract

Land use/land cover change studies assist the administration in understanding on-the-ground circumstances and taking the necessary steps to safeguard and conserve soil and water resources. The present research was conducted for the Rushikulya river basin in Odisha, utilising the Soil and Water Assessment Tool (SWAT) in conjunction with a Geographic Information System (GIS). The input data characteristics necessary to perform the simulation of watershed parameters are a LU/LC map, meteorological data, precipitation data, discharge data, soil data, and slope data. For this study, meteorological information from spanning the years 2000 to 2014 was utilised. The SWAT model was used in this work that estimates the variation effects of LU/LC concern to Rushikulya River Basin. The findings depict that the SWAT model shows excellent outcomes in runoff assessment with

Water Practice & Technology

Water Practice & Technology Vol 18 No 9, 2151 doi: 10.2166/wpt.2023.142

Modeling of water surface profile in non-prismatic compound channels

Vijay Kaushik [a,*], Munendra Kumar[a], Bandita Naik[b] and Abbas Parsaie[c]

[a]Department of Civil Engineering, Delhi Technological University, Delhi 110042, India
[b]Department of Civil Engineering, Methodist College of Engineering, Hyderabad 500001, India
[c]Department of Hydraulic Structures, Faculty of Water and Environmental Engineering, Shahid Chamran University of Ahvaz, Ahvaz, Iran
*Corresponding author. E-mail: vijay&kaushik 2k20phdce01@dtu.ac.in

VK, 0000-0002-7270-4520

ABSTRACT

Estimating the water surface elevation of river systems is one of the most complicated tasks in formulating hydraulic models for flood control and floodplain management. Consequently, utilizing simulation models to calibrate and validate the experimental data is crucial. HEC-RAS is used to calibrate and verify the water surface profiles for various converging compound channels in this investigation. Based on experimental data for converging channels ($\theta = 5°$, 9°, and 12.38°), two distinct flow regimes were evaluated for validation. The predicted water surface profiles for two relative depths ($\beta = 0.25$ and 0.30) follow the same variational pattern as the experimental findings and are slightly lower than the observed values. The MAPE for the simulated and experimental results is less than 3%, indicating the predicted HEC-RAS value performance and accuracy. Therefore, our findings imply that in the case of non-prismatic rivers, the proposed HEC-RAS models are reliable for predicting water surface profiles with a high generalization capacity and do not exhibit overtraining. However, the results demonstrated that numerous variables impacting the water surface profile should be carefully considered since this would increase the disparities between HEC-RAS and experimental data.

Key words: compound channel, converging floodplains, HEC-RAS modeling, water surface profile

HIGHLIGHTS

- In this article, research was conducted for the non-prismatic compound channel with converging floodplains, utilizing the HEC-RAS software.
- The findings depict the HEC-RAS models are accurate for forecasting the water surface profile of non-prismatic rivers, have a high capacity for generalization, and do not display any signs of overexertion.
- The usefulness of HEC-RAS tool for the design of flood control and diversion structures in the non-prismatic rivers.

Energy is essential to life and all living organisms. The sun, directly or indirectly, is the source of all the energy available on Earth. Our energy choices and decisions impact Earth's natural systems in ways we may not be aware of, so it is essential that we choose our energy sources carefully. Electricity from renewable energy sources produces between 90-99% less greenhouse gases (GHGs) compared with coal-fired plants and causes 70-90% less pollution. Focusing on renewable energy sources other than fossil fuels and coals might help in avoiding environmental impacts, specifically from air pollution. Eliminating fuel costs lowers the cost of the electricity produced. It also means the price of electricity isn't susceptible to changes in the price of fuels, like it is with natural gas or coal. This may lead to more stable energy prices over the long term. Finally Renewable technologies are considered as clean sources of energy and optimal use of these resources decreases environmental impacts, produces minimum secondary waste and are sustainable based on the current and future economic and social needs.

1.Dr. Bhukya Laxman, Associate Professor, Methodist College of Engineering & Technology,Hyderabad.
2. Namburi Nireekshana, Assistant Professor, Methodist College of Engineering & Technology,Hyderabad.
3.Mrs.Y.Mastanamma, Associate Professor & HOD, Methodist College of Engineering & Technology, Hyderabad.

9 786205 517949

BHUKYA LAXMAN
NAMBURI NIREEKSHANA
Y MASTANAMMA

ENERGY SCIENCE AND ENGINEERING

LAP LAMBERT Academic Publishing

LAXMAN, NIREEKSHANA, MASTANAMMA

BHUKYA LAXMAN
NAMBURI NIREEKSHANA
Y MASTANAMMA

ENERGY SCIENCE AND ENGINEERING

In recent years, power quality disturbances become most issue which makes many researchers interested to find the best solutions to solve it. Power quality in the power system is the important issue for industrial, commercial and residential applications today. The voltage problem is mainly considered from under-voltage (voltage sag) condition over current caused by short circuit or fault somewhere in the system. In customer opinion a power problem is deviation in voltage, current and frequency that results in failure.Power electronic converters have been developed several tenths of years ago for many types of applications. One of its major applications is for control of electrical machines, mainly used in the beginning for industrial applications, and now propagated in many household appliances. The beginning of the renewable energy story had a moderate influence on the power electronic converters market. Indeed, in the old small wind turbines, the mechanical power was converted to electrical power thanks to induction machines directly connected to the grid. Very quickly, the power of the wind turbine increased and more rules were implemented.

NAMBURI NIREEKSHANA graduated from ACTS, JNTU Hyderabad,received Master of Technology from UET JNTU Hyderabad, Research Scholar in Annamalai University. He is working on load frequency control area with Optimization Techniques.

9 786200 239310

PE Applications to Power systems (PEAPS)

NIREEKSHANA Namburi
RAMACHANDRAN R
G V NARAYANA

Power Electronics Applications to Power Systems

LAMBERT Academic Publishing

Namburi, R, NARAYANA

Water Science and Technology Library

Ramakar Jha · V. P. Singh ·
Vivekanand Singh · L. B. Roy ·
Roshni Thendiyath *Editors*

Hydrological Modeling

Hydraulics, Water Resources and Coastal Engineering

Springer

Water Science and Technology Library

Volume 109

Editors
Ramakar Jha
Department of Civil Engineering
National Institute of Technology
Patna, India

Vivekanand Singh
Department of Civil Engineering
National Institute of Technology Patna
Patna, India

Roshni Thendiyath
Department of Civil Engineering
National Institute of Technology Patna
Patna, India

V. P. Singh
Department of Biological and Agricultural Engineering
Texas A&M University
College Station, TX, USA

L. B. Roy
Department of Civil Engineering
National Institute of Technology Patna
Patna, India

ISSN 0921-092X ISSN 1872-4663 (electronic)
Water Science and Technology Library
ISBN 978-3-030-81357-4 ISBN 978-3-030-81358-1 (eBook)
https://doi.org/10.1007/978-3-030-81358-1

This Springer imprint is published by the registered company Springer Nature Switzerland AG
The registered company address is: Gewerbestrasse 11, 6330 Cham, Switzerland

Chapter 31
Rainfall–Runoff Studies of Brahmani River Basin Using ANN

Swagatika Biswal, Bandita Naik, and K. K. Khatua

Abstract Rainfall–runoff is a very complicated process due to its nonlinear and multidimensional dynamics, hence it is difficult to model. There are various methods for time series based on the model of rainfall and runoff. In the present study, feed-forward back-propagation and auto-regressive integrated moving average models are applied to predict monthly runoff in the Brahmani river of the three stations: Jaraikela, Jenapur, and Tiliga. ANN with different transfer functions like TANSIG and PURELIN is used to find runoff prediction in these areas. Different statistical error analysis is done, to know better transfer function. From the observation, it was concluded that the transfer function gives better results than PURELIN. The predicted runoff found by TANSIG transfer function was again compared with ARIMA model. From the statistical error analysis, it was observed that ANN gave better results than the ARIMA method.

31.1 Introduction

Many natural resources are available on the earth. Water is one of the most important natural resources. Without water, life cannot be imagined on the earth's surface. 71% of the earth's surface is water-covered, and the oceans hold about 96.5% of all earth's water. Water also exists in the air as water vapors, in rivers and lakes, in icecaps and glaciers, in the ground as soil moisture, and in aquifers (Ref. water.usgs.gov). But the problem is that water is not available at the proper place at the proper time. Water is not constant. It always moves on from one place to another. Water in the different catchment areas always changes from one state to another under the effect of solar radiation. The water surface is converted to vapor by evaporation due to solar heat

S. Biswal (✉)
Department of Civil Engineering, CAPGS, BPUT, Rourkela, India

B. Naik
Faculty in Department of Civil Engineering, CAPGS, BPUT, Rourkela, India

K. K. Khatua
Department of Civil Engineering, NIT, Rourkela, Rourkela, India

R. Jha et al. (eds.), *Hydrological Modeling*, Water Science and Technology Library 109,
https://doi.org/10.1007/978-3-030-81358-1_31

Water Science and Technology Library

Ramakar Jha · V. P. Singh ·
Vivekanand Singh · L. B. Roy ·
Roshni Thendiyath *Editors*

River Hydraulics

Hydraulics, Water Resources and Coastal Engineering Vol. 2

Springer

Water Science and Technology Library

Volume 110

Editors
Ramakar Jha
Department of Civil Engineering
National Institute of Technology
Patna, India

Vivekanand Singh
Department of Civil Engineering
National Institute of Technology Patna
Patna, India

Roshni Thendiyath
Department of Civil Engineering
National Institute of Technology Patna
Patna, India

V. P. Singh
Biological and Agricultural Engineering
Texas A&M University
College Station, TX, USA

L. B. Roy
Department of Civil Engineering
National Institute of Technology Patna
Patna, India

ISSN 0921-092X ISSN 1872-4663 (electronic)
Water Science and Technology Library
ISBN 978-3-030-81767-1 ISBN 978-3-030-81768-8 (eBook)
https://doi.org/10.1007/978-3-030-81768-8

This Springer imprint is published by the registered company Springer Nature Switzerland AG
The registered company address is: Gewerbestrasse 11, 6330 Cham, Switzerland

Toggle navigation

- banditanaik1982@gmail.com LOGOUT
-
-
-

- Home
- My data
- Projects
- Refer your Friends
- Royalty Payments
- Marketing Material
- Group Deals

My Projects

- Title
- Subtitle
- PDF Upload
- Bio/Vita
- Author image
- Accepted

Project ID: #229335

Introduction to Climate Change

ISBN:	978-620-5-49149-2
Editor:	rlanguelale
Contributor :	Bandita Naik
Status:	Published

Download eBook

WATER RESOURCES

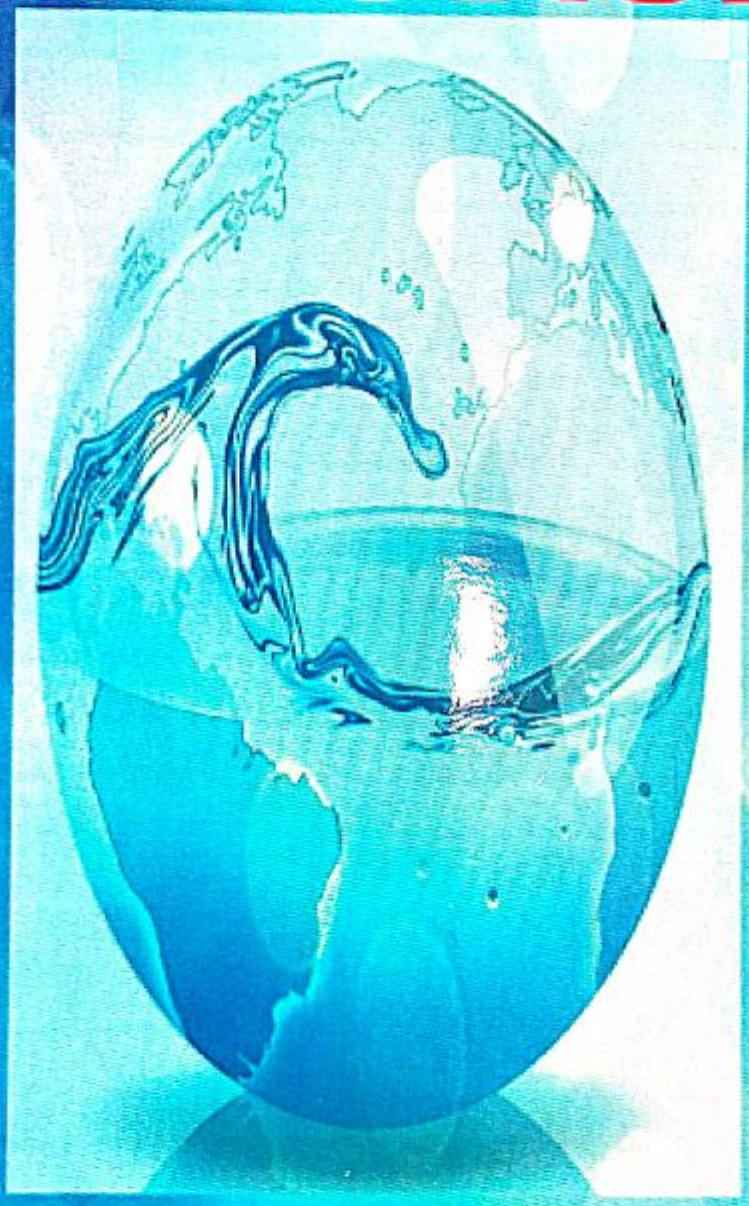

DR. BANDITA NAIK
DR. SUDHAKAR SINGHA
DR. SOUMYA S. SINGHA

NOTION PRESS

India. Singapore. Malaysia.
Published by Notion Press 2022

ISBN 9-7988-873-39-37

Author's Profile

Dr. Soumya S. Singha is presently working as Associate Professor and Head of Department of Civil Engineering at KG Reddy College of Engineering & Technology, Hyderabad, Telangana. She has graduated in 2006 with "Honours" and was a "Gold Medalist" in M.Tech with a specialization in Water Resources Development and Irrigation Engineering in Department of Civil Engineering from NIT, Raipur in the year 2013. She has completed PhD in Water Resources from IIT (ISM) Dhanbad in 2020. She has vast experience in teaching with more than ten years in engineering colleges. She has authored more than fifteen research papers in various National and International SCI/SCIE/SCOPUS indexed peer reviewed journals. She is a reviewer of different renowned International peer reviewed journals. She has four Indian patents publication. She is the author of one text book of Civil Engineering in field of water resources.

Dr. Sudhakar Singha is presently working as Assistant Professor in Civil Engineering Department of GITAM (Deemed to be University), Hyderabad, Telangana. He obtained B.Tech in Civil Engineering from BPUT, Rourkela in 2006, M.Tech (Water Resources Development and Irrigation Engineering) from NIT, Raipur and Ph.D in Water Resources Engineering from IIT (ISM), Dhanbad in year 2013 and 2021, respectively. He was recipient of "Gold Medal Award" in his M.Tech from NIT, Raipur in 2014. He has more than ten years of industry, teaching and research experiences. He is associated with number of professional organizations. He is the corporate member of The Institution of Engineers (India) and Life member of International Association of Engineers. He has published more than twelve National and International Journals in the area of Water Resources and Environmental Engineering. He has four Indian patents publications. He is the author of one Civil Engineering textbook in the field of water resources.

Dr. Bandita Naik is presently working as Associate Professor in Civil Engineering Department of Methodist College of Engineering and Technology, Hyderabad, Telangana. She obtained B.Tech in Civil Engineering from Biju Patanaik University of Technoly, Rourkela in 2005, PhD in Water Resources Engineering from National Institute of Technology, Rourkela in 2017. She has authored more than twenty research papers in various National and International peer reviewed journals. She is the author of one text book of Civil Engineering in field of water resources.

Scientific International Publishing House

ISBN
978-93-5625-397-1

A Textbook of Environmental Science

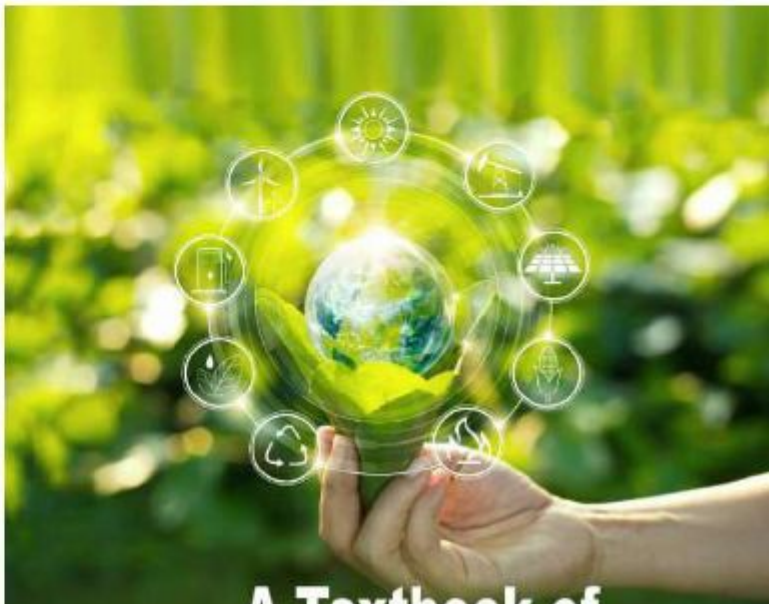

A Textbook of Environmental Science

Dr. SOUMYA S. SINGHA
Dr. SUDHAKAR SINGHA
Dr. BANDITA NAIK

GRENZE Scientific Society

Grenze International Journal of Engineering and Technology, Jan Issue

A Novel Web Application of Product Recommender System based on Sentiment Analysis

Dr Lavanya Pamulaparty[1], Mohammed Adnan[2] and Abdul Moid Khan Mohammed[3]
[1-3]Methodist College of Engineering and Technology/CSE, Hyderabad, India
Email: lavanya.post@gmail.com, mohd.adnan2317@gmail.com, skhan852000@gmail.com

***Abstract*—In present scenario the data overload is a serious problem. for mere humans, its impossible to analyse data manually without error or bias. One prime example of this regarding the review of products on e-commerce websites is that when a customer buys a certain product, he first looks for its ratings and then decides whether to buy that item or not. But only ratings are insufficient to determine the quality of the product. Reviews give us a much clearer and more in-depth understanding of the product. There is a need to summarize the feedback in a meaningful manner. Here's where sentimental analysis comes into play. Sentiment analysis can be automated, decisions can be made based on a significant amount of data rather than plain intuition that isn't always right. This proposed model combines sentiment analysis and a recommendation system to provide users with a comprehensive recommendation of e-commerce products. The aim of this analysis is to determine the orientation of a review then the recommender module provides users with product recommendations by analyzing large amounts of user-supplied data that is ratings and the sentiments of users and other factors like price and the number of sales to provide the user with the best recommendation. This is developed in the Python language.**

***Index Terms*— Sentiment Analysis, Product Reviews, Vader Sentiment.**

I. Introduction

In a world driven by data, the limitations, and possibilities of what we can carry out with the data are unfathomable. Whether it is data from a football game or a student's database, there are times when we can give meaningful execution to the data at hand and use it to solve a variety of issues and make our lives easier.

Companies may have bought mountains of client feedback in today's data-overloaded atmosphere. However, it is still hard for normal people to manually analyse it without inaccuracy or bias. A perfect illustration of this relating to product reviews on e-commerce websites is the fact that when a buyer buys a product, he first checks its ratings before deciding whether to buy it. However, merely ratings are insufficient to adequate for deciding the product's quality. Reviews supply a far more precise and comprehensive picture of the product. Additionally, we may have our own prejudiced, predetermined notions on the issue at hand, which may affect how we understand the material we must analyse. We will also need to synthesise the input into a handful of actionable insights so that it is useful to the user. Users want insights to make an educated decision before buying a product. And they are inadequate. We must devise a more efficient strategy for gaining the most valuable ideas. Here, emotive analysis comes into play and aids the user in condensing evaluations and providing a concise insight. Sentiment analysis may be automated, and choices can be made based on a substantial quantity of data as

Grenze ID: 01.GIJET.9.1.657

Grenze International Journal of Engineering and Technology, Jan Issue

A Cyber Physical System Enabled Intelligent Farming System with Artificial Intelligence, Machine Learning and Cloud Computing

Diana Moses[1], T Praveen Kumar[2], Sharada Varalakshmi[3] and Lavanya Pamulaparty[4]
[1,2]Associate Professor, Methodist College of Engineering and Technology, Hyd, India
[3]Professor, Methodist College of Engineering and Technology, Hyd, India
[4]Professor and Head, Methodist College of Engineering and Technology, Hyd, India

Abstract—**In this proposal, we study the advances of major core technologies and their applicability in creating an Intelligent farming System (IFS). As the world is trending into new technologies and implementations it is a necessary goal to trend up with agriculture also. Cyber Physical System (CPS) plays a very important role in Smart Farming. IOT sensors are capable of providing information about agriculture or Farming fields.**
We have proposed a Cyber Physical System (CPS) enabled smart agriculture system using different technologies like AI&ML, Data Science and Cloud Computing. This CPS based Intelligent Farming system makes use of sensor networks that collects data from different sensors which as a result develop an Intelligent Village Farming. Several Utilities such as Pest management, Crop Stress management, Nutrient management, Water management and Deep Analysis can be done to suggest the farmer regarding the crop and climatic conditions. This smart agriculture or Smart Farming using Cyber Physical System (CPS) is powered by advances in sensor technology, wireless communication technologies and their applicability to farming Chatbot, Computer vision, technology enabling farming, it consists of sensor followed by technological techniques.

Index Terms— **Intelligent Farming System, Crop disease detection, Automated irrigation, Yield prediction, Soil nutrition management.**

I. Introduction

Irrigation was defined as "the application of water supplementary to that supplied directly by precipitation for the production of crops". Although clearly defined, irrigation has not been clearly identified and separated from the wide-ranging area of water development activities, such as major and minor constructions for water harvesting, storing, conveyance and allocation; the drilling of tube-wells; and pumping. Most of the efforts and investments made in many countries for irrigation development result in water resources development and very few in on-farm water use improvement. The application of improved irrigation methods and techniques on small to large farms is expanding rapidly as a result of the increasing demand for higher irrigation efficiency, improved utilization of water and intensification, diversification & optimization. An irrigation system consists of canals and structures to convey regulate and deliver the water to the farmers. Two basic types of irrigation systems exist: open canal systems and pressurized piped systems.

Grenze ID: 01.GIJET.9.1.663

Grenze International Journal of Engineering and Technology, Jan Issue

A Cyber Physical System Enabled Intelligent Farming System with Artificial Intelligence, Machine Learning and Cloud Computing

Diana Moses[1], T Praveen Kumar[2], Sharada Varalakshmi[3] and Lavanya Pamulaparty[4]
[1,2]Associate Professor, Methodist College of Engineering and Technology, Hyd, India
[3]Professor, Methodist College of Engineering and Technology, Hyd, India
[4]Professor and Head, Methodist College of Engineering and Technology, Hyd, India

***Abstract*—In this proposal, we study the advances of major core technologies and their applicability in creating an Intelligent farming System (IFS). As the world is trending into new technologies and implementations it is a necessary goal to trend up with agriculture also. Cyber Physical System (CPS) plays a very important role in Smart Farming. IOT sensors are capable of providing information about agriculture or Farming fields.**

We have proposed a Cyber Physical System (CPS) enabled smart agriculture system using different technologies like AI&ML, Data Science and Cloud Computing. This CPS based Intelligent Farming system makes use of sensor networks that collects data from different sensors which as a result develop an Intelligent Village Farming. Several Utilities such as Pest management, Crop Stress management, Nutrient management, Water management and Deep Analysis can be done to suggest the farmer regarding the crop and climatic conditions. This smart agriculture or Smart Farming using Cyber Physical System (CPS) is powered by advances in sensor technology, wireless communication technologies and their applicability to farming Chatbot, Computer vision, technology enabling farming, it consists of sensor followed by technological techniques.

***Index Terms*— Intelligent Farming System, Crop disease detection, Automated irrigation, Yield prediction, Soil nutrition management.**

I. Introduction

Irrigation was defined as "the application of water supplementary to that supplied directly by precipitation for the production of crops". Although clearly defined, irrigation has not been clearly identified and separated from the wide-ranging area of water development activities, such as major and minor constructions for water harvesting, storing, conveyance and allocation; the drilling of tube-wells; and pumping. Most of the efforts and investments made in many countries for irrigation development result in water resources development and very few in on-farm water use improvement. The application of improved irrigation methods and techniques on small to large farms is expanding rapidly as a result of the increasing demand for higher irrigation efficiency, improved utilization of water and intensification, diversification & optimization. An irrigation system consists of canals and structures to convey regulate and deliver the water to the farmers. Two basic types of irrigation systems exist: open canal systems and pressurized piped systems.

Grenze ID: 01.GIJET.9.1.663

GRENZE Scientific Society

Grenze International Journal of Engineering and Technology, Jan Issue

A Deep Exposition of Data Science: Related Issues and its Applications

Syed Azahad[1], Venkatram Vennam[2] and M.V.D.S. Krishnamurty[3]
[1-3]Department of Computer Science Engineering, MCET, Hyderabad, Telangana
Email: azahadsyed@methdoist.edu.in, venkatram@methodist.edu.in, mkrishnamurty@methodist.edu.in

***Abstract*—Data science is the study of extracting, collecting, gathering, representing, and safeguarding data for use in technical problems or for business goals. Although the term "Data Science" may seem to refer to databases and software engineering, numerous other quantitative and qualitative skills, including non-mathematical skills, are also necessary. Information dissection is the main goal of data science. This essay provides an explanation of what data science is, how it works, and some possible applications. This essay's second section contains several reviews of data science. The full data science method is illustrated in Section III of this essay. The data science-related research topics are all described in Section IV. The report concludes with several recommendations for data science-related future research. The writers of the current study will make an effort to look at the various problems, execution, and challenges in the field of data science.**

***Index Terms*— Information, Data Science, investigation, management, cloud computing.**

I. Introduction

Data science is the aggregation from a sizable amount of data that is combined or free, or, to put it another way, it is the field of data mining and data disclosure, which are generally terms for data scooping and perception research. The statement made by John Tukey on this subject and his conclusion are as follows: "The combination of a few data and a desperate need for an answer does not ensure that a sane answer can be derived from a given set of data".

According to Hal Varian, Google's economist, "the ability to absorb information—to have the capacity to interpret it, to analyze it, to remove an incentive from it, to visualize it, to present it—that will be an enormously vital competence in the next decades. Since information is essentially free and readily available right now. The ability to interpret that knowledge and draw a benefit from it is therefore a complementary rare factor. This science's field covers data sequencing, collection, and presentation, bits of information, and machines that make assumptions about how to handle various problems in various fields.

II. Literary Review

According to Dr. S. Justus (2013), the entrance layers, processes, and capacity frameworks for big data are all improving gradually. In this significant circumstance, test architects and testing groups are not prohibited. They focus on some of the problems that test groups would shortly look into. For adaptive performance benchmarking and quality affirmation in the current machine-learning and examination outstanding tasks at hand, J. Nowling

Grenze ID: 01.GIJET.9.1.661

Grenze International Journal of Engineering and Technology, Jan Issue

Sentimental Analysis of Online Products using Ratings and Reviews

Mr. T. Praveen Kumar[1] and Mr. Sandeep Pamulaparty[2]
[1]Methodist College of Engineering and Technology/Dept of CSE, Hyderabad, India
Email: pravinthumukunta@gmail.com
[2]CISCO/Santa Clara, California, USA
Email: pamulaparty@gmail.com

Abstract—**Every second, we can observe a massive surge of data being generated. Data present abundantly needs to be processed to become meaningful information. One way of processing data and knowing the current trend is through product analysis. This concept can be used by organizations to identify their flaws and enhance their productivity. It is often performed on textual data to help businesses monitor brand and product sentiment in customer feedback, and understand customer needs. In this project, we throw light on the aspect that data generated by textual comments along with the rating contribute the efficient classification of data rather than only the rating and obtain various insights as a part of the analysis. In general, when a person wants to buy a product, he checks for the review of the product and then makes a decision whether to buy or not. In more specific terms, the user checks only the rating and makes a decision. We have understood that sometimes rating is misleading the customers and it alone cannot be the sole parameter to take a decision hence we are comparing ratings and comments for better efficiency and authenticity of product reviews.**

Index Terms— **NLP, SVM, KNN, and Logistic Regression.**

I. Introduction

Researchers already use social data to analyze the sentiment of users' opinions on a product, event, or setting. Moreover, People utilize online comments to convey their interests or attitude in social networks, thanks to the rapid development of Internet technology. We can utilize these comments to extract vital information, such as consumer sentiment for a particular product. One of the most important research tasks in text mining is sentiment categorization. Researchers are already analyzing the sentiment of consumers' opinions on a product, event, or location using social data. In addition, sentiment analysis is frequently referred to as opinion mining, which is an important NLP task. The direction of the sentiments is determined by this sentiment analysis. In respect to text, as neutral, positive, or negative in addition, text analytics, computational linguistics, and natural language processing (NLP) are all used in sentiment analysis to recognize and understand the text. Organizing the user's points of view. The primary purpose of sentiment analysis is to determine the author's perspective on a similar event or the overall polarity of the material. Views of emotional communication might include a user's judgment or appraisal, emotional state, or deliberative state. It's typically used to identify sentiment information disclosed by people in comments, such as movie reviews. Sentiment analysis, also known as option mining, is the process of extracting a reviewer's attitude from a movie, usually in the form of a sentence or a review. Sentiment analysis

Grenze ID: 01.GIJET.9.1.659

GRENZE Scientific Society

Grenze International Journal of Engineering and Technology, Jan Issue

Trends and Paradigms in Machine Learning – A Review

DevaRajashekar[1] and Jujuroo Sowmya[2]
[1-2]Asst.Prof, Department of CSE, Methodist College of Engineering & Technology, Hyderabad, India
Email: rajshekardeva@gmail.com, jsowmya@methodist.edu.in

Abstract—**This paper examines recent advances in the area of machine learning. Machine learning has emerged as a novel approach to producing fresh, precise decisions in the processing of massive amounts of data. In the next applications, where a huge amount of learning data must be analyzed in order to produce a judgement, the learning technique will become increasingly important. The field of automation was creating new interfaces and solutions for precise and effective mining in a variety of applications, including retrieval of information, medical applications, military surveillance, privacy and authentication concerns, astronomy data processing, etc. The development of machine learning techniques using different learning approaches, including the biological system, classification approach, and decision approach, are discussed in this study. In order to produce an approach that relies on training and validation, a machine learning strategy is employed, which involves learning specifics like descriptive characteristics and various predictive analytic algorithms in order to develop the best match option. While there have been many advances in the field of machine learning that have resulted in faster and more accurate learning systems, there is still room for development in the monitoring element. The limitations of machine learning are twofold: while intricacy and information extraction must be kept to a minimum, a higher level of accuracy is required. This study described the evolution and limitations of the current machine learning approaches.**

Index Terms— **Dimensional Reduction Reinforcement Learning, Boosting, Predictive modeling Ensemble Learning, Instance learning, Regression Modeling.**

I. INTRODUCTION

A crucial challenge in many automation applications is the retrieval of data from a huge dataset. The need to automate the current approach drives up the effort put into machine learning for current and upcoming applications. The field of machine learning has recently seen advancements in deep learning [1], Bayesian modelling [2], non-parametric processing [3], etc. The demand for novel machine learning approaches, where a significant signaling request and data accessing, has increased due to the increase in the number of data in the registered data base. New methods to speed up and streamline the process have been prioritized as machine learning has advanced. The dissemination of data is no longer restricted to a single site thanks to the development of new architectures and network configurations, but rather to maintain a vast. Data delivery units are dispersed throughout a large network and communicate with one another. New topologies have emerged throughout the evolution, including heterogeneous networks [6, 4], distributed computing [5], and cloud

Grenze ID: 01.GIJET.9.1.655

Proceedings of the International Conference on Intelligent Data Communication Technologies and Internet of Things (IDCIoT 2023)
IEEE Xplore Part Number: CFP23CV1-ART; ISBN: 978-1-6654-7451-1

Automated Deep Learning with Wavelet Neural Network based Rice Plant Classification

[1]V.Rekha
Assistant Professor,
Agurchand Manmull Jain College,
Chennai, Tamil Nadu, India.
rekhaonmail@gmail.com

[2]Dr.L.Venkateswara Reddy-SM IEEE
Professor, Department of Computer Science and Engineering,
KG Reddy College of Engineering and Technology,
Hyderabad, Telangana, India.
lakkireddy.vi@gmail.com

[3]Dr. Sachin Vasant Chaudhari
Associate Professor, Department of Electronics & Computer Engineering,
Sanjivani College of Engineering,
Kopargaon, India.
chaudharisachinetc@sanjivani.org.in

[4]Arepalli Gopi
Assistant Professor, Department of Computer Science Engineering,
Koneru Lakshmaiah Education Foundation
Guntur (d.t), Andhra Pradesh, India.
gopi.arepalli400@gmail.com

[5]C. Nithiya
Assistant professor, Department of ECE, R.M.K. College of Engineering and Technology,
Puduvoyal, India.
nithiyalingamvlsi@gmail.com

[6]Dr. Shaik Khaleel Ahamed
Associate Professor, Department of CSE,
Methodist College of Engineering and Technology
Hyderabad, Telangana, India.
khaleelska@gmail.com

***Abstract*—In the agricultural sector, a disease that occurs in plants is primarily responsible for the decrease in production and results in massive financial loss. Rice is considered the crucial food crop in Asian nations and is affected by distinct types of diseases. Due to the arrival of deep learning (DL) and computer vision methods, rice plant ailments will be identified and diminish the problem of the agriculturalists to save the crops. Currently, computer aided diagnosis (CAD) methods become accessible to observe pests and crop diseases with the help of plant images. An automatic rice disease prognosis technique could present details regarding preventing and controlling rice ailments for decreasing the monetary loss, decline the insecticide residue, and increase the number and quality of yields. In order to attain this method, authors are advised to advance effective image processing methods for noticing plant diseases. Therefore, this paper presents an Automated Deep Learning with Wavelet Neural Network Based Rice Plant Classification model named ADLWNN model. The proposed ADLWNN model focuses on the effectual recognition and categorization of rice plant images. The proposed ADLWNN model primarily exploits convolutional neural network (CNN) model to extract features from the input rice plant images. Moreover, manta ray optimization algorithm (MRFO) algorithm is applied as a hyperparameter optimizer. Besides, the WNN model is employed for the robust recognition and categorization of rice plant images. The simulation analysis of the ADLWNN model is tested using a set of rice plant images and the results indicated as 98.17% better outcomes for the ADLWNN model over other techniques.**

Keywords*— *Rice plant images; Disease diagnosis; Image classification; Convolution neural network; Machine learning

I. INTRODUCTION

Rice is considered to be a staple food in India and all over the world. Nearly half of the global population relies upon rice [1]. Furthermore, a loss of 10 to 15 percent in rice production happens because of rice plant diseases. Therefore, it will be a great challenge for agricultural field to assuring food security for these large populations. It is believed that main factors for such diseases were bacteria and fungi [2]. Such diseased rice plants lead to a decrease in rice production which results in great economic loss to farmers annually. Therefore, the disease diagnosis in agricultural products at initial level was indispensable to thwarting productivity loss and quality improvement as well [3]. Accordingly, it serves an important role in economic growth of a country. Traditionally, rice pla disease recognition can be executed depending on visua valuation of the indications or depends on the experimental outcome by culturing pathogens in labs [4]. The visual valuation was a subjective method and disposed to error. Where culturing pathogens in lab was taking more time and there was also no guarantee of rendering the outcome in time. Along with such limits, both traditional methods need experts for disease identification and it was tough for agriculturalists to get access to specialists because of interior region of their agricultural domain [5]. Such problems have encouraged the research domain for investigating several techniques for developing automated detection and categorization methods for rice plant diseases [6].

In conventional tactics, the time complexity was important, and it can be hard to accurately detect the disease and evaluate its polluted areas in supporting large farming areas [7]. The recognition of pests/insects and diseases on a timely basis has been shown critical for agricultural outcomes. There was a

978-1-6654-7451-1/23/$31.00 ©2023 IEEE

GRENZE Scientific Society

Grenze International Journal of Engineering and Technology, Jan Issue

Implementation of Kernels, Hybridization and Optimizers to Enhance SVM Classifier Accuracy

Dr.U.Moulali[1], Tariku Birhanu Yadesa[2], A. Sowjanya[3] and Sana Mateen[4]
[1]Associate Professor, CSE Dept, Methodist College of Engineering and Technology, Hyderabad
Email: moulaliu@methodist.edu.in
[2]Tariku Birhanu Yadesa, HOD,Lecture, department of Computer Science, Wollega University Nekemte, Ethiopia
Email: tariku 123@ gmail.com
[3-4]Assistant Professor, CSE Dept, Methodist College of Engineering and Technology, Hyderabad
Email: a.sowjanya@methodist.edu.in, sanamateen@methodist.edu.in

Abstract—**The paper deals with improving the results of SVM (Support Vector Machine) by selecting the best kernel (Radial Bias Function kernel, Linear kernel, Sigmoid kernel, Polynomial kernel) and merging the best kernel with a compatible kernel that will overcome the disadvantages in one kernel and increases the overall accuracy of the prediction and finally, converting the Support Vector Machine into a neural network that accepts an optimizer to improve the model and make it effective, as well as adding a Stochastic Gradient Descent (SGD) optimizer to increase the SVM's prediction accuracy, and using SoftMax and Linear activation functions as SVM kernels gives us an SVM model that is more effective than the original SVM model. Once all three techniques have been finished, the model with the highest accuracy among all models will be chosen. The classification of a class decision obtained on the basis of the SVM hyperplane is based on sub-objects determined by experiments close to the class-to-class hyperplane and which include both precise and incorrectly placed objects in the vector space. In the case of improving the quality of the item separation from the original database, the proposed item classification methods may be recommended for the classification of new items. When you upgrade the SVM section, the default parameters used are used. Comparative analysis of the classification results obtained during a test in the compilation of the Multi-class SVM. MPKF and MKF work and functions, similar to the results obtained in the SVM phase modification test using a stochastic gradient drop optimizer that has the functionality of SoftMax, where the parameter values are randomly determined, ensures the suitability of using these composite characters to enhance the quality of the SVM partition. In many cases, the mixing and preparation of the SVM planes work best in terms of improving the quality of the SVM partition.**

Index Terms— **Machine Learning, Neural Networks, High Dimensional Datasets, Support Vector Machines, SVM Kernels, Hybrid Model, Optimizers, Activation Functions.**

I. INTRODUCTION

The Support Vector Machine (SVM) is normally based on the VC concept and the principle of minimizing structural risk. In some learning environments that require more accurate learning functionality, SVM can be upgraded to meet this goal. This paper describes different Boost-SVM methods, such as changing the SVM

Grenze ID: 01.GIJET.9.1.669

GRENZE Scientific Society

Grenze International Journal of Engineering and Technology, Jan Issue

Analysis of Prediction Algorithm for Recognitions of Skin Disease Report in Hyderabad City

Shaik Abdul Khalandar Basha[1], Dr.U.Moulali[2], Dr. S.Khaleel Ahamed[3] and Aruna varnasi[4]
[1, 4]Sreenidhi Institute of Science and Technology, Hyderabad
Email: abdulshaik@sreenidhi.edu.in
[2, 3]Associate Professor, CSE Dept, Methodist College of Engineering and Technology, Hyderabad
Email: moulali.u@gmail.com

Abstract—**Hyderabad is highly affected by climate change and is reported to be a highly prone skin disease-endemic area. This study investigates the association between skin diseases and climate factors. For selecting the best-fit climate prediction method for skin diseases occurrence in Hyderabad city, we have considered 3 different machine learning regression models namely: Poisson Distributed Lag Model [PDLM], Seasonal Autoregressive Integrated Moving Average Model [SARIMA] and other model Standard Multiple Regression [SMR] directed toward investigate the relationship between skin diseases and climate attributes incident during the time period 2000 to 2018. We verify the models lag predicting skin diseases for the time duration of January month to December month 2019 using the MAPE. ROC curves were considered to examine the prediction rate of a skin disease outburst. The results show that relative humidity and temperature are significant parameters which promote skin diseases where there is no rainfall effect. The PDLM model presents the finest fitting prediction of skin disease occurrence and identification of an outbreak when analyzed for a 6, 9, and 12 month time. Nevertheless, the SARIMA algorithm enacts a better prediction of skin disease occurrence for a short 3 month time period. The standard multiple regressions present a high loss prediction of skin disease incidence. From our results we are encouraged to carry out an extensive analysis to validate and examine the modelwith more data in Hyderabad city and contribute in prevention and control of skin diseases at an early stage.**

I. Introduction

Skin Cancer related Diseases is the most widespread disease during summer and winter around the world. Skin cancer occurrence has increasedsince 3 decades,the skin is the organ most exposed toenvironmental UVR and it is roughly calculated that 40 lakhs skin diseases take place each year. Nearly2 crore people reside in skin cancer effected countries[1].Tropical areas America, Australia, India, central Asia andPacific locations are mostly bundled with skin diseases, and in which southeast india and the central Asia area bear nearly 30% of the presentworldwide diseases bundle due to skin[2]–[4]. Some type of Skin are vulnerable toor higherTemperature that result from worldwide global warming which cover an increasingoccurrence of skin diseases [5]–[7]. The annual investigation by has confirm the increase of skin diseases at higher temperature. In-room temperature UV radiations getcarcinogenic. In human beings, theoccurrence of squamous cell sabal and cell carcinoma rises by 45% and 2.4%, respectively, per 1C rise in atmospheric temperature [8]. These estimates correlate to a rise in the virtual UV dose of around 1.5% per 1C rise. Skin cancer can give rise to a change of skin color with more than 6

Grenze ID: 01.GIJET.9.1.605

Grenze International Journal of Engineering and Technology, Jan Issue

Frequency Domain Feature Statistics for Cardiovascular Disease Diagnosis on Low-Computational Devices

Diana Moses [1], Gladson Maria Britto[2], Deisy C[3] and Dainty[4]
[1]Associate Professor, Methodist College of Engineering and Technolog, Hyd, India
[2]Professor and Dean Mallareddy College of Engineering, Hyd, Ind
[3]Thiagarar College of Engineering, Madurai, India
[4]Technology Lead, Infosys, Atlanta, USA

Abstract—**Towards providing a low cost and readily available healthcare intervention system for rural India, we propose novel methods to analyze ECG on Android mobile devices for diagnostic purposes. In the proposed system, ECG is compressed to reduce the volume of input so as to enable processing on a low computational mobile device. Morphological, wavelet and statistical features are extracted directly from the compressed ECG. The subset of most discriminative features is extracted using information theoretic Dynamic Weighting based Feature Selection. Hybrid classification using majority voting-based classifier fusion is applied to enhance the classification performance. For the 14 MIT Arrhythmia classes, the proposed system achieved classification accuracy of 99.3% and a sensitivity of 100 % and a specificity of 98.9 %. Comparison with other existing methods shows better performance of the proposed method.**

Index Terms— **Android App; ECG Analysis; Feature Extraction; Feature Selection; Hybrid Classifier; Mobile Telecardiology.**

I. Introduction

Cardiovascular diseases (CVDs) are the major cause for morbidity and mortality in developing nations as India. Cardiovascular disease encompasses all types of abnormalities affecting the Heart muscles, Valves and/or the blood vessels. These can be diagnosed using the Electrocardiogram (ECG), which is a device for recording the electrical impulses of the heart. The analysis if ECG demands expert knowledge which is not readily available in rural areas. In order to overcome this, mobile based healthcare intervention strategies were proposed. The two major challenges in mobile based ECG analysis systems include those inherent to mobile applications and ECG Classification.

Challenges inherent to mobile applications for analyzing ECG in a real-time environment are limitation in: storage, computational capacity, bandwidth and associated delays. Accordingly, general mobile based telecardiology architecture has evolved incorporating ECG Compression, low computation methods for feature extraction and classification and strategies to mitigate delays [1]. Despite the risks of losing of clinically significant data, lossy compression was used [2]. Features are generally extracted in time or frequency domain. In realization of the computational capacity of these devices, mobile based systems extract the key features in the time domain only and overlook frequency domain feature extraction methods. Time domain feature extraction methods adopted by many mobile based systems include the Pan Tompkins [3] algorithm for QRS detection and

Grenze ID: 01.GIJET.9.1.654

GRENZE Scientific Society

Grenze International Journal of Engineering and Technology, Jan Issue

An Efficient Approach for Identification of Copy- Move Image Forgery using SURF and SIFT based Techniques

Shaik Rasool[1], Uma N. Dulhare[2], Vasavi Sravanthi Balusa[3], Deepthi Joshi [4] and Shaziya jabeen[5]
[1, 3-5]Methodist College of Engineering and Technology, Hyderabad, India
Email: shaikrasool@outlook.com, vasavibvs@gmail.com, deepthijayam@gmail.com, shaziyajabeen@gmail.com
[2]Muffakham Jah College of Engineering and Technology, Hyderabad, India,
Email: prof.umadulhare@gmail.com

***Abstract*—Internet has changed the world of computers and how we use them. Now there is no field left that may not require internet. It has impacted mostly the fields like image processing, machine learning, cyber security, data mining etc. Technological developments today have made the life so comfortable and easy but also put forward a challenge of authentication of digital data generated from various domains. This has become a major concern for security. To address this concern, we are encapsulating facet point juxtaposition, adaptive over dissection for forgery identification in our proposal. We have based our work on Key point and Section based forgery identification techniques. Adaptive non-intersecting, irregular sections are utilized to uncover suspicious sections in the images. Dissection algorithms are used to assist in this process. Facet points are mined by comparing and juxtaposition each section with its facets. Super pixels are used instead of facet points in the proposed forgery section mining system. The neighbouring sections are melded into facet sections to acquire merged sections which have similar color facets. To end the process morphological operations are used over merged sections to obtain forgery section. The outcomes obtained shows that this proposed algorithm can achieve superior and accurate outcomes even in most critical constraints when compared to other existing approaches.**

***Index Terms*— Image Processing, Forgery Identification, Image Forgery, Juxtaposition, Digital Images.**

I. INTRODUCTION

Digital image processing in this modern era has become one of the most protruding domains for research in multidisciplinary fields. The core of electromagnetic spectrum and security is constituted by digital image processing. It has become the primary focus of research with huge scope to safeguard privacy and maintain confidentiality. Achieving the desired outcomes in image processing remains a challenging task that needs an apt solution. Digital images are primary source for forensics, deep learning, AI and thrust areas. Using deep learning techniques today, we can fake eminent personalities thus by posing challenge to forensics to detect forgery images. The disparity between forgery and original image has been narrowed done deeply that it's almost becoming impractical to identify the difference. This drawback is addressed by proposed work [1].
Image forgery has become very common today in social networks. Copy-move forgery is among well-known digital image manipulation practices today that copies portion of the image and is bonded at a different location

Grenze ID: 01.GIJET.9.1.603

GRENZE Scientific Society

Grenze International Journal of Engineering and Technology, Jan Issue

A Secure Voting System using Iris Recognition

Dr. M. Sharadha Varalakshmi[1], Nikhila Bethi[2], N. Lakshmi Samyu[3] and Samiya Hafsa[4]
[1]Professor, Methodist College of Engineering and Technology/Computer Science and Engineering, Hyderabad, India
Email: msharada@methodist.edu.in
[2-4]Methodist College of Engineering and Technology/Computer Science and Engineering, Hyderabad, India
Email: {saritha760, saivirinchi103, akarshanagoud2001}@gmail.com

***Abstract*—During elections in democratic countries, the voting mechanism is extremely significant.**
India holds elections using either Secret Ballet Voting or Electronic Voting Machines which involves massive costs and manual labor. The election commission is having a lot of problems during the election process. The most common issue that the electoral commission deals with is the polling arrangement and duplicate or voting fraud. Electronic voting machines need more personnel, are time-consuming, and are less reliable. As a result, the system must be tuned to be efficient, leaving no opportunity for poor voting procedures. In this project, a secure and modern voting system employing iris recognition and facial recognition is built to improve the present voting system. The most reliable biometric of human identification is iris recognition. The proposed system allows users to vote only after verifying their iris image Iris recognition system is categorized into Canny Edge Detector, iris Circular Hough transformation, symlet wavelet, iris-based authentication detection.

***Index Terms*— iris, e-voting, secure, hough transform.**

I. Introduction

In any country, the election process is a major administrative task. It employs a number of processes, all of which require human effort. Voting techniques are now transferred to electronic format and used in a variety of automated tasks. This will save time by reducing traditional paper tasks. E-voting is a computer-assisted voting mechanism that can be used both online and offline. Each voter's information is recorded with a unique ID and saved in a database.

Every voter's information is retrieved and confirmed whenever the ballot method is used. In an electronic voting system, voter identification is crucial.

Existing voting systems' core problem is security. An unidentified person may often cast a vote. Some politicians bid to secure elections by unlawful means. Existing systems are very long, difficult, and with time lags. We use an Iris pattern and as a result, the suggested voting mechanism is more secure than the alternating current system.

II. Methodology

Canny Edge Detection:

Canny Edge Detection is a popular edge detection algorithm that was developed by John F. Canny. It takes the Sobel algorithm's output as its input and is a multi-stage algorithm with stages like Noise

Grenze ID: 01.GIJET.9.1.646

GRENZE Scientific Society

Grenze International Journal of Engineering and Technology, Jan Issue

Hrypton: Password Manager App Built using SHA-256 Cryptographic Hash Function

S.Karthik Kumar[1], A. Anudeep[2], M. Dhruvteja[3], and Dr. M. Sharada Varalakshmi[4]
[1-3]Methodist College of Engineering and Technology/Computer Science and Engineering, Hyderabad, India
Email: karthik.sirnam@gmail.com, {arvapally. anudeep, dhruvtejamanjrekar}@gmail.com
[4]M.Tech, Ph.D, Professor, Methodist College of Engineering and Technology/Computer Science and Engineering, Hyderabad, India
Email: msharada@methodist.edu.in

Abstract—**Explosive growth in the number of passwords for web-based Applications and encryption keys far surpass the management's allotted number of users for outsourced data storage. the outsourcing of keys (including passwords and data encryption keys) to the professional password managers (honest-but-curious service providers) which attracts the attention of many users. However, current approaches to conventional data outsourcing scenarios cannot meet the security requirements for crucial outsourcing simultaneously. So, the proposed Hrypton is a modified cryptographic hash function that addresses all three goals above. Under the framework, the key owner can perform privacy, and controllable authorization-enforced encryption with minimum information leakage. To implement Hrypton efficiently, a new cryptographic primitive named Searchable Conditional Proxy Re-Encryption (SC-PRE) combines the techniques of Hidden Vector Encryption (HVE) and Proxy Re-Encryption (PRE) seamlessly and proposes a concrete SCPRE scheme based on existing HVE and PRE schemes.**

Index Terms— **Hash Function, SHA-256, Encryption, Security, Cryptographic.**

I. Introduction

An individual's passwords for multiple online accounts and security features are stored and managed by a password manager, which is a piece of software. With a master password, password managers offer secure access to all password information and store passwords in an encrypted format password.

If your current passwords are weak, the best password managers will alert you. brittle, frequently used, or have been implicated in a data leak. These tools assist you in maintaining good password hygiene by providing fresh, robust, and outstanding login credentials for each session. We advise configuring your password manager to create passwords of at least 20 characters and a variety of character kinds, including uppercase, lowercase, numbers, and symbols.

Password management tools also provide several other standard features. It's common for them to have password generators that can create strong passwords. Many also can automatically fill out Web forms, such as online job applications, order forms on retail sites, and contest forms. By entering your contact information into the tool, it can then pass your name, address, and other contact information into fields on whatever Web form is loaded in your browser. Then, by pressing a button, you can fill out most or all of a

Grenze ID: 01.GIJET.9.1.660

GRENZE Scientific Society

Grenze International Journal of Engineering and Technology, Jan Issue

A Deep Exposition of Data Science: Related Issues and its Applications

Syed Azahad[1], Venkatram Vennam[2] and M.V.D.S. Krishnamurty[3]
[1-3]Department of Computer Science Engineering, MCET, Hyderabad, Telangana
Email: azahadsyed@methdoist.edu.in, venkatram@methodist.edu.in, mkrishnamurty@methodist.edu.in

Abstract—**Data science is the study of extracting, collecting, gathering, representing, and safeguarding data for use in technical problems or for business goals. Although the term "Data Science" may seem to refer to databases and software engineering, numerous other quantitative and qualitative skills, including non-mathematical skills, are also necessary. Information dissection is the main goal of data science. This essay provides an explanation of what data science is, how it works, and some possible applications. This essay's second section contains several reviews of data science. The full data science method is illustrated in Section III of this essay. The data science-related research topics are all described in Section IV. The report concludes with several recommendations for data science-related future research. The writers of the current study will make an effort to look at the various problems, execution, and challenges in the field of data science.**

Index Terms— **Information, Data Science, investigation, management, cloud computing.**

I. Introduction

Data science is the aggregation from a sizable amount of data that is combined or free, or, to put it another way, it is the field of data mining and data disclosure, which are generally terms for data scooping and perception research. The statement made by John Tukey on this subject and his conclusion are as follows: "The combination of a few data and a desperate need for an answer does not ensure that a sane answer can be derived from a given set of data".

According to Hal Varian, Google's economist, "the ability to absorb information—to have the capacity to interpret it, to analyze it, to remove an incentive from it, to visualize it, to present it—that will be an enormously vital competence in the next decades. Since information is essentially free and readily available right now. The ability to interpret that knowledge and draw a benefit from it is therefore a complementary rare factor. This science's field covers data sequencing, collection, and presentation, bits of information, and machines that make assumptions about how to handle various problems in various fields.

II. Literary Review

According to Dr. S. Justus (2013), the entrance layers, processes, and capacity frameworks for big data are all improving gradually. In this significant circumstance, test architects and testing groups are not prohibited. They focus on some of the problems that test groups would shortly look into. For adaptive performance benchmarking and quality affirmation in the current machine-learning and examination outstanding tasks at hand, J. Nowling

Grenze ID: 01.GIJET.9.1.661

Grenze International Journal of Engineering and Technology, Jan Issue

Identifying Vertex Influential Nodes in Considerable Composite Networks using Grid Layout

Srinu Dharavath[1], D Natarajasivan[2] and Senthil Kumaar[3]
[1,2]Department of Computer Science and Engineering, Annamalai University, Annamalai Nagar, Chidambaram
Email: srinudharavathphd@gmail.com., natarajasivan@gmail.com.
[3]Department of Computer Science and Engineering, Methodist College of Engineering and Technology, Hyderabad
Email: aarcse100@gmail.com

Abstract—**Online social networks are famous for various activities like creativity, spreading information, and ideas, for the most part for viral marketing. The main focus in the social influence analysis, known as the influence maximization problem(IMP), aims to select Top-N nodes to maximize the expected number of nodes activated by the Top-N nodes (a.k.a seed nodes). This issue has gotten a lot of attention and has been looking into the issue of IMP; these studies are usually too time-consuming to be useful in a complex social media network. The problem of seed selection is NP-hard. Due to the utilization of time-consuming Monte Carlo simulations, which are confined to small networks, so a greedy method to the IM issue is insufficient? The greedy approach, on the other hand, offers a good approximation assurance. In this paper, we present an algorithm for identifying communities and computing the ranking scores of nodes in the identified communities to solve the IMP with a focus on time efficiency.**

Index Terms— **Top-N influential nodes, Node ranking Score, Information propagation. K-Shell decomposition, Complex networks.**

I. Introduction

In recent years, with the advancement of communication technology and the widespread use of the internet, the number of people using social media sites is on the rise. Online social networks have grown ingrained in the lives of all users. As a result, a vast volume of information and ideas is transmitted every day across networks that may affect a big number of individuals for a brief period [1]. From the last two decades, many researchers have been concerned about the Influence Spread (IS) and influence among social networks, and their results have paved the way for many online applications such as viral marketing [2]. which is a successful strategy and practical platform that is used as a launching pad and spreads through W-O-M/word-of-mouth on social media sites. One of the oldest and most practical kinds of marketing, word-of-mouth, is a simple way of getting an advertising or promotional message out to people. For example, a firm may wish to target a limited number of people (a.k.a seeds) for a trial of a new brand via social-media-networking medium in the hopes that these early adopters would encourage their friends, and they influence their friends, to buy the product. The assumption is that word-of-mouth marketing will help the firm reach a large pool of targeted users. Under the spreading model, this situation is formally characterized as the influence maximization problem[3], which seeks to choose the initial seeds who can encourage the greatest number of consumers to accept a marketed product.
Domingo et al. [3]were the first to present the IMP from the standpoint of the algorithm inspired by the concept

Grenze ID: 01.GIJET.9.1.665

Grenze International Journal of Engineering and Technology, Jan Issue

Short Term Memory Recurrent Neural Network-based Machine Learning Model for Predicting Bit-coin Market Prices

Mr.M.Ravi Kumar[1], Dr. Syed Umar[2] and V. Venkatram[3]
[1,3]Assistant Professor, CSE Dept, Methodist College of Engineering and Technology, Hyderabad
Email: ravi2kinus@gmail.com, venkatram@methodist.edu.in
[2]Professor, Department of computer science, College of Engineering, Wollega University, Nekemte, Oromiya Region, Ethiopia-390
Email: umar332@gmail.com

Abstract—**Machine learning based on Deep neural Network have integrated usages in a variety of domains such as translation, finance, distribution, and medical world as well as cognition. This study illustrates Recurrent Neural Network Learning Model on the basis of LSTM, which analyses the previous values of a crypto currency, Bit coin and predicts the future one. This application estimates the actual and anticipated price of Bit coin, starting with 30 days of the previous price and then extrapolating to forecast the next day's price. At a ratio of 1:9, a regularized data set for modeling is separated into test data and training data. The previous set is divided again, this time between training and validation data. The machine learning from this research should use the usage of the Neural Network library and the Keras framework. You optimize the process by searching for the model's weight using the training data while trying to fit the model. In this article, the batch size and epochs for the fit function are 11 and 30, respectively. The loss is reduced more slowly, then levels off to a more steady amount as learning is processed repeatedly. In other words, over fitting is impossible. As the outcome of the experiment, the machine learning states that the neural network becomes better at processing after studying the graphs of error rates and weight change rates.**

Index Terms— **Bitcoin, Block Chain, price, LSTM, Recurrent Neural Network, prediction.**

I. INTRODUCTION

Artificial intelligence is described as a program that simulates human thought processes and behavior, including natural language processing, automatic inference, computer vision, voice recognition, and knowledge representation. The two categories of learning in Artificial Intelligence are supervised and unsupervised learning, depending on whether a label is in the learning data. To solve an issue, the brain uses strategies including grouping, categorization, and forecasting. A learning model should be established in advance, according to research from [1,2]. Machine learning, with its predictive analysis, provides knowledge and advice suited to the task at hand, calculating patterns and possible outcomes before projecting the most likely results. RNN, when applied to estimation problems dealing with time series data like monthly sales, price index, unemployment rate, exchange rate, and stock price, generates the following data prediction via learning context -> RNN, when

Grenze ID: 01.GIJET.9.1.662

GRENZE Scientific Society

Grenze International Journal of Engineering and Technology, Jan Issue

Multi-Mode Detection and Identification of Biometric using Multilevel Scaler SVM

Dr.Shruthi SK[1], Mr.P.V.Ramanaiah[2] and Mr.Ravi Kumar Munaganuri[3]
[1-3]Assistant Professor,CSE Department, Methodist College of Engineering and Technology

***Abstract*—The Face, iris and fingerprint are most promising biometric authentication system that can be identify and analysis a person as their unique features that can be quickly extracted during the recognition process. To ensure the actual presence of a real legitimate trait in difference to a fake self-pretended synthetic or reconstructed sample is aimportant problem in biometric verification, which needs the development of new and efficient protection measures. Biometric systems are vulnerable to spoofing attack. A dependable and efficient countermeasure is needed in order to combat the epidemic growth in identity theft. The biometric detection and authentication deals with non-ideal scenarios such as blurred images, reflections and also faked by the other users. For this reason, image quality assessment approaches to implement fake detection method in multimodal biometric systems. Image quality assessment approach is used to construct the feature vectors that include quality parameters such as reflection, blur level, color diversity, error rate, noise rate, similarity values and so on. These features are stored as vector in database. Then implement Multi level Support Vector Machine classification algorithm to predict fake biometrics.**

***Index Terms*— Multimodal biometrics, Image Quality, Spoofing attack, Fake detection, Feature Vector.**

I. INTRODUCTION

Biometric is epidemically growing technology for automated acknowledgment or authentication of the uniqueness of a person using distinctive physical or behavioral characteristics such as fingerprints, face, iris, retina, voice, hand geometry and signature etc. To ascertain a personnel identity biometric relies on - who you are or what you do, as conflicting to what you remember such as a PIN number or secrete keyword or what you use -such as an ID card. However, significant advances have been realized in biometrics, several spoofing techniques have been established to deceive the biometric systems, and the protection of such systems against attacks is still an open problem. Among the changed threats examined, the direct or spoofing attacks have provoked the biometric community to study the liabilitiesin contradiction of this type of duplicitous actions in performances such as the fingerprint, the face, the signature, or even the bearing and multimodal tactics.Spoofing attacks arise when a person tries to masquerade as someone else faking the biometrics data that are confined by the acquisition sensor in an attempt to avoid a biometric system and thereby aheadillegal access and advantages. Some type of falsely created artifact e.g. gummy finger, printed iris image, face mask, photograph, audiovisual, 3d Model or imitate the behavior of the actual user (e.g., gait, signature) etc. are used by the imposter to fake the biometric scheme.Consequently, there is an accumulative essential to detect such efforts of attacks to biometric systems. Liveness detection is one of the existing countermeasures in contradiction of spoofing attack. It aims at

Grenze ID: 01.GIJET.9.1.666

Grenze International Journal of Engineering and Technology, Jan Issue

An Intelligent Way to Recognize Digits using Convolutional Neural Networks (CNN) Algorithm

A.Virinchi Sai[1], M. Sai Dhanush[2], M.N. Akarshana[3], and Sandeep R[4]
[1-3]Methodist College of Engineering and Technology/Computer Science and Engineering, Hyderabad, India
Email: saidhanushccs@gmail.com, akarshanagoud2001@gmail.com
[4]Asst.Professor, Methodist College of Engineering and Technology/Computer Science and Engineering, Hyderabad, India
Email: rsandeep@methodist.edu.in

Abstract—**The Handwritten digit recognition issue in pattern recognition systems is one of the more significant technical issues. Applications for digit recognition include data entry forms, bank check processing, postal mail sorting, and more. The capacity to create a practical algorithm that can recognize handwritten digits given by users via a scanner,tablet and other digital devices is at the core of the issue. The study's main goals were to create a machine learning algorithm and an optimization technique to improve the precision of handwritten digits recognition, as well as to analyze the performance of the proposed algorithm with test data set. This model offers a method for recognizing handwritten digits offline that is based on various machine learning techniques. There are several machine learning algorithms such as Support Vector Machine, Random Forest, Multilayer Perceptron, Convolutional Neural Network etc. In this project is aimed to use Convolutional Neural Network to complete the task. The MNIST dataset also used in this project. The main objective of this model is to ensure effective and reliable approaches for recognition of handwritten digits.**

Index Terms— **CNN, Neural Network.**

I. Introduction

The sudden growth of new documents and multimedia news has created new challenges in pattern recognition and machine learning (Cecotti, 2016). Handwriting character recognition has become a common research area due to technological advances such as handwriting capture devices and powerful mobile computers. However, since handwriting focuses on the writer, building a highly reliable recognition system that recognizes any handwritten character input to an application can be challenging.

In this work, we deal with the recognition problem of handwritten numbers, i.e. the numbers 0-9. Handwritten number recognition is usually crucial in various practical applications such as management and economics (Niu & Suen, 2012). These industries require excellent recognition and the highest credibility. For example, unconstrained handwritten digit recognition has been applied to checks and hand-filled forms such as tax forms or postal codes on postcards with excellent results (Lauer, Suen, & Bloch, 2007). Constraint perception refers to the extent to which people believe that factors beyond their control limit their behaviour. In contrast, an unconstrained detection system can be divided into several parts: preprocessing, feature extraction, classification, evaluation, and verification.

Grenze ID: 01.GIJET.9.1.656

Grenze International Journal of Engineering and Technology, Jan Issue

Web Service Ranking and Classification using Intelligent Techniques

Dr. Ramakanta Mohanty
Methodist College of Engineering and Technology, king Koti Road, Abids, Hyderabad, TS
Email: ramakanta5a@gmail.com

Abstract—**In the fastidious ever-growing world of businesses when the constant exchange of web services takes place, it is important for the buyer and seller to understand where their web service stands. A web service is a set of open protocols and standards that allow data to be exchanged between different applications or systems. Web services can be used by software programs written in a variety of programming languages and running on a variety of platforms to exchange data via computer networks such as the Internet in a similar way to inter-process communication on a single computer. The QWS dataset version II is collected from literature which is not having class level. The dataset is normalized using min-max method and employ stratified cross validation to make different fold systems. To make the different web services into different class levels, we employ two different clustering algorithm viz. K-means, and Fuzzy C-means to cluster different web services into different clusters. To test the different class level simulated by clustering algorithm, machine learning algorithm is employed i.e. Genetic Programming (GP), and Random Forest to test the efficacy of the model. From our experimental results, it is observed that C-Fuzzy means clustering provided the best clustering level compared to other techniques. The average accuracy of 99.23% provided by Genetic programming.**

Index Terms— **Fuzzy C-means, K-means, Genetic Programming, Random Forest, Intelligent Techniques, Web Services.**

I. Introduction

The inter connectivity of thousands of different types of computers across the globe that are a component of various networks is known as the Internet. A web service is a defined technique for message transmission between client and server applications on the World Wide Web. A software module called a web service is designed to perform a certain set of tasks. In cloud computing, web services are searchable and dynamically typed across a network. The client that called the web service would be able to receive functionality from the web service [1].

A web service is a collection of open protocols and standards that enable the transfer of data across various software programs or computer systems. In a manner similar to inter-process communication on a single computer, web services may be used by software programs created in a range of programming languages and running on a variety of platforms to exchange data across computer networks like the Internet.

A web service is any piece of software, application, or cloud technology that connects to the internet and exchanges data messages, typically in the form of XML (Extensible Markup Language), using defined web

Grenze ID: 01.GIJET.9.1.640

Analysis of the Regulatory Development Cryptocurrencies for Trading in Business with Deep Learning Techniques

Uma N Dulhare
Professor and Head
Department of CS & AI
Muffakham Jah College of Engineering And Technology
Telangana, India
prof.umadulhare@gmail.com

Shaik Rasool
Assistant Professor
Department of CSE
Methodist College of Engineering and Technology
Telangana, India
shaikrasool@outlook.com

Mohammad Naseer Khan
Principal Software Engineer
Visual Technologies LLC
Dallas, Texas
United States
mohammadnaseerkhan@outlook.com

Bhasker Pant
Department of CSE
Graphic Era Deemed to be University And Graphic Era Hill University
Dehradun, Uttarakhand, India
Bhasker.pant@geu.ac.in

Dr. A. Kakoli Rao
Professor and HOD
Department of CSE
Lloyd Institute of Engineering and Technology
Greater Noida, Uttar Pradesh, India.
hodcse@liet.in

Garima Bhardwaj
Amity University
Greater Noida
Uttar Pradesh, India
gbhardwaj@gn.amity.edu

***Abstract*- As the number of people infected with COVID-19 continues to rise, a number of nations have implemented state wide quarantines. This has resulted in a global financial crisis that is having severe impacts on countries all around the world. As a direct consequence of the epidemic, unemployment rates have increased in a number of different regions, which has a substantial and detrimental effect on trade across the globe. In light of the current state of the economy, Artificial Intelligence (AI) is causing a shift in the manner in which businesses evaluate their bitcoin holdings. The application of AI in a commercial setting has the potential to produce a wide range of beneficial results. We are spared from completing as much manual labour as a direct result of the favourable effects that AI has had on technology. These consequences can be noticed in our day-to-day lives. In the event that there is a pandemic, having knowledge of AI and the various strategies it employs, such as the classifier model, could be beneficial. Humans will be better suited to make decisions if they have rapid access to the analyses and projections that are created by AI and big data. In order to be prepared for the arrival of the new world, the company is putting in more effort, in collaboration with small and medium-sized enterprises (SMEs) and start-ups, to improve the administration of virtual enterprises by having a presence on a variety of different e-trade systems. Artificial intelligence (AI) is currently being utilised in a variety of settings to assist with the process of identifying and implementing workable solutions to a variety of problems that can develop in the workplace. AI is being used to improve business operations in a wide variety of spheres, including marketing, fraud detection, algorithmic trading, customer assistance, portfolio management, and product recommendations based on customer preferences. These are just few of the sectors. These are just a few examples of the kinds of problems that artificial intelligence might be able to solve in the future. Given the present worth of cryptocurrencies, technological developments may also be made in order to improve the performance of the rules that have been provided and produce the most accurate conclusion that is possible.**

Keywords: AI and Machine Learning, Big Data, Business Analytics, and Decision Making.

I. INTRODUCTION

At this point, the COVID-19 virus has spread to all seven continents. People who are in close quarters with an unwell person are more likely to transmit the virus to that person by their coughing, sneezing, and other respiratory movements. There is currently no treatment available for this ailment. When taking medication, the easiest way to avoid becoming ill is to ensure that you follow the dosing instructions to the letter. The COVID-19 outbreak has already reached every region of the world, which has caused the World Health Organization (WHO) to declare a public health emergency [1]. Because of the quick spread of the disease, there has been a noticeable slowdown in economic activity all across the world. The shutdown at the power plant has had a greater impact on the lives of a greater number of people than it has had on the economy. Because of the shockingly high number of fatalities, the economy has been in a state of crisis for some time now, and the unemployment rate is only going to continue to climb higher. Specifically, artificial intelligence is making a substantial contribution, which is contributing to the overall improvement of conditions at this moment. Not only is this method helpful for forecasting, but it also contributes to the diagnosis and treatment of patients. Its ability to fool humans into believing it is human grants it access to regions that are normally off-limits to people. Models that are based on artificial intelligence (AI) can help the economy recover by making it easier to develop skilled labour and deploy machine automation on a wider scale. The epidemic caused by COVID-19 has had an impact on practically all of the world's most significant corporations. In the year 2020, the virus that kills humans has caused problems for industry and trade. This encompasses the entire

978-1-6654-7657-7/22/$31.00 ©2022 IEEE

2022 2nd International Conference on Technological Advancements in Computational Sciences (ICTACS)

Automated Multiclass Classification Using Deep Convolution Neural Network on Dermoscopy Images

Shaik Rasool
Assistant Professor
Department of CSE
Methodist College of Engineering and Technology
Telangana, India.
shaikrasool@outlook.com

Uma N Dulhare
Professor and Head
Department of CS & AI
Muffakham Jha College of Engineering and Technology
Telangana, India.
Prof.umadulhare@gmail.com

Mohammed Naseer Khan
Principal Software Engineer
Visual Technologies LLC
Dallas, Texas,
United States.
mohammednaseerkhan@outlook.com

Dr. Durgaprasad Gangodkar
Department of CSE
Graphic Era Deemed to be University
And Graphic Era Hill University
Dehradun, Uttarakhand, India.
Dr.gangodkar@geu.ac.in

Dr. Ajay Rana
Amity University
Greater Noida
Uttar Pradesh, India.
Ajay_rana@amity.edu

Ravi Kalra, Department of CSE
Lloyd Institute of Engineering and Technology
Greater Noida, Uttar Pradesh, India.
Dean.engineering@liet.in

***Abstract*— Due to the nature of the surgery, treating skin tumours manually takes a long time and can only be done on one individual at a time. As a result, it is evident that computational and analytical methodologies are required for meaningful classification of skin lesions at various stages. We have demonstrated a fully automated method of classifying the wide variety of skin lesions that exist. The automatic dissection of skin lesions and their isolation are two of the most critical and interconnected difficulties in computer-assisted skin cancer detection. Although deep learning models see widespread use, they are typically developed to address only one problem, when it could be more efficient to address both simultaneously. In this research, we propose a model for detecting and labelling skin lesions that makes use of Bootstrapping Ensembles and Convolutional Neural Networks (BE-CNN). This theory was developed by the authors of the study. The CI-SN (Compute-Intensive Segmentation Network) is the backbone of this approach (improved-SN). However, the Compute-Intensive Segmentation Network can detect and categorise skin lesions by creating pre-bootstrapping uneven lesion coverings. The strategy's objective is for the arrangement and division networks to cooperate and learn from one another. To do this, a "bootstrapping" process is used. However, we suggest a novel use of segmentation networks to address issues stemming from both class and pixel variation. On the ISIC-HAM 10000 datasets, we find that the proposed BE-CNN model outperforms the function of separating skin lesions based on the current condition and stages techniques, with a mean accuracy of 92.67%. We reached this result after observing that the suggested model more effectively classified skin lesions into their respective stages than the prevalent condition and stages-based methods. The findings demonstrate that a continuous bootstrapping strategy can be used to partition and classify skin lesions in a connected model. Doing both at once like this would prove the point.**

Keywords*— *Classification of Skin lesion, CNN - Convolutional Neural Network, Compute-Intensive Segmentation Network.

I. INTRODUCTION

The largest organ in the human body is the skin. Cancer of the skin arises when cells in the skin become disorganised and begin to multiply uncontrollably, putting the surrounding tissues at risk[9]. The vast majority of people who develop cancer do so on their skin, making it the most common type. The vast majority of people who struggle with skin conditions are unaware of the nature of their condition or the degree to which it manifests itself. One of the factors that contributes to the rapid progression of various skin diseases is the fact that their symptoms don't always present themselves right away. The average person does not have the level of knowledge required to make educated choices regarding their health and the medical care they receive. Dermatologists are medical practitioners who focus their training and expertise on skin disorders. Unfortunately, expensive laboratory tests may be required in order to properly diagnose and evaluate the severity of a skin condition. Dermatological technologies that are based on lasers and photonics have undergone significant advancements in recent years, which has allowed for faster and more accurate diagnosis and treatment of skin problems. Nevertheless, there is not a significant financial burden associated with this particular diagnosis. As a consequence of this, we offer a method of diagnosis that is predicated on the inspection of photographs. When trying to diagnose skin cancer, dermatologists and other medical experts frequently resort to the use of biopsies as a reliable diagnostic tool. It's possible that this is the best alternative, but I can't make any guarantees. The ABCDE rule [1] and the 7-point criteria [2] are also examples of additional screening methodologies.

However, in order for these therapies to be effective, it is vital to first consult with a dermatologist. In recent years [3, 4], dermatologists have shifted away from relying on alternative ways to identify skin cancer and now employ dermoscopy and microscopic pictures instead. Please be aware that the images have been drastically shrunk, and in order to view them, you will need a specialised micro camera.

978-1-6654-7657-7/22/$31.00 ©2022 IEEE

Proceedings of the International Conference on Edge Computing and Applications (ICECAA 2022)
IEEE Xplore Part Number: CFP22BV8-ART; ISBN: 978-1-6654-8232-5

Improving Multimodal Sentiment Analysis using Prediction-based Word Embeddings

[1] T Praveen Kumar
Department of CSE
Methodist College of Engineering and Technology
Hyderabad, Telangana, India
pravinthumukunta@gmail.com

[2] B.Vishnu Vardhan
Department of CSE
JNTUH College of Manthani
Manthani, Telangana, India.
mailvishnuvardhan@gmail.com

Abstract- **In the digital era, information in large amounts may be discovered in the form of reviews and writings of customers. People create reviews using only text or emojis that express the customer's thoughts or opinions. In most instances, user comments reflect their gut feelings about a product. A significant amount of value is extracted from these remarks by using sentiment analysis. The classification is one of the most pressing challenges in sentiment analysis which is our main agenda in this work. The accuracy is used as a performance evaluator and gives weightage to sentiments given in the form of emojis. A multimodal classification model is utilized here by considering both text and emojis for the final output. The comparative study is also done on the word embedding methods of the Word2Vec model. According to the findings of the experiments, the proposed system outperforms the sentiment analysis models, which considers only text for evaluation.**

Keywords: Multimodal Sentiment Analysis, word embeddings: CBOW and Skipgram, word2vec, Machine Learning

I. INTRODUCTION

In the olden days before the internet people would go and seek opinions from friends or relatives to buy a product [4]. However, nowadays we are witnessing an explosive increase in information product reviews on various social media platforms, as a result of the extraordinary prominence of social media and the increase of usage of smartphones with advanced features. This type of multimodal corpus consists of either Aesthetic (picture), sound (speech), or transcribed verbal (text) data. Thus the opinion of others about a particular product will have a drastic effect on our decision-making process.

Mobile Apps like flip kart, amazon, e-commerce sites like e-bay, social media platforms like Facebook, WhatsApp, LinkedIn or Twitter, etc. help in getting the reviews of various online selling products [5-6]. The sentiment behind these reviews is analyzed by a technique of artificial intelligence which is called as sentiment analysis (SA). The customer's intention of the product is analyzed thoroughly and classified by using a scored word list as either neutral, positive, or negative. The four main types of SA are i) Graded Opinion Mining II) Emotion detection III) Aspect based SA IV) Intent analysis.

The combination of NLP and machine learning methods are used to model the complicated data. In sentiment analysis, there are three main types of algorithms automated systems, Rule-based systems, and hybrid systems. In our research, the SA is done on Text and emojis not merely on only text. A good fusion of this text and emojis will help in extracting meaningful information. For both sellers and consumers, the necessity to analyze reviews in order to comprehend customer feedback has grown. However, due to a large number of reviews so it is not practical to read all of the feedback for a specific item. Using deep learning algorithms, this study will compare alternative analyses of sentiment methodologies for a corpus of mobile phone reviews of prediction of consumer happiness for a mobile phones review. So, in this paper, we worked on a multi-modal SA to analyze reviews on both text and emojis. This technique outperformed the existing methods by increasing in Accuracy of SA.

The paper's structure is Section II is a literature review. The proposed model for Multimodal Sentiment Analysis Using Word Embedding in Section III In Section IV the experiments are implemented described and the results. The conclusion and future work are discussed in Section V.

II. RELATED WORK

In this section, we discussed Multimodal sentiment analysis (MSA). This MSA, which combines verbal and nonverbal information such as visual and audio, has become a popular research topic. To enable multimodal shifting for presenting learning models, Wang et al. [1] constructed a repeating attended variation embedding network. Hazarika [2] proposed multisensory and modality-specific representations for multimodal representation learning. Liu et al. [3] presented a rank model for the multimodal fusion concept to reduce the cost of tensor-based techniques. Hellinger[8] used word embedding and PCA to identify the opinion of Bengali comments. Similar terms appear more frequently in the same context of Word2vec [9]. Opinion mining, an effective feature extraction method based on Word2Vec is proposed [10]. Through Word2Vec and an opinion lexical dictionary, the technique detects polarity clusters of terms in the lexicon. The polarity clusters are used to create the characteristics vector for each text which results in a lower-dimensional vector. Researchers in the field of opinion mining employ ML algorithms to increase accuracy. The research work [11] proposed a method for opinion mining on datasets of 400,000 customer reviews. Their results suggested the good accuracy on "Random Forest" with word embeddings equal to 90.6622%. In the realm of sentiment analysis utilizing deep learning methodologies, on the other hand, a data corpus of 10,662 records was used for opinion mining from the IMDb corpus [12]. In addition, another study used deep learning methods like the MLP,